Monthly Notices
of the
ROYAL ASTRONOMICAL SOCIETY

MNRAS **467,** 369–411 (2017)
Advance Access publication 2017 January 12

doi:10.1093/mnras/stx058

After the fall: late-time spectroscopy of Type IIP supernovae

Jeffrey M. Silverman,[1⋆] Stephanie Pickett,[1] J. Craig Wheeler,[1] Alexei V. Filippenko,[2] József Vinkó,[1,3,4] G. H. Marion,[1,5] S. Bradley Cenko,[6,7] Ryan Chornock,[8] Kelsey I. Clubb,[2] Ryan J. Foley,[9] Melissa L. Graham,[2,10] Patrick L. Kelly,[2] Thomas Matheson[11] and Joseph C. Shields[8]

[1]*Department of Astronomy, University of Texas at Austin, Austin, TX 78712, USA*
[2]*Department of Astronomy, University of California, Berkeley, CA 94720-3411, USA*
[3]*Department of Optics and Quantum Electronics, University of Szeged, Dóm tér 9, 6720 Szeged, Hungary*
[4]*Konkoly Observatory, Research Centre for Astronomy and Earth Sciences, Hungarian Academy of Sciences, H-1121 Budapest, Hungary*
[5]*Harvard–Smithsonian Center for Astrophysics, Cambridge, MA 02138, USA*
[6]*Astrophysics Science Division, NASA Goddard Space Flight Center, Greenbelt, MD 20771, USA*
[7]*Joint Space-Science Institute, University of Maryland, College Park, MD 20742, USA*
[8]*Astrophysical Institute, Department of Physics and Astronomy, Ohio University, Athens, OH 45701, USA*
[9]*Department of Astronomy and Astrophysics, University of California, Santa Cruz, CA 95064, USA*
[10]*Department of Astronomy, University of Washington, Seattle, WA 98195-1580, USA*
[11]*National Optical Astronomy Observatory, Tucson, AZ 85719-4933, USA*

Accepted 2017 January 9. Received 2017 January 7; in original form 2016 October 23

ABSTRACT

Herein we analyse late-time (post-plateau; $103 < t < 1229$ d) optical spectra of low-redshift ($z < 0.016$), hydrogen-rich Type IIP supernovae (SNe IIP). Our newly constructed sample contains 91 nebular spectra of 38 SNe IIP, which is the largest data set of its kind ever analysed in one study, and many of the objects have complementary photometric data. The strongest and most robust result we find is that the luminosities of all spectral features (except those of helium) tend to be higher in objects with steeper late-time *V*-band decline rates. A steep late-time *V*-band slope likely arises from less efficient trapping of γ-rays and positrons, which could be caused by multidimensional effects such as clumping of the ejecta or asphericity of the explosion itself. Furthermore, if γ-rays and positrons can escape more easily, then so can photons via the observed emission lines, leading to more luminous spectral features. It is also shown that SNe IIP with larger progenitor stars have ejecta with a more physically extended oxygen layer that is well-mixed with the hydrogen layer. In addition, we find a subset of objects with evidence for asymmetric ^{56}Ni ejection, likely bipolar in shape. We also compare our observations to theoretical late-time spectral models of SNe IIP from two separate groups and find moderate-to-good agreement with both sets of models. Our SNe IIP spectra are consistent with models of 12–15 $M_\odot$ progenitor stars having relatively low metallicity ($Z \leq 0.01$).

Key words: methods: data analysis – techniques: spectroscopic – supernovae: general.

1 INTRODUCTION

Supernovae (SNe) provide a driving force for the chemical evolution of galaxies. They return material to the interstellar and intergalactic medium to be recycled and used in galaxy and star formation, and they produce some of the heaviest naturally occurring elements. Type II SNe (SNe II) result from the core collapse of a massive ($\gtrsim$8 $M_\odot$), hydrogen-rich star that has produced an iron core at the end of its life. The collapse sends a shock wave through the stellar material that disrupts the star. While stellar physics implies that typical SNe II could come from stars with masses up to 30 $M_\odot$, direct observations have yielded progenitors with masses of only 8–16 $M_\odot$; this is known as the red supergiant (RSG) problem (Smartt 2009). Possibly related to this mystery are the recent results that ∼19 per cent of massive, apparently single stars are in fact the result of a merger (de Mink et al. 2014) and that very few model stars over 20 $M_\odot$ explode as SNe IIP (e.g. Sukhbold et al. 2016).

SNe IIP are classified by their spectra, which are dominated in their photospheric phase by P Cygni profiles of H Balmer lines

⋆ E-mail: jsilverman@astro.as.utexas.edu

(e.g. Barbon, Ciatti & Rosino 1979; Filippenko 1997), and by their light curves, which have a 80–120 d plateau in the *R* and *I* bands (e.g. Faran et al. 2014a), from which the 'P' in SNe IIP comes. Their progenitor stars have a thick hydrogen envelope at the time of explosion, leading to this signature plateau in the light curve. The plateau phase ends once all of the hydrogen in the envelope has recombined. At this point SN IIP light curves show a rapid and steep drop (1–2 mag) before settling on to a linear decline in magnitude space (e.g. Faran et al. 2014a). The energy source at these late times is the deposition of γ-rays and positrons that come from the decay chain ^{56}Ni$\rightarrow$ ^{56}Co$\rightarrow$ ^{56}Fe, with most of the energy at these epochs coming from the second step of this process. This final phase in the life of a SN IIP is known as the radioactive tail (referring to the light-curve power source) or the nebular phase (referring to the spectra, which consist mostly of forbidden emission lines). We focus our efforts in this paper on the spectral observations at such late epochs.

About 40 per cent of all SNe in a volume-limited sample are Type IIP, making them the most common SN subtype (Li et al. 2011a). However, owing to their relative faintness at late times (-13 to -16 mag during the nebular phase; e.g. Faran et al. 2014a), it is difficult to study SNe IIP at these epochs. Of order two dozen previous studies of individual SNe IIP have included nebular spectra, while only a few published works have presented late-time SN IIP spectra of many objects at once (Turatto et al. 1993; Maguire et al. 2012; Spiro et al. 2014; Valenti et al. 2016). One of the largest and most comprehensive studies, Maguire et al. (2012) analysed 35 late-time spectra of nine SNe IIP. The sample studied herein consists of 91 nebular spectra of 38 SNe IIP, making it the largest data set of late-time SN IIP spectra ever analysed in a single study.

The data used in this work are summarized in Section 2, and our methods of nebular-phase determination and spectral-feature measurement, as well as our late-time photometry calculations, are described in Section 3. The analysis of our spectral measurements and their possible correlations with each other and other SN IIP observables can be found in Section 4, while a comparison of our spectral data to theoretical models is discussed in Section 5. We summarize our conclusions in Section 6.

2 DATA SET

2.1 Spectroscopy

To compile the late-time SN IIP spectral data set used herein, we first searched the UC Berkeley Filippenko Group's SuperNova Database (SNDB; Silverman et al. 2012a) for spectra obtained at least 80 d after discovery for all objects classified as SNe II or SNe IIP. After an initial visual inspection, we removed a handful of these spectra that showed strong H Balmer absorption features, indicating that the SN was not yet in the nebular phase. To augment this initial sample, from 2012 through 2014 we undertook a concerted observing campaign to obtain more late-time spectra of SNe IIP using multiple telescopes. This yielded an additional 20 spectra of nine SNe IIP, increasing our data set by $\sim$50 per cent.

About half of the spectra in the present sample were obtained using the Kast double spectrograph (Miller & Stone 1993) on the Shane 3 m telescope at Lick Observatory. The rest of the spectra were obtained with a variety of instruments and telescopes including the UV Schmidt spectrograph (Miller & Stone 1987) on the Shane 3 m telescope at Lick, the Low Resolution Imaging Spectrometer (LRIS; Oke et al. 1995) on the 10 m Keck telescope, the DEep Imaging Multi-Object Spectrograph (DEIMOS; Faber et al. 2003) also on the Keck telescope, the Marcario Low-Resolution Spectrograph (LRS; Hill et al. 1998) on the 9.2 m Hobby–Eberly Telescope (HET) at McDonald Observatory and the Wide-Field Spectrograph (WiFeS; Dopita et al. 2007, 2010) on the 2.3 m Advanced Technology Telescope at Siding Spring Observatory. All data were reduced using modern reduction methods; for more information regarding the data reduction, see Silverman et al. (2012a).

2.2 Photometry

Although this work concentrates on late-time spectroscopic observations of SNe IIP, complementary photometric data at both early and late times can be informative as well. For each object in our sample, we conducted a literature search for both early- and late-time photometric data. The early-time data allow us to constrain the dates of explosion and peak magnitude, while the late-time data can be compared to our spectra obtained at similar epochs.

For any object where no explosion date was found, we instead use the mid-point between the date of the last non-detection and the date of discovery. Our uncertainty on this date is then half the time between the date of discovery and the date of the last non-detection. If, however, the time between discovery and the last non-detection is $>$40 d, we instead define the explosion date as the date of discovery minus 20 d with an uncertainty of 20 d.

For SNe IIP, the magnitude at discovery is often reported in the IAU Circulars and ATels, as opposed to the peak magnitude or the magnitude on the plateau. We assume this 'discovery magnitude' is effectively equal to the plateau magnitude since most SNe IIP are discovered while in the plateau phase. This assumption is supported by the fact that in many cases observations of the same SN IIP reported soon after discovery and within a few days of each other yield consistent magnitudes. Sometimes *R*-band or unfiltered magnitudes are reported, but we ignore these in favour of the more often used *V*-band observations for the peak and plateau magnitudes.

2.3 Possible SN IIL contamination

When constructing a data set of SN IIP observations, one needs to be aware of possible contamination from SNe IIL, which have a 'linear' (in mag per day) decline in their light curves instead of a plateau (e.g. Barbon et al. 1979). The long-standing distinction between SNe IIP and SNe IIL has recently been scrutinized as progressively larger samples of well-sampled SN II light curves have become available. While some authors support this separation into two separate subclasses, others argue that there exists a continuum of light-curve decline rates (e.g. Arcavi et al. 2012; Anderson et al. 2014b; Faran et al. 2014a,b; Sanders et al. 2015). Using the findings of these previous studies, we searched the spectra and light curves of all objects in our sample for characteristics of SNe IIL. This led to a small number of objects being removed.[1]

2.4 The final sample

After further analysis to determine whether a spectrum was truly nebular (see Section 3.1 below for further details), our final sample consists of 91 late-time spectra of 38 SNe IIP, 21 of which have multiple spectra in the data set. More than half of the SNe IIP in our sample (21) have never been studied previously at late times and nearly three-quarters (66) of the spectra analysed herein are

[1] For example SNe 2000dc, 2001cy, 2001fa and 2008es.

previously unpublished. Most objects in the sample were discovered by 'targeted' surveys that favour more-luminous host galaxies, with 34 out of the 38 SNe IIP coming from NGC galaxies. Information regarding each object and spectrum in our data set can be found in Tables A1 and A2, respectively. Upon acceptance of this paper, all spectra herein will be available in electronic format in the SNDB,[2] WISeREP (the Weizmann Interactive Supernova data REPository; Yaron & Gal-Yam 2012)[3] and the Open Supernova Catalog Guillochon et al. 2017).[4]

The rest-frame ages, with respect to explosion, of the spectra studied in this work range from 103 to 1229 d. While ∼100 d may seem young for an SN IIP to be in its nebular phase, our analysis in Section 3.1 indicates that this can indeed happen. Owing to their relative faintness, it is unsurprising that our sample consists of only very low-redshift objects ($z \lesssim 0.016$) with a typical redshift of about 0.005. Fig. 1 shows a subset of the spectra in our final sample from a variety of epochs.

All 38 objects in our sample have published *V*-band absolute plateau magnitudes [$M_{\rm plat}(V)$], the typical value of which is about −16.3 mag, consistent with previous work on SN IIP light curves (e.g. Li et al. 2011a). For nearly two-thirds (25) of the SNe IIP in our data set, we measure *V*-band absolute peak magnitudes [$M_{\rm pk}(V)$] from their light curves, and the typical value of this is approximately −16.6 mag. Late-time photometry was acquired for a different subset of 25 objects in our sample, often in multiple bands. More on the late-time light curves can be found in Section 3.4.

3 METHODS

3.1 How old is old?

To arrive at our final sample of 91 spectra of 38 SNe IIP (Section 2.4), we first needed to determine whether each SN IIP spectrum was truly nebular, or, equivalently, whether the SN IIP was on the radioactive tail at the epoch when a given spectrum was obtained. Previous work on SN IIP observations often defined the late-time nebular phase to begin after some specified epoch, ranging from ∼150 to ∼250 d past explosion; for example, Elmhamdi, Chugai & Danziger (2003b) use 200 d after explosion. Therefore, our first step was to calculate the rest-frame age of each spectrum in our possible sample of 117 spectra of 55 SNe IIP (mostly from the SNDB) with respect to both date of explosion and date of discovery.

Upon visual inspection of these data, however, we found that some relatively young spectra (∼100 d after explosion) appeared to be nebular (i.e. nearly no continuum emission or absorption features). On the other hand, some spectra from significantly later epochs (∼170 d past explosion) were clearly not yet in the nebular phase. Thus, it seems unwise to define the beginning of the nebular phase of all SNe IIP to be a semi-arbitrarily chosen epoch. Different objects having different ages at which they transition to the nebular phase is unsurprising given that SNe IIP evolve at different rates and have a range of plateau lengths (e.g. Faran et al. 2014a). We therefore employ a less strict, but more robust, determination of whether a given spectrum is truly nebular.

As mentioned above, our first method of removing spectra that were obviously not nebular was a visual inspection and comparison to high signal-to-noise ratio (S/N) spectra of very late-time SN IIP data. We then investigated whether the Hα profiles, the strongest feature in SN IIP spectra, showed evidence for P Cygni absorption. If present, this would be an indicator of an optically thick photosphere that should not exist in nebular phases. Unfortunately, our spectra often did not have sufficiently high S/N to confidently determine whether Hα absorption was present.

Our main method of identifying nebular-phase spectra involved forbidden emission lines of oxygen ([O I] λλ6300, 6364) and calcium ([Ca II] λλ7291, 7324). At our desired late epochs, SN IIP spectra are dominated by emission features, including many forbidden lines, so the presence of [O I] and [Ca II] should be a reasonable indicator of being in the nebular phase. Using our spectral-feature fitting routine (see Section 3.2 for further details), we attempted to fit a double-Gaussian function to [O I] λλ6300, 6364 and [Ca II] λλ7291, 7324 in each spectrum. The feature was considered to be present if the peaks of the Gaussian fits were $>2\sigma$ above the locally determined continuum and two distinct peaks were detected. [O I] λλ6300, 6364 is often the stronger of the two features investigated, so this was the main indicator of whether a spectrum was nebular, though [Ca II] λλ7291, 7324 was also detected in many of the same spectra. This search for forbidden lines mostly supported our visual inspection and comparison to high-S/N nebular spectra mentioned above.

Furthermore, a majority of the SNe IIP we investigated had companion photometry (see Section 3.4 for more information). Using these data, we were able to photometrically determine when many of our objects entered the radioactive tail phase of their light curve. For each SN IIP with photometric data, the epochs at which our nebular spectra were obtained were all found to be after the object began its late-time photometric decline. Thus, our spectroscopic and photometric determinations of the beginning of the nebular phase are consistent. This analysis resulted in narrowing the sample from 117 spectra of 55 SNe IIP to our final sample of 91 spectra of 38 SNe IIP (Section 2.4).

3.2 Measuring nebular spectral features

The routine used in this work to measure the emission features in the late-time spectra of SNe IIP is similar to that used to measure emission features in SN Ia spectra also obtained from the SNDB (Silverman, Kong & Filippenko 2012b; Silverman, Ganeshalingam & Filippenko 2013). The method is described in detail in previous work, but here we give a brief summary of the procedure.

Each spectrum is first corrected for its host-galaxy recession velocity and Galactic reddening using the values listed in Table A1, then smoothed using a Savitzky–Golay smoothing filter (Savitzky & Golay 1964). Reddening from the host galaxies is not removed, as most of the objects in the current sample appear to be relatively unreddened by their hosts (i.e. they lack obvious narrow Na I D absorption in our spectra and in publicly available early-time spectra). The significant exception to this statement is SN 2002hh, which has ∼6 mag of extinction from its host (Welch et al. 2007).

Since all of the spectra in our sample are nebular, the continuum level should be nearly non-existent, so we do not include any background or continuum level in our fits. For each feature investigated, the end-points of the emission profile are chosen by hand and the data between these end-points are then fitted with a cubic spline as well as a (multi-)Gaussian function. The number of Gaussians used in each fit depends on the number of detectable, but blended, features in the profile.

It was found that the cubic spline fits captured the peaks of each spectral feature much more accurately than the Gaussian fits.

[2] http://heracles.astro.berkeley.edu/sndb
[3] http://www.weizmann.ac.il/astrophysics/wiserep
[4] https://sne.space

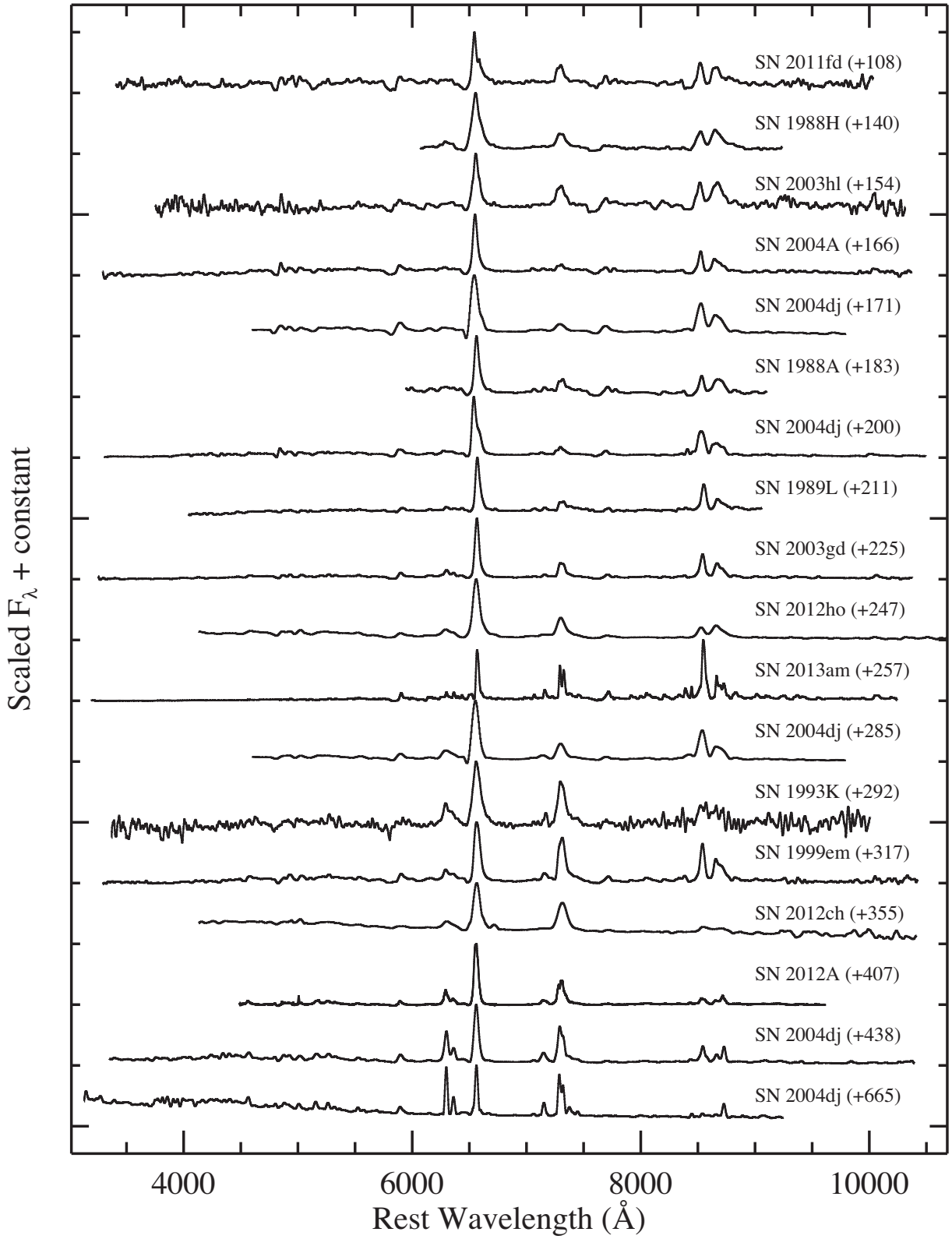

Figure 1. A subset of spectra from our final sample. Each spectrum is labelled with the object name and its rest-frame age relative to explosion. All data have been corrected for host-galaxy recession velocity and Galactic reddening using the values listed in Table A1.

Therefore, the peak of each spline fit was recorded as the peak flux (F_{pk}) and the wavelength at which this peak occurred was used to calculate the peak velocity (v_{pk}) using the relativistic Doppler equation. We also recorded the total flux (F_{tot}) in each spectral feature between the aforementioned end-points. When comparing multiple SNe, it is more instructive to use luminosities than observed fluxes, so we converted all of our measured F_{pk} and F_{tot} values to luminosities (L_{pk} and L_{tot}, respectively). This was accomplished by using the

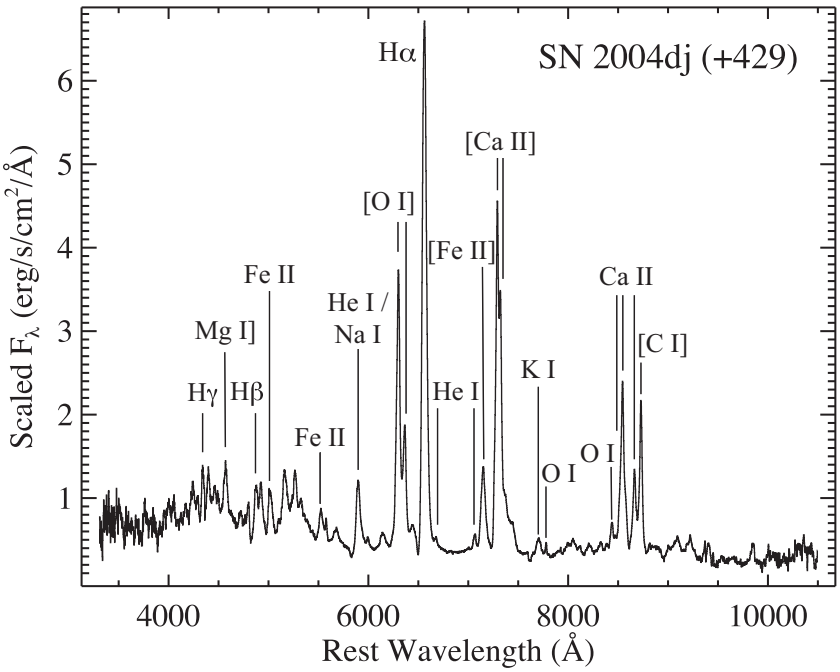

Figure 2. Spectrum of SN 2004dj from 429 d past explosion with all features investigated herein labelled. Also labelled is [C I] λ8727, which is clearly detected here, but rarely seen in most of the spectra in our sample. The spectrum has been corrected for its host-galaxy recession velocity and Galactic reddening using the values listed in Table A1.

mean metric distance to each SN IIP (from the NASA/IPAC Extragalactic Database – NED – and listed in Table A1) or, for the four objects without measured distances, using the redshift (also from NED and listed in Table A1) and $H_0 = 73$ km s^{-1} Mpc^{-1} (Riess et al. 2016). The values of $L_{\rm pk}$, $L_{\rm tot}$and $v_{\rm pk}$ for each spectral feature can be found in Tables A3–A8.

On the other hand, the Gaussian fits appeared to capture the widths of each spectral feature better than the spline fits. Thus, the Gaussian fits were used to determine the half-width at half-maximum intensity (HWHM; e.g. Maguire et al. 2012) and the half-width at zero intensity (HWZI) of each feature. As in Maguire et al. (2012), both of these parameters were corrected for the instrumental resolution of each spectrum (listed in Table A2) using an equation of the form

$$\mathrm{HWHM}_{\rm corrected} = \sqrt{\mathrm{HWHM}^2_{\rm measured} - \mathrm{HWHM}^2_{\rm resolution}}.$$

When comparing the measured values of the HWHM and HWZI, it was found that in the vast majority of cases HWZI ≈2.36 × HWHM as a result of our Gaussian fitting method. Thus, our HWZI measurements did not yield any new information and are ignored throughout the rest of this work. The HWHM for each spectral feature is listed in Tables A3–A8.

In addition to the cubic spline and Gaussian fits, each spectral feature was assigned a descriptor of its overall visual shape or appearance: single-peaked, multipeaked, flat-topped, or other. For extremely low-resolution spectra, the appearance of the spectral profile may not reflect the actual underlying profile, but Maguire et al. (2012) found that for resolutions of ∼14 Å or better one can distinguish the true shape of moderately strong emission features. Some of the spectra in our data set are near this cut-off, but the vast majority have higher resolution. Thus, we should be able to determine the intrinsic shape of the stronger emission profiles in our spectra. In short, we do not detect any flat-topped profiles, though we do find a handful of asymmetric, double-peaked profiles. Section 4.5 discusses the profile shapes in our sample in much greater detail.

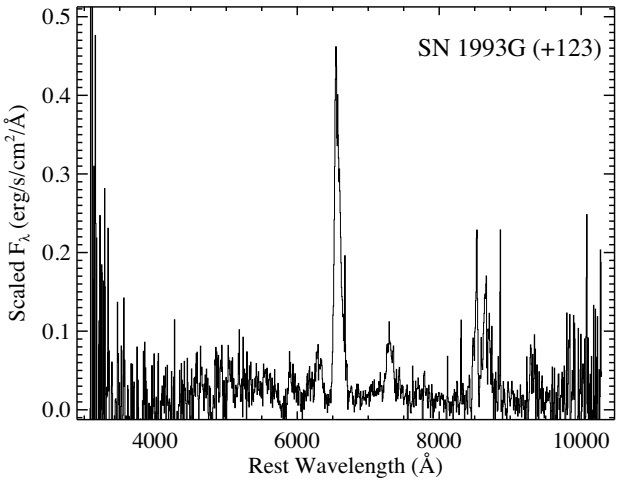

Figure 3. A relatively low-S/N spectrum of SN 1993G from 123 d past explosion. The spectrum has been corrected for its host-galaxy recession velocity and Galactic reddening using the values listed in Table A1.

Using the measurement technique described above, we attempt to fit numerous features in each of our SN IIP spectra. These consist of a combination of permitted and forbidden emission lines of hydrogen, helium, oxygen, magnesium, potassium, calcium and iron. Spectral features of other elements were considered, including carbon, sodium and nickel, but no or very few significant detections of these were found in our spectra. Fig. 2 shows one of our highest S/N spectra, an observation of SN 2004dj from 429 d after explosion; all features investigated herein are labelled. On the other hand, Fig. 3 shows one of our younger and lower S/N spectra, an observation of

SN 1993G from 123 d past explosion. Despite the significant noise in the spectrum, many emission features are readily identified.

3.3 Spectral features investigated

The most prominent feature in late-time spectra of SNe IIP is Hα and we clearly detect it in all 90 (out of 91 total) spectra that extend above 6500 Å. Significantly weaker, but still fit in most of our spectral sample, is Hβ, which occasionally appears blended with another feature near 4910 Å. The H γ line is even weaker, but still confidently detected in many of our spectra. The measured values from the cubic spline and Gaussian fits for all hydrogen lines can be found in Table A3.

At early times, relatively strong helium lines are common in optical spectra of SNe IIP, but in observations at later times they are often not as obvious (e.g. Filippenko 1997). Theoretical models of nebular spectra of SNe IIP, however, sometimes predict quite strong helium lines (e.g. Dessart et al. 2013). The strongest helium feature in the optical is He I λ5876, but the Na I D feature is almost coincident with it and is thought to dominate the emission profile at late times (Leonard et al. 2002b). Despite this, we detect two other helium lines (He I λ6678 and He I λ7065) in many of our spectra with profile shapes consistent with those of He I λ5876. The two redder lines are more prominent in the later epochs studied herein, with He I λ7065 appearing more often than He I λ6678. Given the consistency of these detections and the relatively low resolution of most of our data set, it seems likely that the often-detected emission near ∼5900 Å is dominated by He I λ5876. Detailed spectral modelling could be used to determine more precisely the relative contributions of He I λ5876 and Na I D to the emission profile in each spectrum, but this is beyond the scope of this paper. The measured values from the cubic spline and Gaussian fits for all helium features can be found in Table A4.

As mentioned in Section 3.1, the main criterion for including a spectrum in the current data set was the detection of the [O I] $\lambda\lambda$6300, 6364 doublet. Thus, it is not surprising that this feature was successfully fit in nearly all (89 out of 91) of our spectra. The two observations where it was not detected both show strong [Ca II] $\lambda\lambda$7291, 7324 emission, which led to their inclusion in our sample. Owing to the relatively low resolution of most of the spectra studied herein, the [O I] $\lambda\lambda$6300, 6364 doublet often appears somewhat blended, though two distinct peaks are always discernible. Because of this, we fit this doublet with a cubic spline as before, as well as with a double-Gaussian function. The highest peak of the doublet, used to calculate $F_{\rm pk}$ and $v_{\rm pk}$, was always the bluer component, and $F_{\rm tot}$ represents the total flux in the doublet (i.e. neither individual component). Since the Gaussian fits are used to calculate the HWHM and a double-Gaussian function is used for this doublet, an HWHM value is calculated for each component individually.

Two other oxygen lines are also investigated: O I λ7774 and O I λ8446. Both of these are actually triplets, but their components are so closely spaced that we cannot resolve them and thus fit each feature as a single spectral line. In addition, we find that O I λ7774 is usually blended with a doublet, K I $\lambda\lambda$7665, 7699, which we also fit as a single spectral feature (using the average wavelength of the two components, 7682 Å, as its rest wavelength). This resonance line has been observed in previously published late-time spectra of SNe IIP (Chornock et al. 2010) and theoretical models support this spectral identification (Dessart et al. 2013). Thus, we fit K I λ7682 and O I λ7774 as a doublet (as was done for [O I] $\lambda\lambda$6300, 6364). The peak of the K I emission was usually stronger than that of O I λ7774, so $F_{\rm pk}$ and $v_{\rm pk}$ were calculated with respect to this feature. The measured values from the cubic spline and Gaussian fits for all oxygen and potassium features can be found in Table A5.

Only one magnesium feature is confidently identified in many of our spectra: Mg I] λ4571. It is often relatively weak, especially in spectra from the earlier epochs in our sample, but we are still able to fit its profile in ∼60 per cent of our data set. The measured values from the cubic spline and Gaussian fits for this magnesium feature can be found in Table A6.

A secondary criterion for inclusion in our sample, as mentioned in Section 3.1, was the detection of the [Ca II] $\lambda\lambda$7291, 7324 doublet. This relatively strong feature was detected in almost all of our spectra, though it was sometimes blended on its blue side with other (possibly iron) emission lines. This feature was fit as a doublet, just like [O I] $\lambda\lambda$6300, 6364 discussed above, and $F_{\rm pk}$ and $v_{\rm pk}$ were calculated with respect to whichever of the two components was stronger. The bluer component had larger peak flux in about 3/4 of the spectra, but both components were often of very similar strength. We also identified the Ca II near-infrared (NIR) triplet $\lambda\lambda$8498, 8542, 8662 in most of the spectra in our sample. The bluer two components were often blended and we fit them as a doublet, with the 8542 Å feature being the stronger of the two; thus, $F_{\rm pk}$ and $v_{\rm pk}$ values were measured with respect to that line. The reddest feature in the triplet would sometimes be blended with weak, but noticeable, emission on its red wing (possibly from [C I] λ8727), but this very rarely affected the fitting of the Ca II profile. The measured values from the cubic spline and Gaussian fits for all calcium features can be found in Table A7.

There are numerous iron emission lines (both permitted and forbidden) from various multiplets that fall in the optical range, and this leads to severe blending of the vast majority of these features. In spite of this, we are able to securely and consistently identify three iron features. Emission from both Fe II λ5018 and Fe II λ5527 is detected in many of our spectra, though the lines are sometimes relatively weak and both occasionally have blended emission on their red wings. The strongly blended [Fe II] $\lambda\lambda$7155, 7172 doublet is also often seen in the spectra in our data set and usually appears relatively broad, but with only one distinct peak. Because of this, we fit this doublet with a single-Gaussian function (in addition to the cubic spline), and $v_{\rm pk}$ is calculated relative to 7155 Å, the stronger of the two blended components. We searched for other iron features, including [Fe II] λ5164, Fe II λ5169 and Fe II λ5270, but very few significant detections were made in our spectral sample. The measured values from the cubic spline and Gaussian fits for all iron features can be found in Table A8.

3.4 Late-time photometry

While our spectra are spectrophotometrically accurate in a relative sense, they may not be in an absolute sense owing to factors such as slit losses or cloud cover (see Silverman et al. 2012a, for further details). This limits our ability to measure reliable line fluxes (and luminosities), so a literature search was conducted in order to gather as much accompanying optical photometry as possible for the SNe IIP in our sample. This photometry also allows us to compare our late-time spectral measurements to photometric observables (as described in Section 4). The literature search yielded 77 optical (B, V, R, I and unfiltered) light curves of 25 objects. 15 of these light curves (representing seven SNe IIP) are previously unpublished, but the observations and data reduction pipeline are described by Ganeshalingam et al. (2010).

Using the 22 V-band light curves obtained, we measured the peak absolute magnitude [$M_{\rm pk}(V)$] and the median absolute magnitude

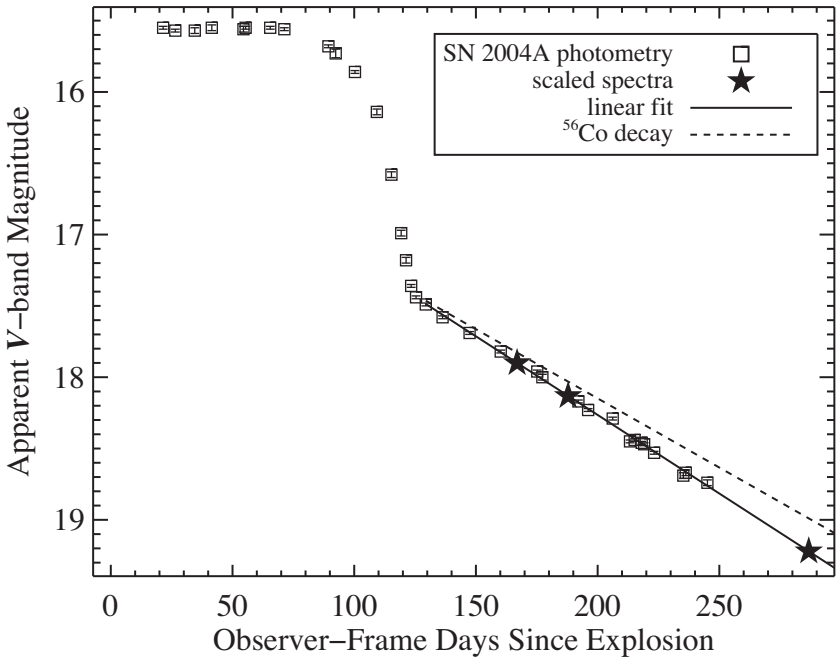

Figure 4. The *V*-band light curve of SN 2004A (open squares) from Gurugubelli et al. (2008). Overplotted is our linear fit to the late-time radioactive tail (solid line) and the decay rate of radioactive ^{56}Co (dashed line), which is 0.97 mag (100 d)$^{-1}$. The interpolated and extrapolated magnitudes for days on which we have spectra of SN 2004A are also plotted (filled stars).

during the plateau phase [$M_{\rm plat}(V)$], where the beginning and end of the plateau was chosen manually for each light curve. For objects with no available *V*-band photometry, $M_{\rm pk}(V)$ (when available) and $M_{\rm plat}(V)$ values from the literature were used. These values are listed in columns 8 and 9 of Table A1.

For each of the 77 light curves acquired, we also manually determined when the late-time radioactive tail began and then fit a line to those data points. For light curves with relatively sparse observations, it was sometimes difficult to determine the exact beginning of the radioactive tail, but oftentimes there was a clear separation in magnitude space between the plateau phase and the nebular phase. Fig. 4 presents an example light curve (the *V*-band data of SN 2004A from Gurugubelli et al. 2008, open squares) along with our linear fit to the late-time radioactive tail (solid line). Overplotted is the decay rate of radioactive ^{56}Co (dashed line), which is 0.97 mag (100 d)$^{-1}$. Lastly, we constructed pseudo-bolometric late-time light curves for all objects with photometry in at least three bands. This yielded 13 *BVRI* light curves, two *BVR* light curves and four *VRI* light curves.

The results of our linear fits to the radioactive tails of the light curves are displayed in Table A9. There, we list the number of photometric points used in each linear fit, the MJD range spanned by those points and the resulting slope of the linear fit and its uncertainty. The late-time rate of decline [in mag (100 d)$^{-1}$] of the SNe IIP is the main parameter in which we are interested, which is why the slopes are the only values from the linear fits listed in the table.

For a given SN IIP, the late-time slope is steeper as the observed bandpass gets redder, consistent with previous work (e.g. Dhungana et al. 2016). As is the case for individual SNe IIP, the mean and median slope for all objects in each band is largest in the reddest bands and smallest in the bluest bands, with *B*, *V* and *R* slower declining than ^{56}Co, and *I* declining slightly faster than ^{56}Co. However, given the relatively large standard deviations, the mean slope of each of the four bands is formally consistent with the ^{56}Co decay rate.

That being said, we find a large range of values for the late-time decline rates. Some of the measured slopes are much smaller (i.e. slower or shallower) than the ^{56}Co decay rate and some much larger (i.e. steeper- or faster-declining). While there are no objects with extremely steep slopes, there are three SNe IIP with slopes that are significantly shallower than the ^{56}Co decay rate (by at least a factor of 2): SNe 2005cs, 2006ov and 2013am. If our determination of the beginning of the late-time radioactive tail was incorrect, then we might have included data from the steep drop-off phase of the light curve. This would then lead to a slope that is much steeper than the ^{56}Co decay rate, and we have no examples of such slopes, so this supports our measurements of the beginning of the late-time tail. As for the three objects with extremely shallow slopes, they also exhibit some of the lowest HWHM values (i.e. narrowest emission lines) in our sample and tend to be low-luminosity SNe IIP, which confirms previous work on these objects (Pastorello et al. 2009; Spiro et al. 2014; Zhang et al. 2014).

As stated above, the initial impetus for gathering these photometric data was to place our spectra on an accurate absolute spectrophotometric scale. To do this, we follow a procedure similar to what was used for SNe Ia spectra by Silverman et al. (2012a). We first calculated synthetic magnitudes from each spectrum of all objects where we were able to obtain late-time photometry. We then interpolated or extrapolated our linear fits of the radioactive decay phase of the light curves in order to calculate the photometric magnitude of each object for days on which we have spectra. Table A10 lists these interpolated/extrapolated magnitudes and their uncertainties in each filter. The filled stars in Fig. 4 represent the *V*-band magnitude of SN 2004A for the three days on which we have spectra.

The synthetic magnitudes from a given spectrum were then compared to the photometric magnitudes (from our linear fits to the late-time light curves) on that same day in order to calculate a scalefactor for each band. The flux values of the spectrum were then multiplied by the median of these scalefactors in order to place

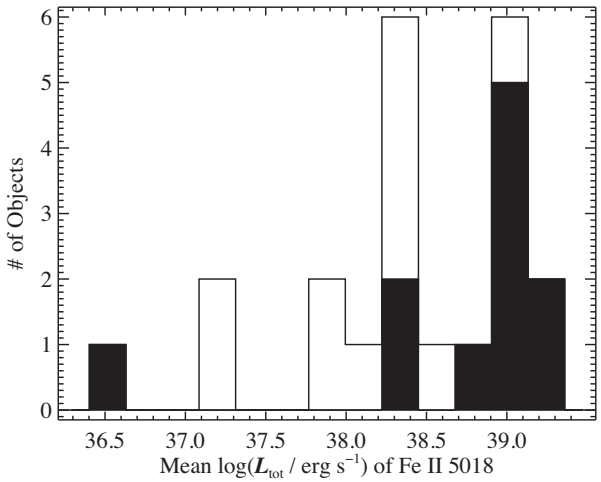

Figure 5. A histogram of the logarithm of the mean L_{tot} of Fe II λ5018 for each object. Filled regions represent objects with $M_{plat}(V)$ brighter than or equal to −16.3 mag; unfilled regions represent objects with $M_{plat}(V)$ fainter than −16.3 mag. The objects with more luminous plateaus tend to have larger values of L_{tot}, implying a direct connection between the energy in the SN ejecta during the plateau and at later times.

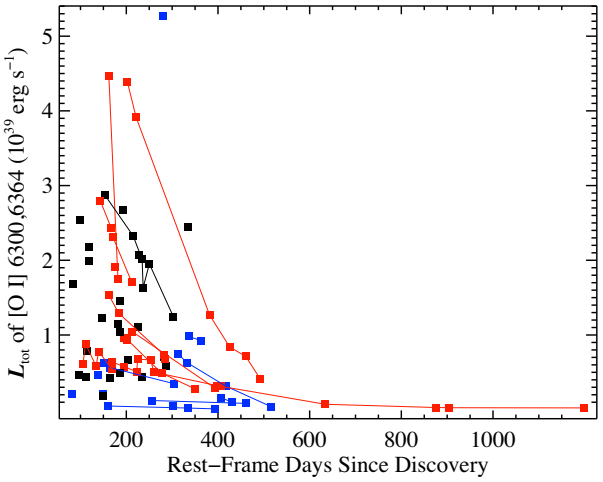

Figure 6. L_{tot} of [O I] λλ6300, 6364 versus time. Blue points are SNe IIP with slower/shallower late-time decline rates than the ^{56}Co decay rate; red points have faster/steeper decline rates; black points have no late-time V-band photometry. Squares represent profiles that are fit well by a double-Gaussian function (as this feature is a doublet); triangles represent more complex-shaped profiles (see Section 4.5 for more information). Filled points are spectra that have been scaled to contemporaneous photometry; open points have not been scaled. Spectra of the same object are connected with solid lines. Uncertainties on these L_{tot} measurements are typically smaller than the data points.

it on an accurate absolute flux scale. We investigated other methods of scaling the spectral flux values, namely using only the R-band scalefactor (since this bandpass contains Hα, the strongest feature in each spectrum) and using the mean of the scalefactors. In both cases, the results were similar to using the median of the scalefactors, and the median led to more consistent results for all spectra of a given SN IIP.

4 ANALYSIS

Using the measured values displayed in Tables A3–A8, we investigated the temporal evolution of each parameter for each spectral feature. We also compared our spectroscopic measurements to the photometric observables $M_{pk}(V)$, $M_{plat}(V)$ and the late-time slope in each optical photometric band (as described in Section 3.4).

4.1 Total luminosity (L_{tot}), peak luminosity (L_{pk})

In previous work, L_{tot} of the strongest emission features (i.e. Hα, [O I] λλ6300, 6364 and [Ca II] λλ7291, 7324) has been measured for a handful of individual SNe IIP. The values we measure for SN 1999em, for example, are very similar to those presented by Elmhamdi et al. (2003a) at similar epochs. On the other hand, our L_{tot} values of these features in SNe 2004et and 2012ec are somewhat lower that what was found by Sahu et al. (2006) and Jerkstrand et al. (2015), respectively.

The values of L_{pk} and L_{tot} for the bluer spectral features investigated in this work tend to be higher for SNe IIP with brighter $M_{plat}(V)$. A Kolmogorov–Smirnov (KS) test indicates that L_{pk} and L_{tot} values of these features for objects with brighter $M_{plat}(V)$ statistically differ from those of objects with fainter $M_{plat}(V)$ ($p = 0.001$–0.04 for L_{pk} and L_{tot} with various bright/faint cut-off values). The specific case of mean L_{tot} values of Fe II λ5018 for each object is shown in Fig. 5. The blue features that exhibit this difference are included in the B and V bands, and it has been seen previously that a more luminous plateau will lead to more luminous lines in these bands at late times (e.g. Valenti et al. 2016), matching what is found herein. According to theoretical models, $M_{plat}(V)$ tends to be brighter for larger progenitor radius and L_{tot} for all emission lines should be higher for larger ^{56}Ni production (e.g. Hamuy et al. 2003; Spiro et al. 2014; Pejcha & Prieto 2015; Valenti et al. 2016). Thus, taking our measured correlation a step further, one might expect a positive correlation between progenitor radius and mass of ^{56}Ni produced, but models show only a moderate connection between these physical parameters (Dessart & Hillier 2011).

One of the strongest and most robust correlations discovered in this work is that L_{tot} and L_{pk} values for all spectral features (except those of helium) tend to be higher for steeper late-time V-band slopes. According to a KS test, L_{pk} and L_{tot} values for objects with late-time V-band slopes steeper than the ^{56}Co decay rate are statistically different than those of objects with shallower V-band slopes ($p = 0.001$–0.05 for all non-helium features studied herein). The L_{tot} values for [O I] λλ6300, 6364 versus time are shown in Fig. 6. Objects with slower/shallower late-time decline rates than the ^{56}Co decay rate are shown in blue while objects with faster/steeper decline rates are shown in red; black points are objects with no late-time V-band photometry. Similar results are obtained when using the median late-time V-band slope as the cut-off instead of the ^{56}Co decay rate. The relatively few pseudo-bolometric late-time slopes in our sample show the same correlation, though slightly weaker, and there is some indication that the correlation also holds for late-time B-band slopes as well. On the other hand, there is no significant correlation between L_{pk} and L_{tot} values and late-time R- and I-band slopes.

To further investigate this correlation, we directly compared the late-time V-band slopes with the median measurements of L_{pk} and L_{tot} (as well as v_{pk} and HWHM) for each SN IIP. Consistent with our results discussed above, the V-band slopes were found to correlate with L_{pk} and L_{tot}, having Pearson correlation coefficients of ∼0.3–0.6, and L_{tot} showing slightly stronger correlations than L_{pk}. As a specific example, Fig. 7 shows that the median values of L_{tot} of Hα for the 21 SNe IIP with late-time V-band photometry are positively

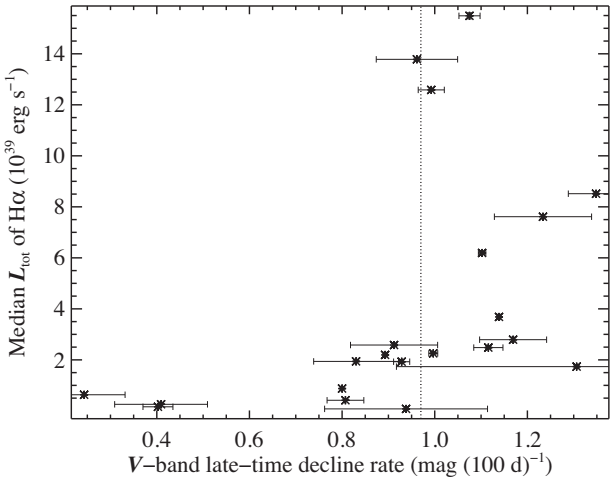

Figure 7. Median L_{tot} values of Hα versus V-band late-time decline rate. The vertical dotted line is the ^{56}Co decay rate; objects to the right of this line (i.e. ones with faster/steeper V-band decline rates) tend to have larger values of L_{tot}.

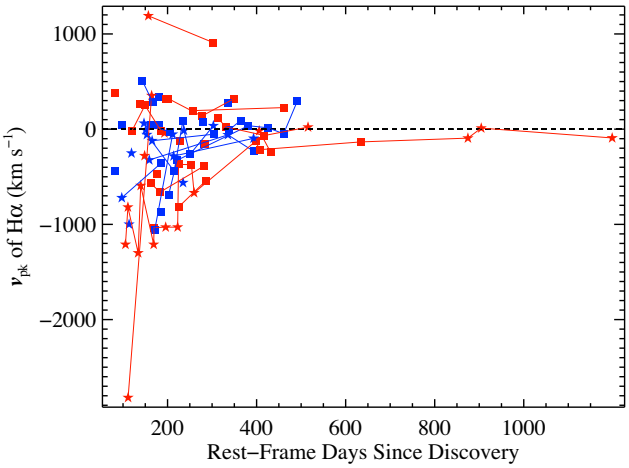

Figure 8. The v_{pk} of Hα versus time. Blue points are SNe IIP with $M_{plat}(V)$ brighter than or equal to −16.3 mag; red points have $M_{plat}(V)$ fainter than −16.3 mag. Squares represent profiles that are fit well by a single-Gaussian function; stars represent profiles whose shapes are more complex (see Section 4.5 for more information). Spectra of the same object are connected with solid lines. Uncertainties in these v_{pk} measurements are typically smaller than the data points. The horizontal dashed line is at zero velocity.

correlated with V-band slope. Also, objects with V-band decline rates that are faster/steeper than the ^{56}Co decay rate (i.e. to the right of the vertical dotted line in the figure) tend to have larger values of L_{tot}. These results are effectively unchanged if we instead use the minimum, maximum, earliest, latest or mean values of L_{tot} and L_{pk}. The median HWHM values also tend to be larger for objects with larger/steeper V-band slopes, especially in the strongest emission lines (i.e. Hα, [O I] λλ6300, 6364 and [Ca II] λλ7291, 7324); see Section 4.3 for more information.

A steep late-time V-band slope likely arises from less efficient trapping of γ-rays and positrons, but there are multiple explanations for this. A relatively small hydrogen envelope may not be sufficiently large or dense to trap γ-rays and positrons efficiently at late time (e.g. Anderson et al. 2014b). In addition, multidimensional effects such as clumping of the ejecta or asphericity of the explosion itself may lead to inefficient trapping (Dessart et al. 2011). Furthermore, at least in SNe Ia, the deposition of γ-rays and positrons is likely dominated by the strength and distribution of magnetic fields (e.g. Penney & Hoeflich 2014). Another explanation for steep late-time decline rates, especially in the bluer optical bands, is the formation of dust that will reprocess blue light into red/infrared light (Sahu et al. 2006). This explanation seems unlikely for the spectra studied herein, however, since significant dust formation is thought to begin more than ∼400 d after explosion, which is significantly older than the majority of our observations. The dust-formation explanation is also likely ruled out by our analysis of the observed profile shapes in Section 4.5.

On the other hand, the three objects towards the left-hand side of Fig. 7 (SNe 2005cs, 2006ov and 2013am) have extremely shallow late-time slopes as well as some of the narrowest emission lines in our sample, and they also tend to be low-luminosity SNe IIP (see also Pastorello et al. 2009; Spiro et al. 2014; Zhang et al. 2014). Shallow late-time slopes have sometimes been attributed to the presence of light echoes (e.g. Otsuka et al. 2012), but this effect also usually appears much later than nearly all of the epochs investigated herein. Instead, there must be some other energy source in addition to the decay of ^{56}Co. Perhaps, larger amounts of other radioactive elements are produced in these objects as compared to the rest of the sample, or additional radiation is being generated in the warmer inner ejecta and propagating into the optically thin and cooler external layers (Utrobin, Chugai & Pastorello 2007). Extra energy could also come from the SN IIP ejecta interacting with circumstellar material, but we find no spectral signatures of such interaction in our data set (see Section 4.5).

Regardless of the root physical cause of the steeper late-time V-band decline rates, if γ-rays and positrons can more easily leak out of the SN ejecta, then so can optical photons via the observed emission lines. This would naturally lead to more luminous spectral features, as we observe. Furthermore, models have shown that more massive progenitors have stronger late-time emission features *and* smaller hydrogen envelopes, which would allow more γ-ray and positron leakage at late times, and thus a steeper light-curve decline (Anderson et al. 2014b).

4.2 Peak velocity (v_{pk})

Our measurements of v_{pk} match well with those in previous work, including, for example, SN 2004et (Jerkstrand et al. 2012). Anderson et al. (2014a) found that v_{pk} of Hα for a sample of SNe IIP was typically in the range −1000 to +500 km s^{-1}, with most of the features blueshifted and approaching zero velocity at later epochs. This is consistent with what is found herein; compare our Fig. 8 to their fig. 4. Opposite to L_{tot} and L_{pk} discussed above, v_{pk} of Hα is found to be anticorrelated with late-time V-band slope. That is, objects with slower/shallower slopes tend to have larger values of Hα v_{pk}. Anderson et al. (2014a), using measurements from earlier in the life of SNe IIP (specifically, the V-band decline rate during the plateau phase and the v_{pk} of Hα measured at $t = 30$ d past explosion), find a similar anticorrelation. Note that, we find no significant correlation or anticorrelation between the Hα v_{pk} value and $M_{pk}(V)$, $M_{plat}(V)$or the late-time decline rates in the B, R, I or pseudo-bolometric light curves.

4.3 Half-width at half-maximum intensity

Our measurements indicate that the HWHM of the spectral features investigated generally decrease with time, with a rapid decline at

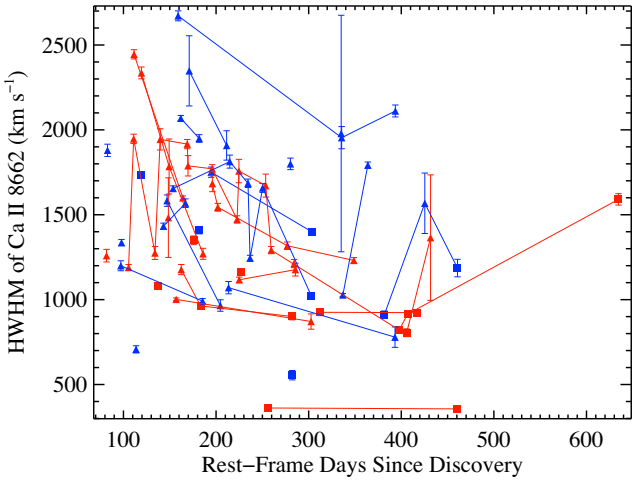

Figure 9. The HWHM of Ca II λ8662 versus time. Blue points are SNe IIP with $M_{\rm plat}(v)$ brighter than or equal to −16.3 mag; red points have $M_{\rm plat}(V)$ fainter than −16.3 mag. Squares represent profiles that are fit well by a single-Gaussian function; triangles represent profiles whose shapes are more complex (see Section 4.5 for more information). Spectra of the same object are connected with solid lines.

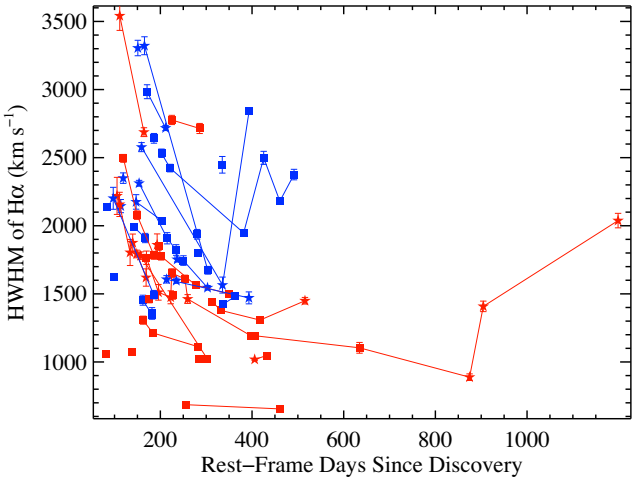

Figure 10. The HWHM of Hα versus time. Blue points are SNe IIP with $M_{\rm plat}(V)$ brighter than or equal to −16.3 mag; red points have $M_{\rm plat}(V)$ fainter than −16.3 mag. Squares represent profiles that are fit well by a single-Gaussian function; stars represent profiles whose shapes are more complex (see Section 4.5 for more information). Spectra of the same object are connected with solid lines.

ages earlier than ∼300 d past explosion and a shallower decline thereafter. This is similar to the results of Maguire et al. (2012), who found relatively flat temporal evolution (for $300 < t < 600$ d past explosion) of the HWHM of Hα, [O I] λ6300, [Ca II] λ7291 and [Fe II] λ7155. The actual range of HWHM values that we measure for these features is also mostly consistent with that of Maguire et al. (2012).

For a few objects, including SN 2004dj with spectra having $t > 600$ d past explosion, the HWHM increases at later times. This is primarily caused by the spectral features getting weaker and broader with time, which leads to smaller $L_{\rm pk}$ values, but larger HWHM values. This evolution is consistent with the findings of Milisavljevic et al. (2012), even though most of their data are from much later epochs. Their work finds a similar amount of decrease in $L_{\rm pk}$ of Hα to what is found in the current study during the first 1–2 yr after explosion. Furthermore, spectra from Milisavljevic et al. (2012), as well as Blair et al. (2015), show Hα and [O I] λλ6300, 6364 profiles that are similar in appearance to those seen in our oldest spectra. These works attribute this evolution of the spectral profiles of SNe IIP at late times to the SNe beginning their transition to the remnant phase.

The typical HWHM we find for the elements that originate from the helium core of the progenitor star (oxygen, calcium and helium; e.g. Dessart & Hillier 2011) are ∼1000–1200 km s^{-1}, except for Ca II λ8662, which is closer to ∼1500 km s^{-1} (see Fig. 9). These values are all smaller than what was predicted by Dessart & Hillier (2011), but they do note that Ca II λ8662 should have larger HWHM values than the rest of the oxygen, calcium and helium lines since it is formed from both the helium core and hydrogen envelope. The lowest minimum HWHM values are measured for [Ca II] and Ca II (∼500–800 km s^{-1}), which implies that they are mixed down to the lowest velocities and innermost radii of the ejecta. The next-lowest minimum HWHM values are found in [O I], O I and He I (900–1000 km s^{-1}), followed by the hydrogen Balmer lines, which have the largest HWHM (with most >1300 km s^{-1}; see Fig. 10 and compare to fig. 5 of Maguire et al. 2012).

Our measurements indicate that the HWHM of Hα and all oxygen spectral features (but not other lines in the Balmer series or calcium features) are larger in SNe IIP with brighter $M_{\rm pk}(V)$ and $M_{\rm plat}(V)$ (see Fig. 10). A KS test indicates the HWHM values of these features for objects with $M_{\rm pk}(V)$ brighter than −16.6 mag [or $M_{\rm plat}(V)$ brighter than −16.3 mag] are statistically different than fainter objects ($p = 0.01$–0.03). Spiro et al. (2014) came to a similar conclusion at slightly earlier epochs, as they found broader spectral-feature profiles at the end of the plateau phase in objects with brighter plateaus.

As mentioned above, the median HWHM values are also found to be larger for objects with larger/steeper V-band slopes, especially in the strongest emission lines (i.e. Hα, [O I] λλ6300, 6364 and [Ca II] λλ7291, 7324). Thus, broad emission lines of [O I] and Hα indicate luminous light-curve plateaus and steep V-band decline rates, which is seen in the models of Dessart et al. (2013). Furthermore, theoretical models indicate that for a given explosion energy, large HWHM values of [O I] features come from a large progenitor mass and radius (Dessart, Livne & Waldman 2010; Dessart & Hillier 2011), while the HWHM of Hα increases with greater mixing within the SN ejecta (Dessart et al. 2013). Therefore, SNe IIP with broader [O I] and Hα emission lines are also likely to have larger progenitors and ejecta with more thoroughly mixed hydrogen and oxygen layers.

4.4 Flux ratios

In addition to individual spectral features discussed previously, we follow what has been done in other late-time SN IIP studies and also investigate some flux ratios of pairs of emission lines. We calculated the Balmer decrement (i.e. the ratio of Hα to Hβ, which were all found to be >3), as well as the ratio between [O I] λλ6300, 6364 and Hβ, but no significant correlations were found with any other observables.

The red-to-blue peak flux ratio of [O I] λλ6300, 6364, defined as $F_{\rm pk}$ of [O I] λ6364 divided by $F_{\rm pk}$ of [O I] λ6300 (e.g. Chugai 1992; Maguire et al. 2012), is calculated for 89 of our 91 spectra. As seen in the top-left panel of Fig. 11, this ratio mostly decreases from ∼1.0 (at $t \approx 100$ d) to ∼0.4–0.5 (at $200 \lesssim t \lesssim 500$ d). There is possibly an increase at even later epochs, but there is only one object (SN

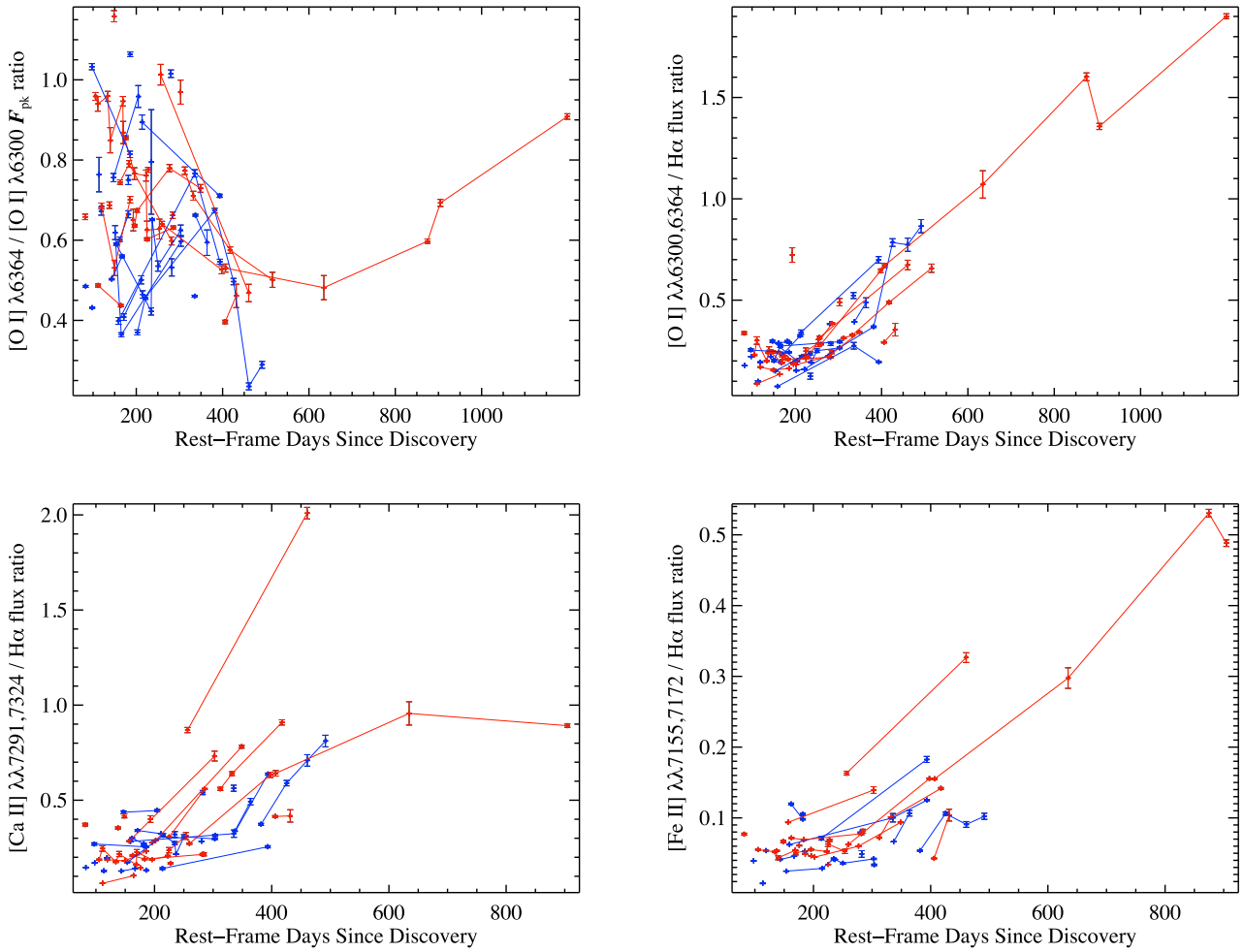

Figure 11. Various flux ratios versus time: the [O I] peak flux ratio (top left), the [O I] λλ6300, 6364 doublet to Hα ratio (top right), the [Ca II] λλ7291, 7324 doublet to Hα ratio (bottom left) and the [Fe II] λλ7155, 7172 doublet to Hα ratio (bottom right). Blue points are SNe IIP with $M_{plat}(V)$ brighter than or equal to −16.3 mag; red points have $M_{plat}(V)$ fainter than −16.3 mag. Spectra of the same object are connected with solid lines.

2004dj) in our sample at such late times. In the optically thick regime this ratio should approach 1, while in the optically thin regime it should approach 1/3. Our measured values are mostly within these limits, and deviations >1 could be caused by the blending of nearby spectral features or electron scattering and clumpiness (Chugai 1992). Fig. 12 of Maguire et al. (2012) displays less scatter than our larger sample, but we both find a relatively smooth decrease in the ratio with time, especially for $t > 200$ d. The [O I] peak flux ratio was also calculated from observations and modelled by Spyromilio & Pinto (1991). The ratios they measure are similar to the values we find, and nearly all of our measurements appear to be fit by their models if one sets the velocity extent of the O-emitting region to 2000–3000 km s^{-1}, the temperature to ∼2000 K, the filling factor to 0.01–0.1 and the mass of O I to ∼1 $M_{\odot}$.

The ratio of F_{tot} of the [O I] λλ6300, 6364 doublet to F_{tot} of Hα was calculated and is shown in the top-right panel of Fig. 11. The ratio is relatively constant in time for $t < 200$ d and then increases (mostly) monotonically thereafter. In the bottom-left and bottom-right panels of Fig. 11, we present the ratio of the [Ca II] λλ7291, 7324 doublet to Hα and the ratio of [Fe II] λλ7155, 7172 to Hα, respectively. Much like the [O I] λλ6300, 6364 to Hα ratio, these both show relatively constant values with time for $t < 200$–250 d and then an increase at later epochs. The results for all of these ratios are very similar to those of Maguire et al. (2012), although they do not present data as early as in our sample and thus do not observe the epoch of nearly constant ratios at $t < 200$–250 d.

For completeness, and to compare with Maguire et al. (2012), we also computed the [Ca II] λλ7291, 7324 to [O I] λλ6300, 6364 ratio, the [Fe II] λλ7155, 7172 to [O I] λλ6300, 6364 ratio and the [Fe II] λλ7155, 7172 to [Ca II] λλ7291, 7324 ratio. All of these ratios showed large scatter versus time. Furthermore, they were mostly consistent with the range of measured values and general temporal behaviour seen by Maguire et al. (2012).

4.5 Spectral-feature shapes

As mentioned in Section 3.2, and denoted by the shapes of the data points in some of the previous figures, each spectral feature in our sample was assigned a descriptor of its overall visual shape or appearance. As most of our spectra have resolution better than 14 Å (∼650 km s^{-1}), the observed shapes should reflect the intrinsic shapes of moderately strong emission features (Maguire et al. 2012). Consistent with the work of Maguire et al. (2012), we found examples of single-peaked profiles and multipeaked profiles, but no evidence was found for flat-topped profiles, which would indicate ejecta layers that are not well-mixed. Of the profiles that were marked as multipeaked, most appeared to be double-peaked and

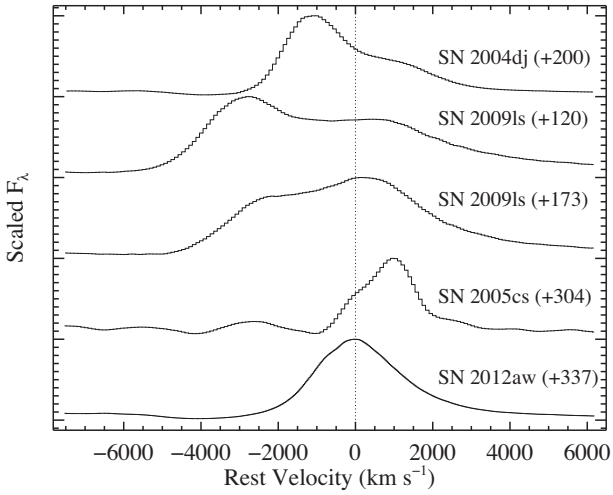

Figure 12. Various Hα profiles. Each spectrum is labelled with its object name and rest-frame age relative to explosion and has been corrected for its host-galaxy recession velocity and Galactic reddening using the values listed in Table A1. The dotted vertical line is the zero velocity of Hα. The top two spectra show a blueshifted peak with a red shoulder, the next two spectra exhibit a redshifted peak with a blue shoulder, and the bottom spectrum has a single-peaked, mostly symmetric profile that peaks at the rest wavelength of Hα.

ones that had more than two distinct peaks were found to be the result of other emission features blended with the lines of interest.

Of the double-peaked profiles, some were caused by noise in the data, some by nearby blended emission lines (as in the multipeaked profiles), and some by narrow emission from the host galaxy of the SN IIP. No narrow emission lines from the SNe themselves were detected in any of our spectra. This type of emission profile could arise from late-time interaction with circumstellar media in the same manner as the so-called SNe IIn-P (e.g. Mauerhan et al. 2013). Removing these noisy, blended or contaminated spectra left only profiles that are double-peaked owing to two separate emission peaks of the same spectral feature in the SN ejecta.

Since Hα is the strongest emission line in the spectra of SNe IIP, it has the highest S/N and thus two distinct peaks can be seen most easily in this feature. We find eight SNe IIP with Hα profiles that have blueshifted peaks with a red shoulder (i.e. a second, weaker, redshifted peak). One of these objects, SN 2009ls, evolves to the opposite profile (i.e. a redshifted peak with a blue shoulder) between our two spectra of that object (120 d past explosion to 173 d past explosion). Three other SNe IIP in our sample exhibit a redshifted peak with a blue shoulder. All of the spectra that show these double-peaked Hα profiles are younger than $\sim$300 d past explosion. Both Hα profiles of SN 2009ls, as well as two other double-peaked Hα profiles and a single-peaked Hα profile (for comparison), are plotted in Fig. 12.

Asymmetric, multipeaked, or otherwise complex profiles were searched for in other emission lines, but they are harder to distinguish than in Hα owing to either their relatively lower flux or blending with other nearby features, or both. The [O I] $\lambda\lambda$6300, 6364, [Ca II] $\lambda\lambda$7291, 7324 and [Fe II] $\lambda\lambda$7155, 7172 doublets are all relatively strong spectral features discussed above, but since they are all doublets it is difficult to identify multiple, distinct emission peaks. No convincing multipeaked profiles were observed in the [Ca II] $\lambda\lambda$7291, 7324 or [Fe II] $\lambda\lambda$7155, 7172 features. On the other hand, seven SNe IIP showed tentative evidence of blueshifted peaks and red shoulders in their [O I] $\lambda\lambda$6300, 6364 profiles.

Of the objects with asymmetric Hα profiles, two (SNe 1988H and 2004dj) showed the same profile shape in [O I] $\lambda\lambda$6300, 6364. Furthermore, SNe IIP with blueshifted Hα peaks tended to have the most negative peak velocities of [O I] $\lambda\lambda$6300, 6364 and [Fe II] $\lambda\lambda$7155, 7172. This is indicative of a blueshifted peak in these features, possibly with a redshifted shoulder, but the asymmetric profile is too weak or too blended to be visually confirmed. Other than this, all objects with asymmetric profiles appear to have typical spectral and photometric observables. This result – that emission lines of different ions in the same spectrum tend to have the same overall profile shape – is consistent with previous work (Maguire et al. 2012).

At very late times (i.e. $t \gtrsim 400$ d), asymmetric or double-peaked profiles in SN IIP spectra are sometimes attributed to the presence of dust (e.g. Jerkstrand et al. 2015), but all of the spectra in the current sample that show these sorts of profiles are younger than this. At the epochs in question ($100 \lesssim t \lesssim 300$ d), Jerkstrand et al. (2015) state that dust will only have a 'small effect' on the optical/NIR spectra of SNe IIP. Instead, it has been proposed that asymmetric ^{56}Ni ejection, possibly bipolar in shape, is responsible for the asymmetric profiles seen at these epochs (e.g. Chugai et al. 2005). In fact, the strange case of the Hα profiles of SN 2009ls mentioned above could be explained by a bipolar ^{56}Ni distribution with a time-variable covering fraction. In this situation, the observed area covered by the ^{56}Ni changes with time such that the approaching lobe of ^{56}Ni is observed first (giving rise to the blueshifted Hα peak seen in the first spectrum); then, at later times, emission from that lobe weakens as the receding lobe of ^{56}Ni becomes visible (leading to the redshifted Hα peak in the second spectrum). It is not obvious, however, how the idea of bipolar ^{56}Ni ejection can explain the prevalence, by a factor of $\sim$2, of blueshifted peaks over redshifted peaks seen in our data.

For most of the objects where we detect asymmetric Hα profiles, previous work has not specifically commented on the profile shape. This study, however, is mostly consistent with examples in the literature that have investigated profile shapes in late-time SNe IIP spectra. SN 1988H exhibited many asymmetric profiles at $\sim$400 d past explosion (Turatto et al. 1993), which matches our detection of such profiles in multiple emission lines at $t = 140$ d past explosion. We find that the well-studied SN 2004dj has a blueshifted Hα peak with a red shoulder in spectra at $136 < t < 438$ d after explosion, which was also observed by Chugai et al. (2005) and Meikle et al. (2011). Furthermore, asymmetry in the ejecta has also been observed via spectropolarimetry of SN 2004dj (Leonard et al. 2006), consistent with bipolar ^{56}Ni ejection. SN 2005cs is one of the few objects that shows the opposite Hα profile (i.e. a redshifted peak with a blue shoulder), and it is seen in both spectra of this object in our sample ($t = 158$ and 304 d past explosion). Pastorello et al. (2006) detect the same Hα profile shape in spectra obtained at similar epochs.

Blueshifted peaks with red shoulders are possibly seen in the Hα profiles of spectra of SN 1999em at $200 < t < 300$ d after explosion (Elmhamdi et al. 2003a), but we find no compelling evidence of an asymmetric Hα profile in our spectra from slightly later epochs ($t = 317$ and 337 d past explosion). At $t > 300$ d past explosion, dust was likely present in SN 2004et (Kotak et al. 2009), and there are indications of a blueshifted Hα peak (Sahu et al. 2006); however, we do not detect an asymmetric Hα profile in our spectra of this object at $202 < t < 355$ d past explosion.

5 COMPARISONS TO THEORETICAL MODELS

In the following subsections, we compare our late-time spectral data of SNe IIP to two recent studies that presented sets of theoretical spectra: Dessart et al. (2013) and Jerkstrand et al. (2014). In general, the vast majority of our spectra match only moderately well to models from the former, but match quite well to models from the latter.

5.1 Dessart et al. (2013) models

Dessart et al. (2013) model 15 $M_{\odot}$ stars as the progenitors of SNe IIP. Adjustable parameters in their models include the mixing length, the amount of convective overshoot, the amount of stellar rotation and the progenitor metallicity. They produce and then evolve many pre-SN progenitors and then model the SN IIP ejecta from early to late times. As pointed out by Dessart et al. (2013), one of the shortcomings of their model spectra is that He I lines are overproduced (especially the 7065 Å line) relative to the observations to which they compare. In this work, we clearly detect He I λ7065 emission in about half of our late-time spectra, although it is usually weaker than what is predicted by the models of Dessart et al. (2013).

We compared every spectrum in our sample to six models run by Dessart et al. (2013), which varied progenitor metallicity (Z) and mixing length parameter (α). Late-time spectra at a variety of epochs were produced for each model, so the spectra in our sample were compared to each model spectrum at the closest epoch. Using visual inspection and a basic cross-correlation algorithm, the model that was most consistent with each spectrum was chosen. Then the model that best fit the majority of the spectra of a given object was deemed the model most consistent with that SN IIP.

Usually, no model fits an individual spectrum very well. Aside from the models showing too much helium emission, as mentioned above, they also sometimes incorrectly predict the relative peak fluxes of the strongest lines (i.e. hydrogen, oxygen and calcium). Furthermore, there was often more than one model that matched an individual object relatively well. Specifically, models where the only difference was metallicity and the values of Z were in the middle of the range tested (i.e. 0.008–0.020) looked very similar. Our final analysis indicates that five objects do not match any model reasonably well, while half of the SNe IIP in our data set are consistent with models with either $Z = 0.002$ or $\alpha = 3$. In addition, it appears that most of the objects are consistent with models with relatively low metallicity ($Z \leq 0.01$). Of the objects in our sample that have published metallicity measurements at the SN site, we find the metallicities to be in the range $0.003 \lesssim Z \lesssim 0.014$, with a typical value of $\sim$0.011 (e.g. Anderson et al. 2016; Taddia et al. 2016), for $Z_{\odot} = 0.0134$ (Asplund et al. 2009). Thus, SNe IIP do tend to be found in low (i.e. subsolar) metallicity regions, but perhaps not quite *as* low as the Dessart et al. (2013) models would suggest.

Fig. 13 shows SN 2004et (top row) and SN 2012aw (bottom row) overplotted with models from Dessart et al. (2013). SN 2004et is consistent with their 'z8m3' model ($Z = 0.008$ and $\alpha = 1.6$; top-left panel), even though Hα, oxygen and calcium emission features are slightly weaker in the model while the helium features are too strong. A less good match is found with their 'z4m2' model ($Z = 0.040$ and $\alpha = 1.6$) and is shown in the top-right panel of the figure. SN 2012aw resembles the 'z4m2' model (in the bottom-left panel of Fig. 13) of Dessart et al. (2013), which comes from a star with $Z = 0.040$ and $\alpha = 1.6$, and is one of the few objects that is consistent with a higher value of Z. Like the comparison to SN 2004et, this model spectrum has Hα, oxygen and calcium features that are a little too weak and helium features that are too strong. Their 'z2m3' model ($Z = 0.002$ and $\alpha = 1.6$) is less consistent with SN 2012aw and is shown in the bottom-right panel.

5.2 Jerkstrand et al. (2014) models

Jerkstrand et al. (2014) present late-time spectra of SN 2012aw, along with theoretical spectra derived from stellar evolution and explosion models. They produce late-time spectra of a variety of models with a nearly constant explosion energy that we can compare to all of the objects in our sample. In general, the model spectra of Jerkstrand et al. (2014) show stronger [O I] $\lambda\lambda$6300, 6364 emission for larger progenitor masses while all emission lines tend to weaken with time.

Using the same procedure outlined in Section 5.1 above, we compared every spectrum in our sample to the model spectrum at the closest epoch from each of the four progenitor masses (12, 15, 19 and 25 $M_{\odot}$) modelled by Jerkstrand et al. (2014). The model that was most consistent with each object was again determined by which model best fits the majority of the spectra of each object. Even more so than with the models of Dessart et al. (2013), there were many cases where two models from Jerkstrand et al. (2014) resembled the same spectrum or object equally well. Thus, we caution against making precise interpretations of progenitor mass from these model comparisons.

While the model spectra of Jerkstrand et al. (2014) often match quite well to our data, there are some issues. For example, as pointed out by Jerkstrand et al. (2014), their models overproduce Hα emission and underproduce the Ca II NIR triplet, which we confirm in many of the comparisons to our spectral sample. Furthermore, their models sometimes overproduce helium emission, like the models of Dessart et al. (2013) discussed above, and occasionally incorrectly predict the strength of the [Ca II] $\lambda\lambda$7291, 7324 doublet.

SNe 2005cs and 2013am, as mentioned in Section 3.4, have some of the lowest HWHM values (i.e. narrowest emission lines) in our sample and are not fit very well by any of the Jerkstrand et al. (2014) models (see the upper-left panel in Fig. 14). We do note, however, that a different suite of models with narrower emission lines was produced by the same group and presented by Maguire et al. (2012); they match SN 2005cs, as well as other narrow-lined SNe IIP, very well.

Using the Jerkstrand et al. (2014) models, we find that most of the objects in our sample (30) resemble their 12 $M_{\odot}$ model. The other eight objects in our sample matched slightly better with their 15 $M_{\odot}$ model. There were a few individual spectra that were consistent with 19 and 25 $M_{\odot}$ models, but they usually also resembled the 15 $M_{\odot}$ model. Therefore, the comparisons of our observations to the models of Jerkstrand et al. (2014) appear to support the RSG problem (Smartt 2009) in that our SNe IIP tend to prefer progenitors with masses smaller than $\sim$16 $M_{\odot}$. A literature search yielded observed progenitor masses for 13 of the objects in our sample and all of them are consistent with our findings, having masses in the range 8–18 $M_{\odot}$ (Smartt 2009; Van Dyk et al. 2012; Maund et al. 2013; Tomasella et al. 2013; Maund, Reilly & Mattila 2014; Bose et al. 2015). This result has also been found by Jerkstrand et al. (2015) using a sample of 12 SNe IIP. We caution, however, that this result is complicated by the fact that de Mink et al. (2014) find that $\sim$19 per cent of apparently single, massive stars actually come from mergers. Observational signatures of such systems may be found in future analyses of late-time SN IIP spectra, but few predictions currently exist.

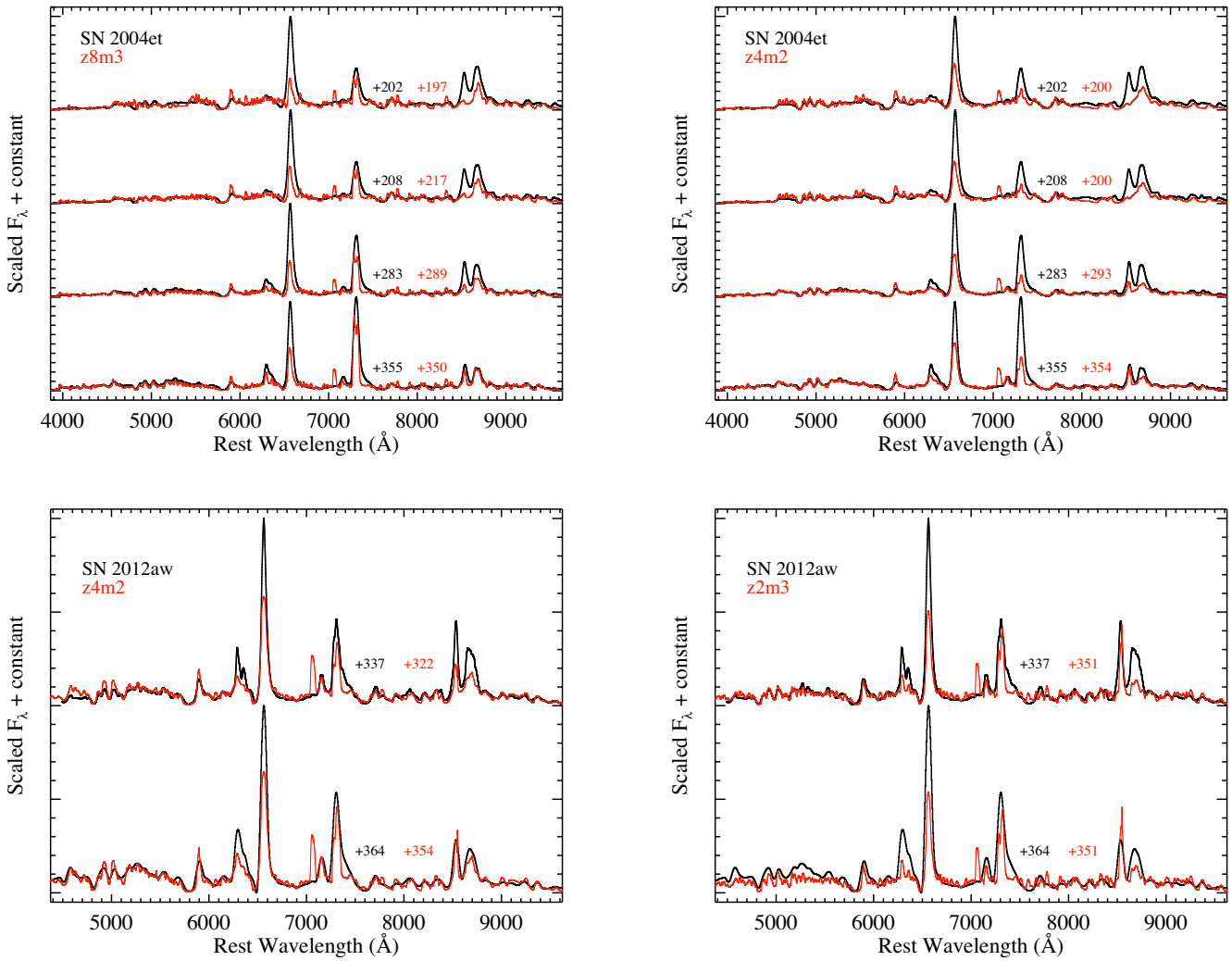

Figure 13. A comparison between two SNe IIP and models from Dessart et al. (2013). SN 2004et (top row) is consistent with the 'z8m3' model ($Z = 0.008$ and $\alpha = 1.6$, top-left panel) and less so with the 'z4m2' model ($Z = 0.040$ and $\alpha = 1.6$, top-right panel). On the other hand, SN 2012aw (bottom row) resembles the 'z4m2' model ($Z = 0.040$ and $\alpha = 1.6$, bottom-left panel) and is less consistent with the 'z2m3' model ($Z = 0.002$ and $\alpha = 1.6$, bottom-right panel). Each spectrum is labelled with its rest-frame age relative to explosion (black) and the age of the overplotted model spectrum relative to explosion (red). All data have been corrected for host-galaxy recession velocity and Galactic reddening using the values listed in Table A1.

As mentioned above, the upper-left panel of Fig. 14 shows the narrow-lined SN 2013am and the 12 $M_\odot$ Jerkstrand et al. (2014) model. While numerous emission features are present in both the data and the model, and the relative strengths of many features match quite well, the emission lines in the model are significantly broader than those in the data. The upper-right panel of Fig. 14 displays SN 2012aw and its best-matching model from Jerkstrand et al. (2014), again the 12 $M_\odot$ model. The middle row of Fig. 14 shows two more objects, SNe 2004A and 2004et, that are fit well by the 12 $M_\odot$ model, and the bottom row contains spectra of SNe 2008ij and 2012fg, two of the relatively few objects that are more consistent with their 15 $M_\odot$ model.

To highlight the variance caused by different progenitor masses in the model spectra from Jerkstrand et al. (2014), we present our late-time spectra of SN 2012aw overplotted with each of their four progenitor mass models in Fig. 15. The top-left panel shows the 12 $M_\odot$ model, which is the same as what is shown in the top-right panel of Fig. 14. The model spectra in each of the other panels are less consistent with the observed spectra of SN 2012aw, especially in the strength of the [O I] λλ6300, 6364 feature.

6 SUMMARY AND CONCLUSIONS

In this work, we present 91 late-time, nebular spectra of 38 SNe IIP, which is the largest data set of its kind ever analysed in one study. We have multiple spectra of most of the objects and many of the SNe IIP have not been studied by other researchers at late times. Furthermore, most of the spectra presented herein are previously unpublished. The observations span 103–1229 d relative to explosion and are found at distances smaller than 69 Mpc, with a typical distance of ∼21 Mpc. In order to determine whether a spectrum was truly nebular, and thus should be included in our data set, we required that the [O I] λλ6300, 6364 doublet show two distinct peaks that were $>2\sigma$ above the local continuum. In one case, detection of two distinct peaks of [Ca II] λλ7291, 7324 was allowed instead.

We also gathered photometric data for most of the objects in our sample, including $M_{\rm plat}(V)$ values for every object and $M_{\rm pk}(V)$ values for nearly two-thirds of them. Also studied were 77 late-time optical light curves of 25 SNe IIP, which allowed us to scale spectra of these objects to interpolated/extrapolated photometry in

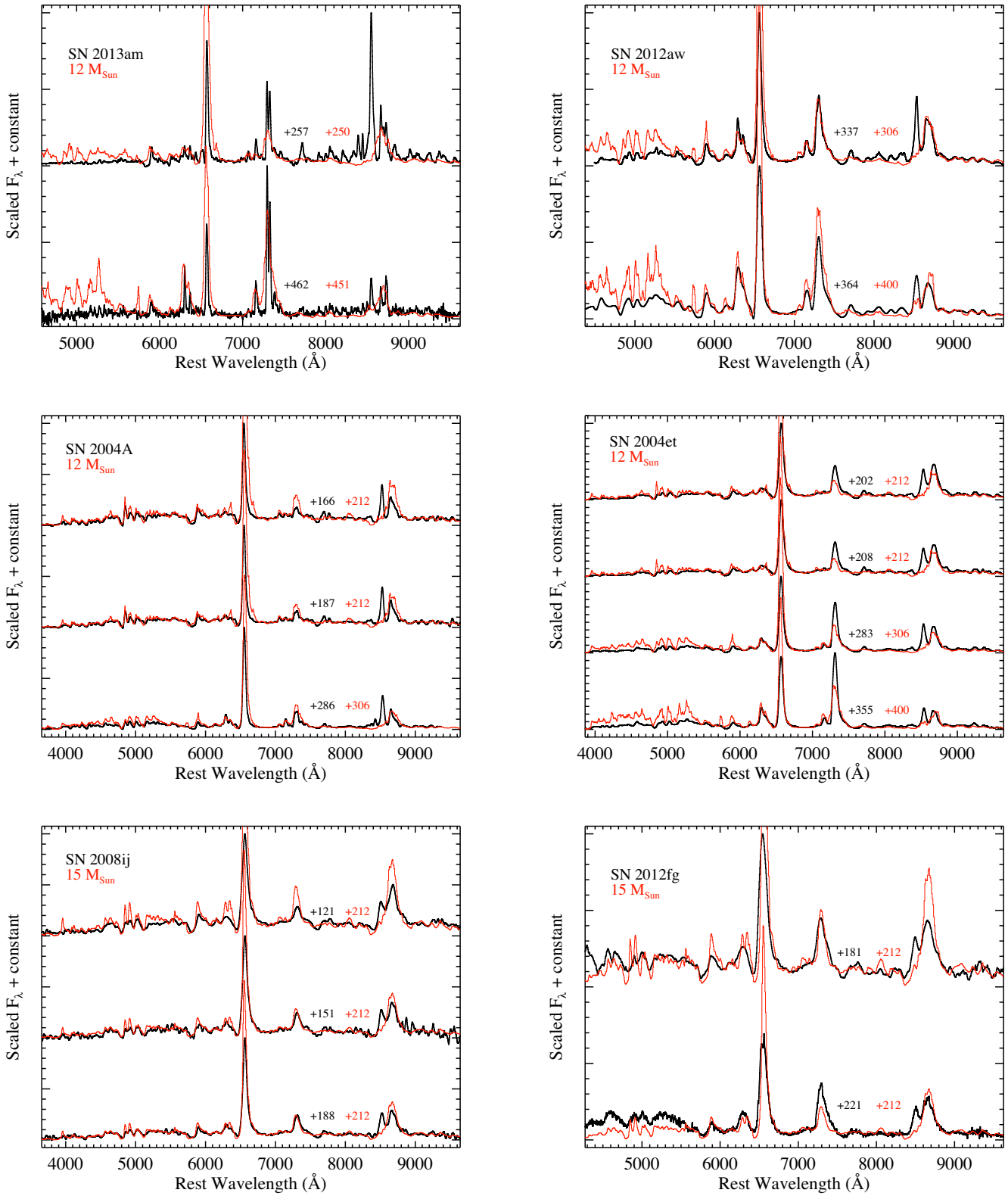

Figure 14. A comparison between SNe IIP and Jerkstrand et al. (2014) models. SN 2013am (upper left) is a narrow-lined SN IIP and somewhat resembles the 12 $M_\odot$ model, even though its emission features are much narrower than those in the model. SN 2012aw (upper right) also matches best to the 12 $M_\odot$ model and was discussed by Jerkstrand et al. (2014). SNe 2004A and 2004et (middle row) are consistent with the 12 $M_\odot$ model, while SNe 2008ij and 2012fg (bottom row) are consistent with the 15 $M_\odot$ model. Each spectrum is labelled with its rest-frame age relative to explosion (black) and the age of the overplotted model spectrum relative to explosion (red). All data have been corrected for host-galaxy recession velocity and Galactic reddening using the values listed in Table A1.

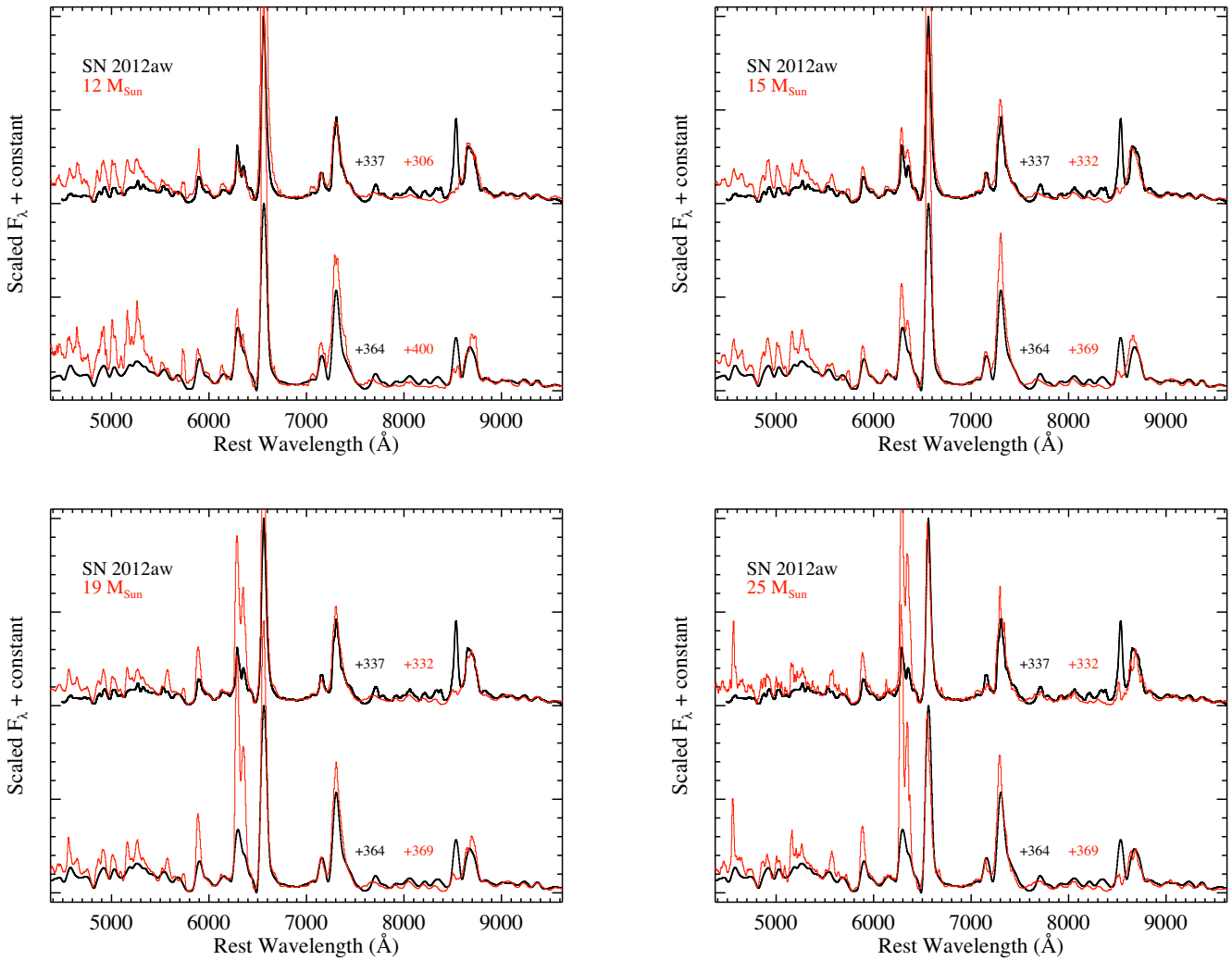

Figure 15. A comparison between SN 2012aw and models of four different progenitor masses from Jerkstrand et al. (2014). SN 2012aw matches best to the 12 $M_\odot$ model (top-left panel) and was discussed by Jerkstrand et al. (2014). Other progenitor masses include 15 $M_\odot$ (top-right panel), 19 $M_\odot$ (bottom-left panel) and 25 $M_\odot$ (bottom-right panel). Each spectrum is labelled with its rest-frame age relative to explosion (black) and the age of the overplotted model spectrum relative to explosion (red). All data have been corrected for host-galaxy recession velocity and Galactic reddening using the values listed in Table A1.

order to put them on an accurate absolute flux scale. The late-time linear decline rates in multiple bands were measured from these data.

In each spectrum, we searched for various permitted and forbidden emission lines from hydrogen, helium, oxygen, magnesium, potassium, calcium and iron. The resulting measurements can be found in Tables A3–A8.

Overall, our spectral-feature measurements are consistent with previous work on individual SNe IIP and relatively small samples of objects. The L_{pk} and L_{tot} values of the bluer spectral features investigated in this work tend to be higher for SNe IIP with brighter $M_{plat}(V)$, possibly indicating a positive correlation between progenitor radius and mass of ^{56}Ni produced. The strongest and most robust result we found is that L_{tot} and L_{pk} values for all spectral features (except those of helium) tend to be higher for steeper late-time V-band and pseudo-bolometric slopes (and HWHM values are bigger for steeper V-band slopes for the strongest lines as well). A steep late-time V-band slope likely arises from less efficient trapping of γ-rays and positrons, which could be caused by multidimensional effects such as clumping of the ejecta or asphericity of the explosion itself. Assuming that γ-rays and positrons can escape relatively easily, photons should be able to as well via the observed emission lines, leading to more-luminous spectral features.

The v_{pk} of Hα appears mostly blueshifted and approaches zero velocity at later epochs, and is found to be anticorrelated with the late-time V-band slope. HWHM values for all spectral features studied tend to decrease with time and median HWHM values are found to be larger for objects with steeper late-time V-band slopes. In addition, the HWHM of Hα and all oxygen spectral features are larger for SNe IIP with brighter $M_{pk}(V)$ and $M_{plat}(V)$. These observations imply that SNe IIP with larger progenitor stars should also have ejecta with a more physically extended oxygen layer that is well mixed with the hydrogen layer (e.g. Dessart et al. 2013).

Various spectral flux ratios are also calculated and investigated herein. We find the peak flux ratio of the [O I] λλ6300, 6364 doublet to mostly decrease from ∼1.0 to ∼0.4—0.5 as the SN IIP ejecta transition from optically thick to optically thin. Also, the ratio of each of the [O I] λλ6300, 6364, [Ca II] λλ7291, 7324 and [Fe II] λλ7155, 7172 doublets to Hα shows the same general trend of roughly constant values for $t \lesssim 200$–250 d and then increasing with time thereafter.

The overall appearance of the shape of each measured spectral profile was also investigated. The vast majority of emission lines were found to be single-peaked and none were seen to have flat tops, similar to what was found by Maguire et al. (2012). We found eight SNe IIP showing Hα profiles with blueshifted peaks and a red shoulder, while three objects had the opposite asymmetric profile, all at epochs earlier than 300 d past explosion. One object (SN 2009ls) is included in both of those categories; it evolves from the former case to the latter between our two observations. These profile shapes are possibly caused by asymmetric ^{56}Ni ejection, likely bipolar in shape (e.g. Chugai et al. 2005).

Lastly, comparisons were made to theoretical late-time spectral models of SNe IIP from Dessart et al. (2013) and Jerkstrand et al. (2014). Most of the objects in our sample were consistent with the Dessart et al. (2013) models with relatively low metallicity ($Z \leq 0.01$). When comparing our data set to the models of Jerkstrand et al. (2014), 30 SNe IIP were most similar to their 12 $M_{\odot}$ model, while the other eight objects were better matched by the 15 $M_{\odot}$ model. This seems to support the RSG problem (Smartt 2009) and is consistent with direct observations of the progenitors of some of the SNe IIP in our sample.

Although the current sample constitutes the largest late-time SN IIP spectral data set ever studied, it still contains relatively few objects and only a handful with spectra at more than two epochs. Future analyses similar to the one undertaken herein would benefit greatly by expanding the total sample of nebular SN IIP spectra. The relatively low luminosity of SNe IIP at late times makes obtaining such spectra difficult, even in the era of 10 m telescopes. Thus, the upcoming 30-m-class telescopes (GMT, E-ELT and TMT) will be key to extending this work. Discovering nearby SNe IIP in greater numbers and in a wider variety of host-galaxy types would also be beneficial. Large, 'untargeted' transient searches coming online soon, such as the Zwicky Transient Factory (Bellm 2014; Smith et al. 2014) and LSST (Ivezić & the LSST Science Collaboration 2013), should be able to find most of the nearby SNe IIP.

ACKNOWLEDGEMENTS

We would like to thank the referee, in addition to J. Anderson, A. Clocchiatti, L. Dessart, A. Jerkstrand, K. Maguire, A. Piro, I. Shivvers, J. Spyromilio and S. Valenti, for helpful discussions that helped improve this paper. We are also indebted to many observers and data reducers, especially M. Childress, B. Cobb, O. Fox, M. Ganeshalingam, L. Ho, I. Kleiser, F. Serduke, I. Shivvers, T. Steele, B. Tucker, D. Wong and W. Zhang, as well as the staffs at the Lick, Keck, McDonald and Siding Spring Observatories, who made this work possible. Research at Lick Observatory is partially supported by a generous gift from Google.

The HET is a joint project of the University of Texas at Austin, the Pennsylvania State University, Stanford University, Ludwig-Maximilians-Universität München, and Georg-August-Universität Göttingen. The HET is named in honour of its principal benefactors, William P. Hobby and Robert E. Eberly. The Marcario Low-Resolution Spectrograph is named for Mike Marcario of High Lonesome Optics who fabricated several optics for the instrument but died before its completion. The LRS is a joint project of the HET partnership and the Instituto de Astronomía de la Universidad Nacional Autónoma de México.

Some of the data presented herein were obtained at the W. M. Keck Observatory, which is operated as a scientific partnership among the California Institute of Technology, the University of California and NASA; the observatory was made possible by the generous financial support of the W. M. Keck Foundation. The authors wish to recognize and acknowledge the very significant cultural role and reverence that the summit of Mauna Kea has always had within the indigenous Hawaiian community; we are most fortunate to have the opportunity to conduct observations from this mountain.

This research has made use of the NASA/IPAC Extragalactic Database (NED), which is operated by the Jet Propulsion Laboratory, California Institute of Technology, under contract with NASA.

JMS is supported by an NSF Astronomy and Astrophysics Postdoctoral Fellowship under award AST-1302771. JCW's supernova group at UT Austin is supported by NSF Grant AST 11-09801. JV is supported by Hungarian OTKA Grant NN 107637. AVF's group at UC Berkeley has been supported by Gary & Cynthia Bengier, the Richard & Rhoda Goldman Fund, the Christopher R. Redlich Fund, the TABASGO Foundation and NSF grant AST-1211916. RJF is supported in part by NSF grant AST-1518052 and from fellowships from the Alfred P. Sloan Foundation and the David and Lucile Packard Foundation.

REFERENCES

Anderson J. P. et al., 2014a, MNRAS, 441, 671
Anderson J. P. et al., 2014b, ApJ, 786, 67
Anderson J. P. et al., 2016, A&A, 589, A110
Arcavi I. et al., 2012, ApJ, 756, L30
Asplund M., Grevesse N., Sauval A. J., Scott P., 2009, ARA&A, 47, 481
Barbarino C. et al., 2015, MNRAS, 448, 2312
Barbon R., Ciatti F., Rosino L., 1979, A&A, 72, 287
Bellm E., 2014, in Wozniak P. R., Graham M. J., Mahabal A. A., Seaman R., eds, The Third Hot-wiring the Transient Universe Workshop. Los Alamos Nat. Laboratory, p. 27
Benetti S., Cappellaro E., Turatto M., 1991, A&A, 247, 410
Blair W. P. et al., 2015, ApJ, 800, 118
Bose S. et al., 2013, MNRAS, 433, 1871
Bose S. et al., 2015, MNRAS, 450, 2373
Cappellaro E., Danziger I. J., della Valle M., Gouiffes C., Turatto M., 1995, A&A, 293, 723
Chornock R., Filippenko A. V., Li W., Silverman J. M., 2010, ApJ, 713, 1363
Chugai N. N., 1992, Sov. Astron. Lett., 18, 239
Chugai N. N., Fabrika S. N., Sholukhova O. N., Goranskij V. P., Abolmasov P. K., Vlasyuk V. V., 2005, Astron. Lett., 31, 792
Clocchiatti A. et al., 1996, AJ, 111, 1286
de Mink S. E., Sana H., Langer N., Izzard R. G., Schneider F. R. N., 2014, ApJ, 782, 7
Dessart L., Hillier D. J., 2011, MNRAS, 410, 1739
Dessart L., Livne E., Waldman R., 2010, MNRAS, 408, 827
Dessart L., Hillier D. J., Livne E., Yoon S.-C., Woosley S., Waldman R., Langer N., 2011, MNRAS, 414, 2985
Dessart L., Hillier D. J., Waldman R., Livne E., 2013, MNRAS, 433, 1745
Dhungana G. et al., 2016, ApJ, 822, 6
Dopita M., Hart J., McGregor P., Oates P., Bloxham G., Jones D., 2007, Ap&SS, 310, 255
Dopita M. et al., 2010, Ap&SS, 327, 245
Drake A. J. et al., 2012, Cent. Bur. Electron. Telegrams, 3118, 1
Elmhamdi A. et al., 2003a, MNRAS, 338, 939
Elmhamdi A., Chugai N. N., Danziger I. J., 2003b, A&A, 404, 1077
Faber S. M. et al., 2003, in Iye M., Moorwood A. F. M., eds, Proc. SPIE Conf. Ser. Vol. 4841, Instrument Design and Performance for Optical/Infrared Ground-based Telescopes. SPIE, Bellingham, p. 1657
Faran T. et al., 2014a, MNRAS, 442, 844

Faran T. et al., 2014b, MNRAS, 445, 554
Filippenko A. V., 1997, ARA&A, 35, 309
Forti G., Boattini A., Tombelli M., Herbst W., Vinton G., 1993, IAU Circ., 5719, 3
Ganeshalingam M. et al., 2010, ApJS, 190, 418
Guillochon J., Parrent J., Kelley L. Z., Margutti R., 2017, ApJ, 835, 64
Gurugubelli U. K., Sahu D. K., Anupama G. C., Chakradhari N. K., 2008, Bull. Astron. Soc. India, 36, 79
Hamuy M. et al., 2003, Nature, 424, 651
Hill G. J., Nicklas H. E., MacQueen P. J., Tejada C., Cobos Duenas F. J., Mitsch W., 1998, in D'Odorico S., ed., Proc. SPIE Conf. Ser. Vol. 3355, Optical Astronomical Instrumentation. SPIE, Bellingham, p. 375
Itagaki K. et al., 2012, Cent. Bur. Electron. Telegrams. LSST Project Science Team, 3338, 1
Ivezić Ž., the LSST Science Collaboration, 2013, LSST Science Requirements Document.
Jerkstrand A., Fransson C., Maguire K., Smartt S., Ergon M., Spyromilio J., 2012, A&A, 546, A28
Jerkstrand A., Smartt S. J., Fraser M., Fransson C., Sollerman J., Taddia F., Kotak R., 2014, MNRAS, 439, 3694
Jerkstrand A. et al., 2015, MNRAS, 448, 2482
Koff R. A., Magill L., Kotak R., Pastorello A., Ochner P., Lykke J., 2011, Cent. Bur. Electron. Telegrams, 2791, 1
Kotak R. et al., 2009, ApJ, 704, 306
Leonard D. C. et al., 2002a, PASP, 114, 35
Leonard D. C., Filippenko A. V., Chornock R., Foley R. J., 2002b, PASP, 114, 1333
Leonard D. C. et al., 2006, Nature, 440, 505
Li W., Filippenko A. V., 2008, Cent. Bur. Electron. Telegrams, 1470, 1
Li W., Fan Y., Qiu Y. L., Hu J. Y., Schwartz M., 2001, IAU Circ., 7591, 1
Li W., Van Dyk S. D., Filippenko A. V., Cuillandre J.-C., 2005, PASP, 117, 121
Li W., Wang X., Van Dyk S. D., Cuillandre J.-C., Foley R. J., Filippenko A. V., 2007, ApJ, 661, 1013
Li W. et al., 2011a, MNRAS, 412, 1441
Li G. et al., 2011b, Cent. Bur. Electron. Telegrams, 2721, 1
Liller W., Adams M., Wilson B., Sventek P., Hale A., Camilleri P., Pesci S., Evans R., 1992, IAU Circ., 5570, 3
Maguire K. et al., 2012, MNRAS, 420, 3451
Mauerhan J. C. et al., 2013, MNRAS, 431, 2599
Maund J. R. et al., 2013, MNRAS, 431, L102
Maund J. R., Reilly E., Mattila S., 2014, MNRAS, 438, 938
Meikle W. P. S. et al., 2011, ApJ, 732, 109
Milisavljevic D., Fesen R. A., Chevalier R. A., Kirshner R. P., Challis P., Turatto M., 2012, ApJ, 751, 25
Miller J. S., Stone R. P. S., 1987, Lick Obs. Technical Report 48, Lick Observatory, Santa Cruz, CA
Miller J. S., Stone R. P. S., 1993, Lick Obs. Technical Report 66, Lick Observatory, Santa Cruz, CA
Moore M., Li W., Boles T., 2003, IAU Circ., 8184, 2
Nakano S., Itagaki K., 2006, Cent. Bur. Electron. Telegrams, 727, 1
Nakano S., Kadota K., Kryachko T., Korotkiy S., 2008, Cent. Bur. Electron. Telegrams, 1626, 1
Nishiyama K., Kabashima F., 2009, Cent. Bur. Electron. Telegrams, 2041, 1
Oke J. B. et al., 1995, PASP, 107, 375
Olivares E. F. et al., 2010, ApJ, 715, 833
Otsuka M. et al., 2012, ApJ, 744, 26
Papenkova M., Li W. D., 1999, IAU Circ., 7337, 3
Pastorello A. et al., 2006, MNRAS, 370, 1752
Pastorello A. et al., 2009, MNRAS, 394, 2266
Pejcha O., Prieto J. L., 2015, ApJ, 799, 215
Penney R., Hoeflich P., 2014, ApJ, 795, 84
Pennypacker C., Perlmutter S., 1989, IAU Circ., 4791, 1
Perlmutter S., Pennypacker C., Djorgovski S., Meylan G., 1988, IAU Circ., 4560, 1
Perlmutter S., Pennypacker C., Marvin H., Sasseen T., Smith C., Muller R., 1990, IAU Circ., 4992, 1
Pozzo M. et al., 2006, MNRAS, 368, 1169
Riess A. G. et al., 2016, ApJ, 826, 56
Ruiz-Lapuente P., Canal R., Kidger M., Lopez R., 1990, AJ, 100, 782
Sahu D. K., Anupama G. C., Srividya S., Muneer S., 2006, MNRAS, 372, 1315
Sanders N. E. et al., 2015, ApJ, 799, 208
Sarneczky K., 2012, Cent. Bur. Electron. Telegrams, 3253, 3
Savitzky A., Golay M. J. E., 1964, Anal. Chem., 36, 1627
Schlafly E. F., Finkbeiner D. P., 2011, ApJ, 737, 103
Schmidt B. P. et al., 1993, AJ, 105, 2236
Silverman J. M. et al., 2012a, MNRAS, 425, 1789
Silverman J. M., Kong J. J., Filippenko A. V., 2012b, MNRAS, 425, 1819
Silverman J. M., Ganeshalingam M., Filippenko A. V., 2013, MNRAS, 430, 1030
Smartt S. J., 2009, ARA&A, 47, 63
Smith R. M. et al., 2014, in Ramsay S. K., McLean I. S., Takami H., eds, Proc. SPIEConf. Ser. Vol. 9147, Ground-based and Airborne Instrumentation for Astronomy V. SPIE, Bellingham, p. 914779
Spiro S. et al., 2014, MNRAS, 439, 2873
Spyromilio J., Pinto P. A., 1991, in Danziger I. J., Kjaer K., eds, European Southern Observatory Conf. Workshop Proc. Vol. 37, Supernova 1987A and other supernovae. European Southern Observatory (ESO), Garching, p. 423
Steele T. N., Silverman J. M., Ganeshalingam M., Lee N., Li W., Filippenko A. V., 2008, Cent. Bur. Electron. Telegrams, 1275, 1
Sukhbold T., Ertl T., Woosley S. E., Brown J. M., Janka H.-T., 2016, ApJ, 821, 38
Taddia F. et al., 2016, A&A, 587, L7
Tomasella L. et al., 2013, MNRAS, 434, 1636
Treffers R. R., Leibundgut B., Filippenko A. V., Richmond M. W., 1993a, IAU Circ., 5718, 1
Treffers R. R., Leibundgut B., Filippenko A. V., Richmond M. W., 1993b, IAU Circ., 5841, 2
Tsvetkov D. Y., 2006, Perem. Zvezdy, 26, 3
Tsvetkov D. Y., Volnova A. A., Shulga A. P., Korotkiy S. A., Elmhamdi A., Danziger I. J., Ereshko M. V., 2006, A&A, 460, 769
Turatto M., Cappellaro E., Benetti S., Danziger I. J., 1993, MNRAS, 265, 471
Uomoto A., 1989, IAU Circ., 4792, 3
Utrobin V. P., Chugai N. N., Pastorello A., 2007, A&A, 475, 973
Valenti S. et al., 2016, MNRAS, 459, 3939
Van Dyk S. D., Li W., Filippenko A. V., 2003, PASP, 115, 1289
Van Dyk S. D. et al., 2012, ApJ, 756, 131
Vinkó J. et al., 2006, MNRAS, 369, 1780
Vinkó J. et al., 2009, ApJ, 695, 619
Welch D. L., Clayton G. C., Campbell A., Barlow M. J., Sugerman B. E. K., Meixner M., Bank S. H. R., 2007, ApJ, 669, 525
Williams A., Martin R., Schmidtke P. C., Phillips M. M., Maza J., Wischnjewsky M., 1993, IAU Circ., 5733, 1
Yamaoka H., 2007, Cent. Bur. Electron. Telegrams, 1042, 1
Yamaoka H., Itagaki K., Klotz A., Pollas C., Boer M., 2004, IAU Circ., 8413, 2
Yaron O., Gal-Yam A., 2012, PASP, 124, 668
Yaron O. et al., 2013, Astron. Telegram, 4910, 1
Zhang J. et al., 2014, ApJ, 797, 5

APPENDIX A: TABLES OF OBJECTS, SPECTRA, SPECTRAL MEASUREMENTS AND PHOTOMETRY

Table A1. Summary of SNe IIP.

SN name	Host galaxy	cz (km s^{-1})[a]	Distance (Mpc)[a]	$E(B-V)_{MW}$ (mag)[b]	MJD of discovery	Approx. MJD of explosion[c]	$M_{plat}(V)$ (mag)[c]	$M_{pk}(V)$ (mag)[c]	Reference(s)[d]
SN 1988A	NGC 4579	1520	19.58	0.036	47177	47176 (2)	−16.9 (0.1)	−17.8 (0.3)	1
SN 1988H	NGC 5878	1991	30.36	0.126	47224	47203 (2)	−16.7 (0.5)	−16.8 (0.5)	2
SN 1989L	NGC 7339	1313	22.97	0.033	47679	47650 (2)	−16.3 (0.5)	–	3,4
SN 1990E	NGC 1035	1241	17.43	0.022	47938	47935 (2)	−16.6 (0.4)	−16.7 (0.4)	5
SN 1990H	NGC 3294	1586	29.74	0.018	47991	47918 (2)	−15.7 (0.5)	–	6
SN 1990K	NGC 150	1583	21.01	0.012	48037	48017 (5)	−17.2 (0.5)	−17.2 (0.5)	7
SN 1992ad	NGC 4411	1280	16.80	0.026	48805	48804 (2)	−16.1 (0.5)	–	8
SN 1992bt	NGC 3780	2398	42.62	0.012	48976	48956 (20)	−16.6 (0.5)	–	9
SN 1992H	NGC 5377	1793	27.65	0.015	48664	48661 (3)	−16.9 (0.3)	−17.7 (0.3)	10
SN 1993G	NGC 3690	3121	–	0.014	49052	49042 (9)	−16.5 (0.3)	−16.6 (0.3)	11,12
SN 1993K	NGC 2223	2722	39.83	0.056	49075	49065 (9)	−17.5 (0.3)	−17.5 (0.3)	13
SN 1999em	NGC 1637	717	11.08	0.036	51481	51476 (2)	−16.2 (0.2)	−16.8 (0.3)	14
SN 1999gq	NGC 4523	261	16.80	0.034	51536	51516 (20)	−16.6 (0.5)	–	15
SN 2001X	NGC 5921	1481	22.56	0.035	51968	51962 (5)	−16.1 (0.4)	−16.7 (0.4)	16,17
SN 2002hh	NGC 6946	48	5.62	0.303	52579	52576 (2)	−16.6 (0.3)	−16.7 (0.5)	18
SN 2003gd	NGC 628	657	9.01	0.061	52803	52715 (3)	−16.0 (0.2)	−16.2 (0.2)	19
SN 2003hl	NGC 772	2473	30.93	0.064	52872	52866 (4)	−15.2 (0.5)	−15.9 (0.1)	20
SN 2004A	NGC 6207	851	18.58	0.022	53014	53010 (3)	−15.9 (0.1)	−16.1 (0.3)	21
SN 2004dj	NGC 2403	132	3.47	0.035	53218	53187 (4)	−15.7 (0.4)	−15.7 (0.4)	22
SN 2004et	NGC 6946	48	5.62	0.302	53276	53270 (1)	−16.0 (0.1)	−16.0 (0.1)	23,24
SN 2005ay	NGC 3938	809	19.80	0.018	53457	53453 (3)	−15.7 (0.3)	−15.9 (0.3)	25
SN 2005cs	NGC 5194	462	7.97	0.032	53550	53549 (1)	−15.3 (0.1)	−15.6 (0.1)	26
SN 2006my	NGC 4651	803	23.70	0.024	54048	53958 (20)	−16.8 (0.5)	–	27,28
SN 2006ov	NGC 4303	1565	16.36	0.020	54064	53974 (6)	−15.1 (0.3)	−15.1 (0.3)	29
SN 2007gw	NGC 4161	4899	48.40	0.010	54337	54217 (20)	−17.5 (0.5)	–	30,31
SN 2008ex	UGC 11428	3945	–	0.201	54696	54694 (2)	−16.3 (0.5)	−16.4 (0.5)	32
SN 2008ij	NGC 6643	1484	20.88	0.053	54820	54818 (2)	−16.1 (0.5)	–	33
SN 2009ls	NGC 3423	1010	11.10	0.026	55159	55150 (8)	−15.4 (0.5)	–	34,35
SN 2011cj	UGC 9356	2224	–	0.024	55691	55688 (2)	−15.4 (0.5)	–	36
SN 2011fd	NGC 2273B	2102	28.10	0.064	55794	55783 (20)	−17.1 (0.5)	–	37
SN 2012A	NGC 3239	752	9.96	0.029	55934	55933 (2)	−15.5 (0.2)	−16.0 (0.2)	38
SN 2012aw[e]	NGC 3351	779	10.11	0.025	56003	56003 (1)	−16.5 (0.1)	−16.6 (0.3)	39
SN 2012ch	SDSS J150602+412534	2590	–	0.016	56065	56045 (20)	−16.4 (0.5)	–	40
SN 2012ec	NGC 1084	1406	20.51	0.023	56151	56143 (2)	−16.5 (0.2)	−16.7 (0.2)	41
SN 2012fg[f]	NGC 2857	4887	69.05	0.020	56208	56198 (10)	−18.4 (0.5)	−19.1 (0.5)	42
SN 2012ho	MCG -01-57-21	2971	35.97	0.046	56268	56255 (14)	−17.9 (0.5)	–	43
SN 2013ab[g]	NGC 5669	1370	22.24	0.025	56341	56340 (1)	−16.7 (0.1)	−17.2 (0.2)	44
SN 2013am[h]	NGC 3623	806	12.77	0.022	56373	56372 (1)	−14.5 (0.5)	−14.7 (0.5)	45

[a]Redshifts and distances are from NED; the latter is the mean metric distance.

[b]Milky Way reddening values come from Schlafly & Finkbeiner (2011).

[c]Uncertainties are in parentheses.

[d](1) Ruiz-Lapuente et al. (1990), (2) Perlmutter et al. (1988), (3) Pennypacker & Perlmutter (1989), (4) Uomoto (1989), (5) Schmidt et al. (1993), (6) Perlmutter et al. (1990), (7) Cappellaro et al. (1995), (8) Liller et al. (1992), (9) Treffers et al. (1993b), (10) Clocchiatti et al. (1996), (11) Forti et al. (1993), (12) Treffers et al. (1993a), (13) Williams et al. (1993), (14) Elmhamdi et al. (2003a), (15) Papenkova & Li (1999), (16) Li et al. (2001), (17) Tsvetkov (2006), (18) Pozzo et al. (2006), (19) Van Dyk, Li & Filippenko (2003), (20) Moore, Li & Boles (2003), (21) Gurugubelli et al. (2008), (22) Vinkó et al. (2006), (23) Yamaoka et al. (2004), (24) Li et al. (2005), (25) Tsvetkov et al. (2006), (26) Pastorello et al. (2006), (27) Nakano & Itagaki (2006), (28) Li et al. (2007), (29) Spiro et al. (2014), (30) Yamaoka (2007), (31) Steele et al. (2008), (32) Li & Filippenko (2008), (33) Nakano et al. (2008), (34) Yamaoka (2007), (35) Nishiyama & Kabashima (2009), (36) Li et al. (2011b), (37) Koff et al. (2011), (38) Tomasella et al. (2013), (39) Bose et al. (2013), (40) Drake et al. (2012), (41) Barbarino et al. (2015), (42) Sarneczky (2012), (43) Itagaki et al. (2012), (44) Bose et al. (2015), (45) Yaron et al. (2013).

[e]SN 2012aw is also known as PTF12bvh.

[f]SN 2012fg is also known as PTF12jxe.

[g]SN 2013ab is also known as iPTF13ut.

[h]SN 2013am is also known as iPTF13aaz.

Table A2. Summary of SNe IIP spectra.

SN name	MJD[a]	Age since discovery[b]	Instrument[c]	Wavelength range (Å)	Resolution[d] (Å)	Previous publication
SN 1988A	47339.262	162	UVSchmidt	3482–9253	12	–
SN 1988A	47359.195	182	UVSchmidt	5940–9104	12	–
SN 1988H	47343.245	119	UVSchmidt	6072–9239	12	–
SN 1989L	47861.000	182	UVSchmidt	4042–9060	12	–
SN 1990E	48089.000	151	UVSchmidt	3936–7023	12	–
SN 1990E	48103.479	165	UVSchmidt	3859–7001	12	Schmidt et al. (1993)
SN 1990E	48133.000	195	UVSchmidt	6692–9809	12	–
SN 1990E	48242.214	303	UVSchmidt	5776–8913	12	–
SN 1990H	48184.523	193	UVSchmidt	5769–8883	12	–
SN 1990K	48184.356	147	UVSchmidt	5770–8883	12	–
SN 1990K	48242.163	205	UVSchmidt	5770–8903	12	–
SN 1992ad	49030.441	225	Kast	3077–10 431	6/11	–
SN 1992ad	49091.391	286	Kast	3286–9957	6/11	–
SN 1992bt	49212.174	235	Kast	3194–9722	6/11	–
SN 1992H	48867.208	202	Kast	4231–6998	6/11	–
SN 1992H	48886.144	221	Kast	4245–7018	6/11	Filippenko (1997)
SN 1992H	49047.470	382	Kast	3135–9801	6/11	Filippenko (1997)
SN 1992H	49091.435	425	Kast	3241–9941	6/11	–
SN 1992H	49127.000	461	UVSchmidt	3499–11 008	12	–
SN 1992H	49158.000	492	UVSchmidt	3596–11 058	12	–
SN 1993G	49166.270	114	Kast	3078–10 293	6/11	–
SN 1993K	49359.301	282	Kast	3369–10 009	6/11	–
SN 1999em	51793.515	312	Kast	3292–10 425	6/11	Leonard et al. (2002a)
SN 1999em	51813.494	332	Kast	3292–7781	6/11	Leonard et al. (2002a)
SN 1999em	51899.000	418	Kast	3252–10 495	6/11	–
SN 1999em	51997.244	516	LRIS	4330–6854	5.5/7	Leonard et al. (2002a)
SN 1999gq	51618.399	83	Kast	3297–10 491	6/11	–
SN 2001X	52144.206	176	Kast	3284–10 349	6/11	Faran et al. (2014a)
SN 2002hh	52737.499	159	Kast	3241–10 398	6/11	Pozzo et al. (2006)
SN 2002hh	52914.170	336	Kast	3299–10 398	6/11	–
SN 2002hh	52972.211	394	LRIS	3153–9418	5.5/7	Pozzo et al. (2006)
SN 2003gd	52940.372	138	Kast	3253–10 377	6/11	Faran et al. (2014a)
SN 2003hl	53021.178	148	Kast	3293–10 315	6/11	Faran et al. (2014a)
SN 2004A	53176.403	162	Kast	3291–10 371	6/11	–
SN 2004A	53197.367	183	Kast	3291–10 371	6/11	–
SN 2004A	53296.230	282	LRIS	3073–9373	5.5/7	–
SN 2004dj	53323.000	105	LRIS	3071–9396	5.5/7	–
SN 2004dj	53328.529	111	Kast	4648–9846	6/11	Leonard et al. (2006)
SN 2004dj	53351.525	134	LRIS	3299–9316	5.5/7	–
SN 2004dj	53357.267	140	Kast	4598–9796	6/11	Leonard et al. (2006)
SN 2004dj	53386.432	169	Kast	3305–10 495	6/11	–
SN 2004dj	53387.235	170	Kast	4598–9796	6/11	Leonard et al. (2006)
SN 2004dj	53413.426	196	LRIS	3778–9246	5.5/7	–
SN 2004dj	53440.272	223	LRIS	3399–9256	5.5/7	–
SN 2004dj	53442.332	225	Kast	4598–9796	6/11	Leonard et al. (2006)
SN 2004dj	53471.233	254	Kast	4598–9796	6/11	Leonard et al. (2006)
SN 2004dj	53477.182	260	Kast	3309–10 395	6/11	–
SN 2004dj	53615.494	398	Kast	3309–10 495	6/11	–
SN 2004dj	53624.499	407	Kast	3349–10 395	6/11	–
SN 2004dj	53852.292	635	LRIS	3129–9246	5.5/7	–
SN 2004dj	54092.484	875	DEIMOS	4582–7227	2	Vinkó et al. (2009)
SN 2004dj	54122.398	905	DEIMOS	4440–9565	2	Meikle et al. (2011)
SN 2004dj	54416.603	1199	LRIS	3738–6837	3.5	–
SN 2004et	53471.494	196	Kast	3309–10 398	6/11	Faran et al. (2014a)
SN 2004et	53477.421	202	Kast	3309–10 398	6/11	Faran et al. (2014a)
SN 2004et	53552.428	277	Kast	3399–10 398	6/11	Faran et al. (2014a)
SN 2004et	53624.354	349	Kast	3349–10 398	6/11	Faran et al. (2014a)

Table A2 – *continued*

SN name	MJD[a]	Age since discovery[b]	Instrument[c]	Wavelength range (Å)	Resolution[d] (Å)	Previous publication
SN 2005ay	53741.579	284	Kast	3301–10 472	6/11	Faran et al. (2014a)
SN 2005cs	53706.659	157	DEIMOS	3902–9054	2	Faran et al. (2014a)
SN 2005cs	53852.529	303	LRIS	3183–9236	5.5/7	Faran et al. (2014a)
SN 2006my	54145.661	98	LRIS	3191–9213	5.5/7	–
SN 2006ov	54145.654	82	LRIS	3183–9190	5.5/7	–
SN 2007gw	54525.500	186	Kast	4327–9701	6/11	–
SN 2008ex	54979.455	280	Kast	3393–10 561	6/11	–
SN 2008ij	54939.536	119	Kast	3437–9851	6/11	–
SN 2008ij	54969.495	149	Kast	3668–9889	6/11	–
SN 2008ij	55006.308	186	Kast	3453–10 647	6/11	–
SN 2009ls	55270.308	111	Kast	3438–10 764	6/11	–
SN 2009ls	55323.268	164	Kast	3428–10 724	6/11	–
SN 2011cj	55919.550	227	Kast	3405–10 671	6/11	–
SN 2011fd	55891.403	97	Kast	3406–10 034	6/11	–
SN 2011fd	55980.213	185	Kast	3438–9855	6/11	–
SN 2012A	56340.305	406	DEIMOS	4489–9617	2	–
SN 2012A	56366.145	432	LRS	4154–10 773	17	–
SN 2012aw[e]	56340.323	337	DEIMOS	4488–9616	2	–
SN 2012aw[e]	56367.343	364	LRS	4177–10 660	17	–
SN 2012ch	56402.461	335	LRS	4132–10 414	17	–
SN 2012ec	56365.000	213	WiFeS	3551–9244	2	–
SN 2012ec	56545.543	393	DEIMOS	4429–9595	2	–
SN 2012fg[f]	56381.301	171	LRS	4200–10 524	17	–
SN 2012fg[f]	56422.301	211	LRIS	3099–10 120	5.5/7	–
SN 2012ho	56422.611	154	LRIS	3119–10 185	5.5/7	–
SN 2012ho	56484.387	215	LRS	4131–10 694	17	–
SN 2012ho	56504.339	235	LRS	4131–10 694	17	–
SN 2012ho	56506.551	237	DEIMOS	4382–9545	2	–
SN 2012ho	56520.295	250	LRS	4131–10 694	17	–
SN 2012ho	56573.439	303	DEIMOS	4442–9532	2	–
SN 2013ab[g]	56484.348	143	DEIMOS	4430–9581	2	–
SN 2013ab[g]	56508.212	167	Kast	3436–10 552	6/11	–
SN 2013am[h]	56629.632	256	LRIS	3192–10 243	5.5/7	–
SN 2013am[h]	56834.287	461	DEIMOS	4501–9641	2	–

[a]Modified JD (if not rounded to the whole day, modified JD at the mid-point of the observation).
[b]Phases of spectra are in rest-frame days since discovery using the redshift and discovery date presented in Table A1.
[c]Instruments: UVSchmidt (Shane 3 m), Kast (Shane 3 m), LRIS (Keck 10 m), DEIMOS (Keck 10 m), LRS (HET 10 m), WiFeS (ATT 2.3 m).
[d]Typical FWHM spectral resolution for the instrument and set-up; if two numbers are listed then they represent the blue- and red-side resolutions, respectively.
[e]SN 2012aw is also known as PTF12bvh.
[f]SN 2012fg is also known as PTF12jxe.
[g]SN 2013ab is also known as iPTF13ut.
[h]SN 2013am is also known as iPTF13aaz.

Table A3. Spectral-feature measurements of hydrogen.

SN name	Age since discovery[a]	$\log\left(\frac{L_{\rm tot}}{\rm ergs^{-1}}\right)$	$\log\left(\frac{L_{\rm pk}}{\rm ergs^{-1}\,\AA^{-1}}\right)$	$v_{\rm pk}$ (100 km s^{-1})	HWHM (1000 km s^{-1})
			Hα		
SN 1988A	162	40.19 (0.03)	38.38 (0.02)	0.40 (0.05)	1.45 (0.04)
SN 1988A	182	39.77 (0.04)	37.98 (0.03)	0.43 (0.05)	1.35 (0.03)
SN 1988H	119	40.05 (0.02)	38.06 (0.02)	−2.52 (0.05)	2.35 (0.04)
SN 1989L	182	39.59 (0.06)	37.82 (0.04)	3.39 (0.17)	1.36 (0.04)
SN 1990E	151	39.49 (0.09)	37.37 (0.06)	−0.09 (0.05)	3.30 (0.06)
SN 1990E	165	39.31 (0.11)	37.18 (0.06)	−1.22 (0.05)	3.32 (0.07)
SN 1990E	304	39.07 (0.06)	37.21 (0.04)	−0.53 (0.05)	1.67 (0.03)
SN 1990H	193	39.57 (0.17)	37.77 (0.10)	−0.41 (0.05)	1.86 (0.08)
SN 1990K	147	39.61 (0.07)	37.71 (0.05)	0.62 (0.05)	2.17 (0.05)
SN 1990K	205	39.52 (0.05)	37.58 (0.03)	−0.30 (0.05)	2.04 (0.02)
SN 1992ad	225	39.72 (0.01)	37.65 (0.01)	−8.16 (0.05)	2.78 (0.03)
SN 1992ad	286	39.18 (0.03)	37.12 (0.02)	−5.43 (0.05)	2.71 (0.04)
SN 1992bt	235	39.55 (0.11)	37.70 (0.06)	−5.62 (0.05)	1.60 (0.02)
SN 1992H	203	40.46 (0.01)	38.40 (0.01)	−6.89 (0.05)	2.53 (0.03)
SN 1992H	221	40.39 (0.01)	38.35 (0.01)	−3.27 (0.05)	2.42 (0.03)
SN 1992H	382	39.54 (0.04)	37.61 (0.04)	0.36 (0.05)	1.95 (0.02)
SN 1992H	425	39.03 (0.09)	37.00 (0.06)	0.15 (0.05)	2.50 (0.05)
SN 1992H	461	38.96 (0.14)	36.97 (0.09)	−0.48 (0.05)	2.18 (0.02)
SN 1992H	492	38.68 (0.13)	36.68 (0.09)	2.97 (0.15)	2.38 (0.04)
SN 1993G	114	39.90 (0.08)	37.95 (0.06)	−9.99 (0.05)	2.14 (0.05)
SN 1993K	282	39.39 (0.06)	37.48 (0.04)	−1.59 (0.05)	1.80 (0.02)
SN 1999em	312	39.38 (0.03)	37.54 (0.02)	1.14 (0.06)	1.44 (0.02)
SN 1999em	332	39.29 (0.03)	37.48 (0.02)	0.22 (0.05)	1.38 (0.02)
SN 1999em	418	38.81 (0.03)	37.02 (0.02)	−0.67 (0.05)	1.31 (0.02)
SN 1999em	516	37.81 (0.07)	35.98 (0.03)	0.21 (0.05)	1.45 (0.02)
SN 1999gq	83	39.98 (0.01)	37.99 (0.01)	−4.43 (0.05)	2.14 (0.02)
SN 2001X	176	39.93 (0.02)	38.11 (0.01)	−4.68 (0.05)	1.46 (0.03)
SN 2002hh	159	38.82 (0.04)	36.78 (0.04)	−3.24 (0.05)	2.58 (0.03)
SN 2002hh	336	37.90 (0.25)	36.11 (0.14)	−0.60 (0.05)	1.56 (0.06)
SN 2002hh	394	37.75 (0.03)	35.67 (0.03)	−2.32 (0.05)	2.84 (0.03)
SN 2003gd	138	39.29 (0.05)	37.57 (0.02)	2.61 (0.13)	1.07 (0.02)
SN 2003hl	149	38.94 (0.10)	37.08 (0.06)	−2.79 (0.05)	1.79 (0.03)
SN 2004A	162	39.80 (0.04)	38.03 (0.03)	−5.70 (0.05)	1.31 (0.03)
SN 2004A	183	39.79 (0.04)	38.04 (0.03)	−6.61 (0.05)	1.21 (0.02)
SN 2004A	282	39.53 (0.05)	37.81 (0.02)	−3.87 (0.05)	1.11 (0.02)
SN 2004dj	106	39.42 (0.06)	37.59 (0.05)	−12.11 (0.05)	2.22 (0.14)
SN 2004dj	111	39.47 (0.24)	37.49 (0.13)	−8.19 (0.05)	2.16 (0.09)
SN 2004dj	134	39.46 (0.06)	37.67 (0.05)	−13.00 (0.05)	1.80 (0.10)
SN 2004dj	140	39.49 (0.26)	37.54 (0.13)	−5.93 (0.05)	1.87 (0.06)
SN 2004dj	169	39.46 (0.04)	37.64 (0.03)	−12.11 (0.05)	1.62 (0.06)
SN 2004dj	170	39.49 (0.25)	37.57 (0.13)	−10.34 (0.05)	1.77 (0.05)
SN 2004dj	196	39.48 (0.06)	37.70 (0.04)	−10.29 (0.05)	1.51 (0.06)
SN 2004dj	223	39.36 (0.06)	37.57 (0.04)	−10.29 (0.05)	1.47 (0.05)
SN 2004dj	225	39.43 (0.24)	37.54 (0.12)	−3.70 (0.05)	1.65 (0.03)
SN 2004dj	254	39.36 (0.23)	37.48 (0.12)	−3.73 (0.05)	1.61 (0.03)
SN 2004dj	260	39.25 (0.04)	37.43 (0.03)	−6.68 (0.05)	1.46 (0.03)
SN 2004dj	398	38.70 (0.02)	36.95 (0.01)	−1.27 (0.05)	1.19 (0.01)
SN 2004dj	407	38.67 (0.03)	36.92 (0.02)	−2.16 (0.05)	1.19 (0.02)
SN 2004dj	635	37.83 (0.19)	36.15 (0.10)	−1.34 (0.05)	1.10 (0.04)
SN 2004dj	875	37.26 (0.04)	35.77 (0.06)	−0.94 (0.05)	0.89 (0.02)
SN 2004dj	905	37.29 (0.03)	35.65 (0.03)	0.11 (0.05)	1.41 (0.04)
SN 2004dj	1199	37.10 (0.01)	35.49 (0.01)	−0.92 (0.05)	2.04 (0.05)
SN 2004et	196	39.72 (0.01)	37.80 (0.01)	3.20 (0.16)	1.85 (0.03)
SN 2004et	202	39.71 (0.01)	37.81 (0.01)	3.20 (0.16)	1.78 (0.03)
SN 2004et	277	39.34 (0.02)	37.48 (0.01)	1.37 (0.07)	1.56 (0.02)
SN 2004et	349	38.92 (0.02)	37.07 (0.01)	3.18 (0.16)	1.50 (0.02)
SN 2005ay	284	39.45 (0.15)	37.75 (0.07)	−1.60 (0.05)	1.02 (0.02)
SN 2005cs	157	38.32 (0.02)	36.44 (0.01)	11.91 (0.60)	1.78 (0.03)
SN 2005cs	303	38.05 (0.13)	36.37 (0.06)	9.09 (0.45)	1.02 (0.02)
SN 2006my	98	40.06 (0.01)	38.18 (0.01)	0.45 (0.05)	1.63 (0.01)
SN 2006ov	82	38.80 (0.08)	37.16 (0.07)	3.77 (0.19)	1.06 (0.02)

Table A3 – *continued*

SN name	Age since discovery[a]	$\log\left(\frac{L_{\rm tot}}{\rm ergs^{-1}}\right)$	$\log\left(\frac{L_{\rm pk}}{\rm ergs^{-1}\AA^{-1}}\right)$	$v_{\rm pk}$ (100 km s^{-1})	HWHM (1000 km s^{-1})
SN 2007gw	186	39.70 (0.05)	37.67 (0.04)	−8.70 (0.05)	2.64 (0.04)
SN 2008ex	280	40.14 (0.02)	38.21 (0.01)	0.78 (0.05)	1.94 (0.04)
SN 2008ij	119	40.07 (0.02)	38.05 (0.02)	−0.24 (0.05)	2.49 (0.03)
SN 2008ij	149	39.07 (0.03)	37.11 (0.02)	2.50 (0.13)	2.08 (0.03)
SN 2008ij	186	39.48 (0.02)	37.58 (0.02)	−0.22 (0.05)	1.78 (0.03)
SN 2009ls	111	39.70 (0.01)	37.60 (0.01)	−28.20 (0.05)	3.54 (0.11)
SN 2009ls	164	39.50 (0.01)	37.43 (0.01)	3.52 (0.18)	2.69 (0.03)
SN 2011cj	227	39.97 (0.09)	38.16 (0.05)	−1.20 (0.05)	1.49 (0.03)
SN 2011fd	97	39.26 (0.10)	37.37 (0.07)	−7.20 (0.05)	2.20 (0.08)
SN 2011fd	185	39.63 (0.05)	37.80 (0.02)	−3.57 (0.05)	1.49 (0.03)
SN 2012A	406	38.74 (0.04)	37.06 (0.03)	−0.17 (0.05)	1.02 (0.01)
SN 2012A	432	38.45 (0.32)	36.73 (0.17)	−2.42 (0.05)	1.05 (0.02)
SN 2012aw[b]	337	39.40 (0.01)	37.59 (0.01)	−0.14 (0.05)	1.42 (0.01)
SN 2012aw[b]	364	39.28 (0.14)	37.43 (0.08)	0.91 (0.05)	1.48 (0.02)
SN 2012ch	335	39.67 (0.12)	37.66 (0.07)	2.79 (0.14)	2.45 (0.06)
SN 2012ec	214	39.48 (0.13)	37.70 (0.11)	−2.83 (0.05)	1.61 (0.03)
SN 2012ec	393	38.62 (0.10)	37.03 (0.10)	−0.97 (0.05)	1.47 (0.04)
SN 2012fg[c]	171	40.00 (0.05)	37.87 (0.03)	−10.64 (0.05)	2.98 (0.05)
SN 2012fg[c]	211	39.72 (0.03)	37.68 (0.03)	−0.54 (0.05)	2.72 (0.02)
SN 2012ho	154	40.28 (0.01)	38.30 (0.01)	−0.58 (0.05)	2.31 (0.02)
SN 2012ho	215	40.02 (0.11)	38.08 (0.07)	−4.41 (0.05)	1.91 (0.04)
SN 2012ho	235	39.93 (0.13)	37.99 (0.07)	0.91 (0.05)	1.82 (0.04)
SN 2012ho	237	39.93 (0.03)	38.08 (0.04)	−0.13 (0.05)	1.75 (0.02)
SN 2012ho	250	39.89 (0.14)	37.98 (0.07)	−2.65 (0.05)	1.74 (0.04)
SN 2012ho	303	39.67 (0.04)	37.89 (0.05)	0.36 (0.05)	1.54 (0.02)
SN 2013ab[d]	143	40.10 (0.01)	38.17 (0.01)	5.10 (0.26)	1.99 (0.02)
SN 2013ab[d]	167	40.10 (0.01)	38.17 (0.01)	2.81 (0.14)	1.91 (0.03)
SN 2013am[e]	256	38.59 (0.05)	37.05 (0.04)	1.95 (0.10)	0.69 (0.02)
SN 2013am[e]	461	38.10 (0.06)	36.62 (0.03)	2.26 (0.11)	0.66 (0.01)
			Hβ		
SN 1988A	162	39.21 (0.08)	37.49 (0.05)	−0.38 (0.06)	1.80 (0.03)
SN 1990E	151	38.30 (0.12)	36.54 (0.11)	5.75 (0.29)	4.10 (0.23)
SN 1992ad	225	38.41 (0.03)	36.70 (0.03)	10.12 (0.51)	2.72 (0.05)
SN 1992ad	286	38.03 (0.09)	36.43 (0.06)	6.59 (0.33)	2.15 (0.08)
SN 1992H	203	39.12 (0.06)	37.46 (0.05)	−11.71 (0.06)	1.78 (0.06)
SN 1992H	221	39.03 (0.04)	37.39 (0.03)	−9.35 (0.06)	1.61 (0.04)
SN 1999em	312	38.10 (0.16)	36.50 (0.14)	13.38 (0.67)	1.56 (0.04)
SN 1999em	332	38.17 (0.06)	36.49 (0.05)	11.03 (0.55)	1.73 (0.02)
SN 1999em	418	38.04 (0.05)	36.32 (0.03)	14.66 (0.73)	2.13 (0.02)
SN 1999em	516	36.93 (0.13)	35.41 (0.11)	−1.30 (0.06)	1.45 (0.13)
SN 1999gq	83	38.92 (0.04)	37.19 (0.03)	−7.63 (0.06)	1.94 (0.04)
SN 2001X	176	38.92 (0.08)	37.28 (0.05)	−6.12 (0.06)	1.34 (0.04)
SN 2002hh	336	36.93 (0.42)	35.48 (0.22)	0.75 (0.06)	0.82 (0.01)
SN 2003gd	138	38.11 (0.09)	36.38 (0.07)	3.33 (0.17)	1.76 (0.03)
SN 2003hl	149	38.04 (0.47)	36.57 (0.28)	−3.69 (0.06)	0.87 (0.02)
SN 2004A	162	38.94 (0.19)	37.32 (0.11)	−5.92 (0.06)	1.37 (0.06)
SN 2004A	183	38.84 (0.19)	37.26 (0.11)	−5.93 (0.06)	1.17 (0.04)
SN 2004A	282	38.34 (0.12)	36.71 (0.07)	−4.82 (0.06)	1.37 (0.04)
SN 2004dj	106	38.66 (0.21)	37.01 (0.13)	−12.31 (0.06)	1.59 (0.08)
SN 2004dj	111	38.65 (0.26)	36.83 (0.23)	−6.66 (0.06)	2.77 (0.05)
SN 2004dj	134	38.58 (0.22)	36.94 (0.14)	−15.95 (0.06)	1.48 (0.08)
SN 2004dj	140	38.61 (0.27)	36.77 (0.23)	−6.57 (0.06)	2.69 (0.05)
SN 2004dj	169	38.46 (0.19)	36.82 (0.12)	−9.86 (0.06)	1.48 (0.07)
SN 2004dj	170	38.51 (0.24)	36.66 (0.21)	−6.57 (0.06)	2.76 (0.04)
SN 2004dj	196	38.41 (0.16)	36.74 (0.10)	−13.56 (0.06)	1.54 (0.06)
SN 2004dj	223	38.26 (0.12)	36.54 (0.08)	−5.00 (0.06)	1.65 (0.04)
SN 2004dj	225	38.37 (0.18)	36.50 (0.16)	2.28 (0.11)	3.52 (0.06)
SN 2004dj	254	38.29 (0.14)	36.44 (0.13)	13.96 (0.70)	4.05 (0.06)
SN 2004dj	260	38.14 (0.07)	36.41 (0.05)	2.24 (0.11)	1.85 (0.02)
SN 2004dj	398	37.86 (0.04)	36.17 (0.03)	7.30 (0.37)	2.18 (0.04)
SN 2004dj	407	37.82 (0.04)	36.14 (0.03)	10.84 (0.54)	2.22 (0.04)
SN 2004dj	635	37.38 (0.03)	35.73 (0.03)	13.32 (0.67)	3.44 (0.09)

Table A3 – *continued*

SN name	Age since discovery[a]	$\log\left(\frac{L_{\rm tot}}{\rm ergs^{-1}}\right)$	$\log\left(\frac{L_{\rm pk}}{\rm ergs^{-1}\,\AA^{-1}}\right)$	$v_{\rm pk}$ (100 km s^{-1})	HWHM (1000 km s^{-1})
SN 2004et	196	38.40 (0.05)	36.66 (0.04)	1.94 (0.10)	1.96 (0.06)
SN 2004et	202	38.30 (0.06)	36.57 (0.04)	0.77 (0.06)	1.93 (0.05)
SN 2004et	277	37.98 (0.03)	36.26 (0.03)	9.17 (0.46)	2.00 (0.04)
SN 2004et	349	37.68 (0.04)	36.01 (0.04)	10.29 (0.51)	2.29 (0.04)
SN 2005ay	284	38.49 (0.34)	37.00 (0.18)	0.59 (0.06)	0.93 (0.01)
SN 2005cs	157	37.45 (0.08)	35.82 (0.04)	18.49 (0.92)	2.07 (0.06)
SN 2005cs	303	37.32 (0.06)	35.68 (0.04)	11.43 (0.57)	2.01 (0.06)
SN 2006my	98	39.05 (0.03)	37.33 (0.03)	6.94 (0.35)	1.58 (0.03)
SN 2007gw	186	38.58 (0.07)	36.99 (0.07)	9.98 (0.50)	2.16 (0.13)
SN 2008ex	280	38.78 (0.10)	37.14 (0.07)	4.58 (0.23)	1.44 (0.05)
SN 2008ij	119	38.92 (0.13)	37.18 (0.10)	−2.66 (0.06)	2.35 (0.03)
SN 2008ij	149	37.62 (0.16)	36.08 (0.11)	−6.23 (0.06)	1.11 (0.04)
SN 2008ij	186	38.14 (0.11)	36.51 (0.08)	−0.29 (0.06)	1.60 (0.03)
SN 2011cj	227	39.10 (0.19)	37.54 (0.11)	−1.18 (0.06)	1.24 (0.03)
SN 2011fd	97	38.49 (0.15)	36.76 (0.11)	−7.37 (0.06)	1.83 (0.03)
SN 2011fd	185	38.56 (0.22)	37.00 (0.13)	1.20 (0.06)	1.26 (0.01)
SN 2012A	432	37.87 (0.49)	36.07 (0.22)	0.49 (0.06)	1.93 (0.03)
SN 2012aw[b]	337	38.05 (0.01)	36.39 (0.01)	10.53 (0.53)	1.80 (0.01)
SN 2012aw[b]	364	38.09 (0.16)	36.41 (0.12)	7.09 (0.35)	2.21 (0.06)
SN 2012ec	214	38.75 (0.08)	37.03 (0.08)	1.01 (0.06)	2.89 (0.08)
SN 2012ec	393	37.73 (0.12)	36.62 (0.09)	−0.45 (0.06)	0.55 (0.02)
SN 2012ho	154	38.92 (0.08)	37.40 (0.09)	−0.57 (0.06)	1.76 (0.06)
SN 2012ho	215	38.98 (0.10)	37.16 (0.08)	0.33 (0.06)	3.05 (0.07)
SN 2012ho	235	38.95 (0.11)	37.13 (0.09)	0.33 (0.06)	3.13 (0.06)
SN 2012ho	237	38.53 (0.13)	37.10 (0.11)	0.27 (0.06)	1.38 (0.07)
SN 2012ho	250	38.93 (0.10)	37.10 (0.08)	2.77 (0.14)	3.22 (0.07)
SN 2012ho	303	38.36 (0.13)	36.94 (0.09)	1.65 (0.08)	1.19 (0.05)
SN 2013ab[d]	143	39.17 (0.02)	37.52 (0.01)	4.91 (0.25)	1.62 (0.02)
SN 2013ab[d]	167	39.14 (0.06)	37.45 (0.04)	1.05 (0.06)	1.49 (0.03)
			H γ		
SN 1988A	162	38.47 (0.34)	36.96 (0.25)	−1.55 (0.07)	1.19 (0.02)
SN 1990E	151	38.35 (0.25)	36.54 (0.20)	18.12 (0.91)	2.37 (0.05)
SN 1992ad	225	38.39 (0.11)	36.74 (0.08)	6.58 (0.33)	2.34 (0.05)
SN 1992ad	286	38.20 (0.24)	36.63 (0.15)	22.82 (1.14)	1.55 (0.03)
SN 1999em	312	37.84 (0.11)	36.26 (0.08)	6.52 (0.33)	1.57 (0.04)
SN 1999em	332	37.92 (0.07)	36.31 (0.06)	−0.31 (0.07)	1.72 (0.03)
SN 1999em	418	37.85 (0.06)	36.23 (0.05)	−1.56 (0.07)	1.97 (0.05)
SN 2001X	176	38.30 (0.20)	36.78 (0.14)	−7.95 (0.07)	1.27 (0.02)
SN 2002hh	159	36.46 (0.78)	35.20 (0.70)	−7.05 (0.07)	0.91 (0.09)
SN 2002hh	336	36.68 (0.35)	35.17 (0.20)	−0.45 (0.07)	1.14 (0.01)
SN 2003hl	149	37.85 (0.43)	36.38 (0.32)	−6.76 (0.07)	1.10 (0.04)
SN 2004A	162	38.32 (0.17)	36.74 (0.12)	−7.04 (0.07)	1.31 (0.04)
SN 2004A	183	38.24 (0.20)	36.73 (0.14)	−2.81 (0.07)	1.21 (0.02)
SN 2004A	282	38.11 (0.12)	36.56 (0.09)	−3.01 (0.07)	1.26 (0.02)
SN 2004dj	106	38.22 (0.10)	36.63 (0.07)	−4.13 (0.07)	1.46 (0.02)
SN 2004dj	134	38.12 (0.11)	36.54 (0.07)	−6.90 (0.07)	1.44 (0.02)
SN 2004dj	169	38.05 (0.10)	36.47 (0.08)	−4.16 (0.07)	1.46 (0.03)
SN 2004dj	196	38.08 (0.11)	36.53 (0.08)	−5.54 (0.07)	1.38 (0.02)
SN 2004dj	223	38.02 (0.11)	36.46 (0.08)	−2.75 (0.07)	1.39 (0.03)
SN 2004dj	260	37.96 (0.10)	36.39 (0.08)	−1.43 (0.07)	1.41 (0.02)
SN 2004dj	398	37.85 (0.05)	36.22 (0.04)	2.75 (0.14)	1.96 (0.04)
SN 2004dj	407	37.83 (0.04)	36.20 (0.03)	4.12 (0.21)	2.08 (0.04)
SN 2004et	277	37.56 (0.03)	35.98 (0.03)	6.17 (0.31)	2.53 (0.04)
SN 2004et	349	37.24 (0.10)	35.85 (0.10)	3.76 (0.19)	1.73 (0.05)
SN 2005ay	284	38.05 (0.19)	36.60 (0.16)	−3.94 (0.07)	1.25 (0.03)
SN 2006my	98	38.37 (0.04)	36.87 (0.03)	−1.56 (0.07)	1.30 (0.01)
SN 2006ov	82	37.62 (0.20)	36.25 (0.17)	6.10 (0.30)	1.16 (0.05)
SN 2008ex	280	38.10 (0.70)	36.64 (0.43)	−7.54 (0.07)	1.01 (0.05)
SN 2008ij	119	38.51 (0.12)	36.80 (0.09)	−5.34 (0.07)	2.32 (0.03)
SN 2009ls	111	37.87 (0.05)	36.35 (0.04)	3.51 (0.18)	2.45 (0.05)
SN 2009ls	164	37.67 (0.08)	36.05 (0.07)	17.41 (0.87)	2.27 (0.08)
SN 2011cj	227	38.90 (0.12)	37.30 (0.09)	−1.52 (0.07)	2.10 (0.06)

Table A3 – *continued*

SN name	Age since discovery[a]	$\log\left(\frac{L_{\rm tot}}{\rm ergs^{-1}}\right)$	$\log\left(\frac{L_{\rm pk}}{\rm ergs^{-1}\,\AA^{-1}}\right)$	$v_{\rm pk}$ (100 km s^{-1})	HWHM (1000 km s^{-1})
SN 2011fd	97	38.22 (0.22)	36.70 (0.17)	−4.29 (0.07)	1.30 (0.04)
SN 2011fd	185	38.47 (0.15)	36.94 (0.12)	1.01 (0.07)	1.46 (0.01)
SN 2012A	432	37.90 (0.11)	36.01 (0.10)	6.61 (0.33)	3.75 (0.06)
SN 2012aw[b]	364	37.95 (0.10)	36.17 (0.09)	−2.03 (0.07)	4.03 (0.13)
SN 2012ch	335	39.18 (0.02)	37.23 (0.01)	21.15 (1.06)	8.86 (0.28)
SN 2012fg[c]	171	38.82 (0.32)	37.20 (0.30)	9.66 (0.48)	2.52 (0.22)
SN 2012ho	215	38.88 (0.03)	36.94 (0.02)	−4.12 (0.07)	6.86 (0.48)
SN 2012ho	235	38.99 (0.03)	37.01 (0.03)	27.74 (1.39)	7.86 (0.69)
SN 2012ho	250	38.79 (0.06)	36.99 (0.06)	−4.12 (0.07)	5.08 (0.30)
SN 2013ab[d]	167	38.45 (0.09)	36.87 (0.07)	−0.03 (0.07)	1.71 (0.04)

Notes. Uncertainties are in parentheses.
[a]Phases of spectra are in rest-frame days since discovery using the redshift and discovery date presented in Table A1.
[b]SN 2012aw is also known as PTF12bvh.
[c]SN 2012fg is also known as PTF12jxe.
[d]SN 2013ab is also known as iPTF13ut.
[e]SN 2013am is also known as iPTF13aaz.

Table A4. Spectral-feature measurements of helium.

SN name	Age since discovery[a]	$\log\left(\frac{L_{\rm tot}}{\rm ergs^{-1}}\right)$	$\log\left(\frac{L_{\rm pk}}{\rm ergs^{-1}\,\AA^{-1}}\right)$	$v_{\rm pk}$ (100 km s^{-1})	HWHM (1000 km s^{-1})
		He I λ5876			
SN 1988A	162	39.49 (0.04)	37.81 (0.03)	3.54 (0.18)	1.43 (0.03)
SN 1989L	182	38.95 (0.05)	37.05 (0.03)	9.70 (0.48)	2.91 (0.03)
SN 1990E	151	38.80 (0.05)	36.79 (0.04)	10.73 (0.54)	4.38 (0.08)
SN 1990E	165	38.71 (0.03)	36.61 (0.02)	2.79 (0.14)	5.42 (0.14)
SN 1990E	304	37.99 (0.16)	36.27 (0.14)	3.51 (0.18)	1.99 (0.09)
SN 1990H	193	39.08 (0.10)	37.52 (0.09)	−17.23 (0.05)	1.34 (0.03)
SN 1990K	205	38.51 (0.21)	36.95 (0.15)	−19.37 (0.05)	0.92 (0.02)
SN 1992ad	225	38.53 (0.06)	36.64 (0.06)	1.83 (0.09)	2.69 (0.03)
SN 1992ad	286	37.83 (0.16)	36.31 (0.12)	−5.20 (0.05)	1.06 (0.03)
SN 1992H	203	39.43 (0.11)	37.60 (0.09)	10.81 (0.54)	2.03 (0.04)
SN 1992H	221	39.45 (0.03)	37.47 (0.01)	2.85 (0.14)	2.82 (0.04)
SN 1992H	382	38.69 (0.09)	36.75 (0.08)	11.77 (0.59)	2.91 (0.09)
SN 1992H	425	38.56 (0.04)	36.52 (0.04)	−0.12 (0.05)	5.00 (0.18)
SN 1992H	461	38.55 (0.10)	36.43 (0.07)	15.84 (0.79)	3.73 (0.06)
SN 1992H	492	38.32 (0.16)	36.24 (0.11)	17.15 (0.86)	3.47 (0.24)
SN 1993G	114	38.46 (0.26)	36.90 (0.15)	0.87 (0.05)	0.86 (0.02)
SN 1999em	312	38.44 (0.04)	36.72 (0.02)	6.48 (0.32)	1.46 (0.03)
SN 1999em	332	38.44 (0.04)	36.68 (0.03)	5.45 (0.27)	1.62 (0.02)
SN 1999em	418	38.00 (0.06)	36.33 (0.05)	0.40 (0.05)	1.47 (0.03)
SN 1999em	516	37.31 (0.09)	35.58 (0.07)	0.44 (0.05)	1.74 (0.05)
SN 1999gq	83	38.92 (0.04)	37.22 (0.03)	3.98 (0.20)	2.25 (0.03)
SN 2001X	176	39.03 (0.04)	37.35 (0.04)	0.92 (0.05)	1.94 (0.04)
SN 2002hh	159	37.34 (0.09)	35.71 (0.08)	1.05 (0.05)	1.94 (0.04)
SN 2002hh	336	36.83 (0.10)	35.26 (0.09)	−10.07 (0.05)	1.48 (0.04)
SN 2002hh	394	36.82 (0.06)	34.86 (0.05)	12.99 (0.65)	3.36 (0.16)
SN 2003gd	138	38.29 (0.03)	36.60 (0.03)	5.09 (0.25)	1.40 (0.03)
SN 2003hl	149	38.21 (0.14)	36.45 (0.11)	−2.76 (0.05)	2.01 (0.05)
SN 2004A	162	38.92 (0.03)	37.24 (0.02)	−1.96 (0.05)	1.46 (0.03)
SN 2004A	183	38.81 (0.05)	37.15 (0.04)	0.09 (0.05)	1.35 (0.03)
SN 2004A	282	38.34 (0.06)	36.68 (0.04)	−0.83 (0.05)	1.28 (0.03)
SN 2004dj	106	38.98 (0.03)	37.02 (0.03)	−2.80 (0.05)	2.35 (0.05)
SN 2004dj	111	39.00 (0.09)	37.01 (0.07)	1.48 (0.07)	2.69 (0.07)
SN 2004dj	134	38.85 (0.04)	36.93 (0.03)	−4.78 (0.05)	2.24 (0.05)
SN 2004dj	140	38.86 (0.11)	36.89 (0.08)	3.93 (0.20)	2.56 (0.07)
SN 2004dj	169	38.68 (0.03)	36.77 (0.03)	−2.77 (0.05)	2.20 (0.05)
SN 2004dj	170	38.76 (0.12)	36.79 (0.09)	3.98 (0.20)	2.58 (0.08)

Table A4 – *continued*

SN name	Age since discovery[a]	$\log\left(\frac{L_{\rm tot}}{\rm ergs^{-1}}\right)$	$\log\left(\frac{L_{\rm pk}}{\rm ergs^{-1}\AA^{-1}}\right)$	$v_{\rm pk}$ (100 km s^{-1})	HWHM (1000 km s^{-1})
SN 2004dj	196	38.64 (0.03)	36.76 (0.02)	−0.74 (0.05)	2.07 (0.05)
SN 2004dj	223	38.50 (0.03)	36.63 (0.01)	0.25 (0.05)	1.98 (0.04)
SN 2004dj	225	38.58 (0.14)	36.65 (0.10)	3.88 (0.19)	2.30 (0.05)
SN 2004dj	254	38.52 (0.15)	36.58 (0.10)	6.42 (0.32)	2.33 (0.06)
SN 2004dj	260	38.38 (0.02)	36.52 (0.01)	1.25 (0.06)	1.95 (0.04)
SN 2004dj	398	38.06 (0.02)	36.20 (0.02)	3.26 (0.16)	2.06 (0.05)
SN 2004dj	407	37.96 (0.04)	36.16 (0.02)	2.21 (0.11)	1.80 (0.02)
SN 2004dj	635	37.48 (0.02)	35.65 (0.02)	1.27 (0.06)	2.78 (0.07)
SN 2004dj	875	36.45 (0.01)	35.45 (0.03)	−2.47 (0.05)	0.63 (0.04)
SN 2004dj	905	36.54 (0.01)	35.37 (0.01)	−2.98 (0.05)	1.26 (0.06)
SN 2004et	196	38.65 (0.02)	36.87 (0.02)	10.05 (0.50)	2.05 (0.02)
SN 2004et	202	38.68 (0.02)	36.84 (0.02)	9.08 (0.45)	2.21 (0.02)
SN 2004et	277	38.21 (0.03)	36.43 (0.03)	8.06 (0.40)	1.86 (0.02)
SN 2004et	349	37.64 (0.05)	36.06 (0.05)	7.24 (0.36)	1.73 (0.03)
SN 2005ay	284	38.27 (0.11)	36.67 (0.10)	2.48 (0.12)	1.38 (0.04)
SN 2005cs	157	37.78 (0.01)	36.21 (0.01)	9.95 (0.50)	1.82 (0.06)
SN 2005cs	303	37.50 (0.08)	35.80 (0.06)	6.11 (0.31)	1.52 (0.03)
SN 2006my	98	39.19 (0.01)	37.36 (0.01)	2.91 (0.15)	1.91 (0.03)
SN 2006ov	82	38.16 (0.03)	36.43 (0.03)	4.97 (0.25)	1.52 (0.03)
SN 2007gw	186	38.95 (0.04)	37.08 (0.05)	−4.85 (0.05)	2.93 (0.14)
SN 2008ex	280	39.33 (0.06)	37.49 (0.05)	6.64 (0.33)	2.18 (0.04)
SN 2008ij	119	39.27 (0.04)	37.38 (0.03)	6.85 (0.34)	2.67 (0.04)
SN 2008ij	149	37.98 (0.19)	36.26 (0.16)	14.01 (0.70)	1.82 (0.07)
SN 2008ij	186	38.46 (0.10)	36.69 (0.09)	5.86 (0.29)	1.77 (0.02)
SN 2009ls	111	38.79 (0.01)	36.97 (0.02)	2.70 (0.14)	3.19 (0.06)
SN 2009ls	164	38.19 (0.08)	36.61 (0.08)	6.61 (0.33)	2.09 (0.08)
SN 2011cj	227	38.80 (0.07)	37.27 (0.06)	−2.48 (0.05)	1.48 (0.04)
SN 2011fd	97	38.54 (0.08)	36.80 (0.04)	0.72 (0.05)	1.63 (0.04)
SN 2011fd	185	38.52 (0.08)	36.97 (0.07)	−1.35 (0.05)	1.34 (0.04)
SN 2012A	406	37.34 (0.17)	35.82 (0.10)	−0.10 (0.05)	0.86 (0.02)
SN 2012A	432	37.58 (0.11)	35.68 (0.08)	3.59 (0.18)	2.38 (0.06)
SN 2012aw[b]	337	38.47 (0.01)	36.74 (0.01)	−0.08 (0.05)	1.59 (0.02)
SN 2012aw[b]	364	38.54 (0.09)	36.65 (0.07)	3.39 (0.17)	2.04 (0.05)
SN 2012ch	335	39.03 (0.02)	37.13 (0.02)	0.92 (0.05)	6.96 (0.37)
SN 2012ec	214	38.76 (0.05)	36.95 (0.05)	5.98 (0.30)	2.70 (0.06)
SN 2012ec	393	38.20 (0.02)	36.40 (0.03)	4.96 (0.25)	2.85 (0.13)
SN 2012fg[c]	171	38.95 (0.11)	37.18 (0.10)	−5.36 (0.05)	2.41 (0.17)
SN 2012fg[c]	211	38.76 (0.09)	36.91 (0.08)	0.94 (0.05)	1.49 (0.10)
SN 2012ho	154	39.33 (0.02)	37.45 (0.01)	−0.89 (0.05)	2.45 (0.03)
SN 2012ho	215	39.07 (0.05)	37.11 (0.04)	−0.16 (0.05)	2.80 (0.06)
SN 2012ho	235	38.99 (0.05)	37.04 (0.03)	5.64 (0.28)	2.91 (0.05)
SN 2012ho	237	38.94 (0.02)	37.00 (0.02)	−0.40 (0.05)	2.63 (0.04)
SN 2012ho	250	38.91 (0.06)	36.99 (0.05)	−0.27 (0.05)	2.72 (0.05)
SN 2012ho	303	38.48 (0.10)	36.80 (0.10)	−3.81 (0.05)	1.98 (0.08)
SN 2013ab[d]	143	39.13 (0.01)	37.51 (0.01)	7.26 (0.36)	2.13 (0.02)
SN 2013ab[d]	167	39.04 (0.02)	37.38 (0.01)	8.05 (0.40)	2.21 (0.02)
SN 2013am[e]	256	37.75 (0.05)	36.23 (0.02)	6.34 (0.32)	0.84 (0.02)
SN 2013am[e]	461	37.43 (0.19)	35.91 (0.17)	6.74 (0.34)	1.02 (0.02)
			He I λ6678		
SN 1988A	162	39.15 (0.04)	37.61 (0.04)	−1.23 (0.04)	1.56 (0.03)
SN 1988A	182	38.61 (0.04)	37.09 (0.04)	−2.90 (0.05)	1.63 (0.03)
SN 1989L	182	38.51 (0.03)	37.02 (0.02)	−5.93 (0.04)	2.03 (0.12)
SN 1993K	282	37.98 (0.20)	36.66 (0.18)	−4.94 (0.04)	0.84 (0.09)
SN 1999em	312	37.49 (0.03)	36.44 (0.03)	−5.36 (0.05)	1.31 (0.22)
SN 1999em	418	37.24 (0.03)	35.89 (0.03)	−4.46 (0.05)	1.45 (0.15)
SN 1999em	516	36.69 (0.19)	35.14 (0.16)	−8.31 (0.05)	1.07 (0.11)
SN 2001X	176	38.66 (0.02)	37.21 (0.02)	−8.49 (0.05)	1.86 (0.07)
SN 2003gd	138	37.56 (0.02)	36.30 (0.02)	0.62 (0.04)	1.95 (0.10)
SN 2003hl	149	37.65 (0.10)	36.33 (0.10)	−1.82 (0.05)	0.94 (0.12)
SN 2004A	162	38.59 (0.03)	37.05 (0.02)	−12.10 (0.05)	2.09 (0.07)
SN 2004A	183	38.47 (0.04)	36.97 (0.04)	−6.11 (0.05)	1.65 (0.03)

Table A4 – *continued*

SN name	Age since discovery[a]	$\log\left(\frac{L_{\rm tot}}{\rm ergs^{-1}}\right)$	$\log\left(\frac{L_{\rm pk}}{\rm ergs^{-1}\AA^{-1}}\right)$	$v_{\rm pk}$ (100 km s^{-1})	HWHM (1000 km s^{-1})
SN 2004A	282	37.86 (0.02)	36.50 (0.02)	−10.30 (0.05)	1.45 (0.12)
SN 2004dj	398	37.36 (0.02)	35.84 (0.02)	−0.87 (0.04)	2.08 (0.03)
SN 2004dj	407	37.43 (0.02)	35.84 (0.02)	−3.50 (0.05)	2.36 (0.04)
SN 2004dj	635	37.10 (0.01)	35.49 (0.01)	−5.40 (0.05)	2.27 (0.09)
SN 2005ay	284	37.80 (0.22)	36.50 (0.17)	−3.60 (0.05)	1.00 (0.08)
SN 2005cs	157	37.30 (0.02)	35.90 (0.02)	3.14 (0.16)	1.16 (0.02)
SN 2005cs	303	36.97 (0.08)	35.44 (0.07)	1.38 (0.07)	1.32 (0.05)
SN 2008ex	280	39.02 (0.03)	37.49 (0.03)	−5.27 (0.04)	2.17 (0.12)
SN 2008ij	119	38.99 (0.04)	37.46 (0.03)	−2.54 (0.05)	1.90 (0.05)
SN 2008ij	149	37.79 (0.04)	36.36 (0.05)	−7.63 (0.05)	1.81 (0.42)
SN 2008ij	186	38.05 (0.02)	36.69 (0.02)	−3.15 (0.04)	2.44 (0.41)
SN 2009ls	164	37.91 (0.01)	36.62 (0.01)	0.67 (0.04)	2.41 (0.29)
SN 2011cj	227	38.63 (0.06)	37.20 (0.04)	−4.26 (0.05)	2.33 (0.29)
SN 2011fd	97	38.16 (0.03)	36.81 (0.02)	−14.66 (0.05)	2.45 (0.61)
SN 2011fd	185	38.28 (0.05)	36.86 (0.04)	−6.61 (0.05)	1.40 (0.12)
SN 2012aw[b]	337	37.70 (0.01)	36.45 (0.01)	−4.15 (0.05)	1.90 (0.18)
SN 2012ec	393	37.42 (0.02)	36.30 (0.02)	−1.20 (0.04)	0.83 (0.03)
SN 2013am[e]	256	37.37 (0.05)	35.90 (0.03)	2.33 (0.12)	0.93 (0.03)
			He I λ7065		
SN 1988A	162	39.35 (0.03)	37.61 (0.02)	1.80 (0.09)	1.78 (0.03)
SN 1988A	182	38.79 (0.03)	37.11 (0.02)	1.75 (0.09)	1.47 (0.02)
SN 1989L	182	38.36 (0.04)	37.03 (0.04)	3.19 (0.16)	1.55 (0.06)
SN 1993K	282	37.77 (0.46)	36.37 (0.30)	−2.53 (0.04)	0.44 (0.01)
SN 1999em	312	37.74 (0.04)	36.38 (0.04)	3.04 (0.15)	1.12 (0.05)
SN 1999em	332	37.60 (0.03)	36.31 (0.03)	−0.18 (0.04)	1.17 (0.07)
SN 1999em	418	37.14 (0.03)	35.81 (0.03)	−0.38 (0.04)	1.19 (0.09)
SN 2001X	176	38.85 (0.02)	37.16 (0.02)	−1.24 (0.04)	1.58 (0.03)
SN 2003gd	138	37.96 (0.02)	36.27 (0.02)	0.28 (0.04)	1.78 (0.04)
SN 2003hl	149	37.83 (0.04)	36.29 (0.04)	−1.07 (0.04)	1.01 (0.14)
SN 2004A	162	38.62 (0.05)	37.10 (0.04)	−5.09 (0.04)	1.26 (0.03)
SN 2004A	183	38.53 (0.04)	37.04 (0.03)	−3.41 (0.04)	1.15 (0.02)
SN 2004A	282	38.01 (0.05)	36.53 (0.04)	−4.26 (0.04)	0.99 (0.01)
SN 2004dj	106	38.22 (0.03)	36.64 (0.03)	−10.73 (0.04)	1.73 (0.03)
SN 2004dj	134	38.12 (0.04)	36.59 (0.04)	−9.93 (0.04)	1.46 (0.02)
SN 2004dj	140	38.15 (0.06)	36.56 (0.06)	−6.98 (0.04)	3.18 (0.03)
SN 2004dj	169	37.97 (0.03)	36.49 (0.03)	−7.44 (0.04)	1.63 (0.02)
SN 2004dj	170	38.01 (0.07)	36.47 (0.07)	−10.62 (0.04)	2.87 (0.04)
SN 2004dj	196	37.93 (0.03)	36.45 (0.03)	−7.44 (0.04)	1.71 (0.03)
SN 2004dj	223	37.71 (0.02)	36.31 (0.01)	1.29 (0.06)	2.35 (0.02)
SN 2004dj	225	37.82 (0.10)	36.34 (0.10)	−8.60 (0.04)	2.57 (0.03)
SN 2004dj	254	37.81 (0.11)	36.26 (0.12)	−10.62 (0.04)	2.57 (0.03)
SN 2004dj	260	37.82 (0.01)	36.22 (0.01)	−0.51 (0.04)	2.05 (0.02)
SN 2004dj	398	37.42 (0.02)	35.87 (0.02)	0.29 (0.04)	1.47 (0.02)
SN 2004dj	407	37.43 (0.02)	35.85 (0.02)	0.32 (0.04)	1.60 (0.02)
SN 2004dj	635	37.09 (0.02)	35.47 (0.02)	−2.08 (0.04)	1.87 (0.04)
SN 2005ay	284	38.04 (0.05)	36.43 (0.04)	−1.32 (0.04)	1.38 (0.05)
SN 2005cs	157	37.37 (0.03)	35.84 (0.02)	−3.13 (0.04)	1.29 (0.03)
SN 2005cs	303	36.98 (0.09)	35.48 (0.07)	−0.35 (0.04)	0.91 (0.06)
SN 2008ex	280	38.76 (0.04)	37.34 (0.03)	4.36 (0.22)	2.35 (0.45)
SN 2008ij	119	38.69 (0.02)	37.19 (0.02)	1.10 (0.06)	2.30 (0.06)
SN 2008ij	149	37.55 (0.11)	36.09 (0.11)	−2.15 (0.04)	0.97 (0.16)
SN 2008ij	186	37.87 (0.02)	36.43 (0.02)	2.71 (0.14)	1.52 (0.21)
SN 2009ls	111	38.25 (0.03)	36.74 (0.02)	7.68 (0.38)	1.75 (0.03)
SN 2009ls	164	38.38 (0.01)	36.56 (0.01)	5.99 (0.30)	1.98 (0.02)
SN 2011cj	227	38.78 (0.01)	37.14 (0.01)	0.68 (0.04)	1.67 (0.02)
SN 2011fd	97	38.39 (0.04)	36.71 (0.03)	−4.91 (0.04)	1.72 (0.09)
SN 2011fd	185	38.31 (0.04)	36.79 (0.03)	−1.49 (0.04)	1.50 (0.15)
SN 2012aw[b]	337	37.80 (0.01)	36.37 (0.01)	−2.22 (0.04)	1.63 (0.02)
SN 2012ec	393	37.77 (0.03)	36.20 (0.02)	−2.44 (0.04)	1.68 (0.11)
SN 2013ab[d]	167	38.91 (0.01)	37.22 (0.01)	5.74 (0.29)	2.38 (0.03)

Table A4 – *continued*

SN name	Age since discovery[a]	$\log\left(\frac{L_{tot}}{ergs^{-1}}\right)$	$\log\left(\frac{L_{pk}}{ergs^{-1}\text{Å}^{-1}}\right)$	v_{pk} (100 km s^{-1})	HWHM (1000 km s^{-1})
SN 2013am[e]	256	37.49 (0.06)	36.13 (0.05)	2.12 (0.11)	0.56 (0.01)

Notes. Uncertainties are in parentheses.
[a]Phases of spectra are in rest-frame days since discovery using the redshift and discovery date presented in Table A1.
[b]SN 2012aw is also known as PTF12bvh.
[c]SN 2012fg is also known as PTF12jxe.
[d]SN 2013ab is also known as iPTF13ut.
[e]SN 2013am is also known as iPTF13aaz.

Table A5. Spectral-feature measurements of oxygen.

SN name	Age since discovery[a]	$\log\left(\frac{L_{tot}}{ergs^{-1}}\right)$	$\log\left(\frac{L_{pk}}{ergs^{-1}\text{Å}^{-1}}\right)$	v_{pk}[b] (100 km s^{-1})	HWHM$_1$[c] (1000 km s^{-1})	HWHM$_2$[d] (1000 km s^{-1})
			[O I] λλ6300,6364			
SN 1988A	162	39.65 (0.03)	37.64 (0.03)	−0.17 (0.05)	2.85 (0.18)	1.48 (0.08)
SN 1988A	182	39.24 (0.04)	37.20 (0.05)	−0.20 (0.05)	2.62 (0.25)	1.53 (0.10)
SN 1988H	119	39.34 (0.04)	37.37 (0.04)	−5.80 (0.05)	1.82 (0.07)	1.28 (0.05)
SN 1989L	182	39.06 (0.05)	37.09 (0.06)	−2.86 (0.05)	2.03 (0.05)	1.35 (0.06)
SN 1990E	151	38.80 (0.09)	36.75 (0.08)	−5.12 (0.05)	2.42 (0.14)	1.73 (0.09)
SN 1990E	165	38.75 (0.04)	36.63 (0.03)	1.15 (0.06)	4.12 (0.67)	1.72 (0.46)
SN 1990E	304	38.54 (0.06)	36.66 (0.05)	−2.22 (0.05)	1.39 (0.04)	0.91 (0.05)
SN 1990H	193	39.43 (0.13)	37.63 (0.11)	2.93 (0.15)	0.81 (0.03)	1.69 (0.16)
SN 1990K	147	39.09 (0.04)	37.16 (0.04)	−0.85 (0.05)	2.25 (0.22)	1.38 (0.13)
SN 1990K	205	38.82 (0.09)	36.99 (0.09)	−30.68 (0.05)	1.18 (0.07)	1.01 (0.10)
SN 1992ad	225	39.05 (0.02)	37.04 (0.01)	−7.30 (0.05)	1.61 (0.02)	1.79 (0.05)
SN 1992ad	286	38.77 (0.02)	36.75 (0.02)	−8.24 (0.05)	1.54 (0.02)	1.96 (0.07)
SN 1992bt	235	38.65 (0.48)	36.85 (0.31)	−4.12 (0.05)	1.41 (0.13)	0.73 (0.05)
SN 1992H	203	39.64 (0.05)	37.62 (0.06)	−11.35 (0.05)	3.01 (0.20)	1.67 (0.12)
SN 1992H	221	39.59 (0.03)	37.58 (0.03)	−5.74 (0.05)	2.34 (0.04)	1.50 (0.04)
SN 1992H	382	39.10 (0.03)	37.18 (0.02)	−4.87 (0.05)	1.34 (0.03)	1.64 (0.10)
SN 1992H	425	38.92 (0.05)	36.76 (0.05)	−4.33 (0.05)	2.78 (0.09)	2.57 (0.23)
SN 1992H	461	38.85 (0.11)	36.74 (0.07)	2.96 (0.15)	2.73 (0.02)	1.43 (0.07)
SN 1992H	492	38.62 (0.09)	36.50 (0.06)	1.04 (0.05)	2.70 (0.16)	2.04 (0.50)
SN 1993G	114	38.90 (0.17)	37.08 (0.17)	−7.58 (0.05)	0.98 (0.04)	0.96 (0.06)
SN 1993K	282	38.85 (0.12)	36.98 (0.06)	−4.64 (0.05)	0.96 (0.03)	1.14 (0.08)
SN 1999em	312	38.87 (0.04)	36.89 (0.03)	−3.59 (0.05)	1.23 (0.02)	1.90 (0.07)
SN 1999em	332	38.80 (0.05)	36.85 (0.03)	−1.71 (0.05)	1.19 (0.02)	1.57 (0.05)
SN 1999em	418	38.50 (0.04)	36.60 (0.03)	−1.70 (0.05)	1.05 (0.01)	1.49 (0.04)
SN 1999em	516	37.62 (0.11)	35.79 (0.09)	−0.72 (0.05)	0.82 (0.02)	2.26 (0.16)
SN 1999gq	83	39.22 (0.02)	37.20 (0.01)	−4.73 (0.05)	2.83 (0.79)	2.77 (2.14)
SN 2001X	176	39.28 (0.02)	37.23 (0.02)	−8.29 (0.05)	2.01 (0.05)	1.86 (0.05)
SN 2002hh	159	37.69 (0.07)	35.82 (0.05)	2.21 (0.11)	2.11 (0.08)	1.36 (0.29)
SN 2002hh	336	37.34 (0.04)	35.25 (0.03)	8.78 (0.44)	2.32 (0.24)	1.87 (0.20)
SN 2002hh	394	37.04 (0.03)	35.14 (0.04)	4.07 (0.20)	1.61 (0.12)	1.73 (0.30)
SN 2003gd	138	38.67 (0.04)	36.75 (0.02)	0.77 (0.05)	1.37 (0.02)	0.99 (0.03)
SN 2003hl	149	38.33 (0.04)	36.39 (0.04)	−3.77 (1.33)	1.24 (0.30)	1.11 (0.19)
SN 2004A	162	39.18 (0.02)	37.15 (0.02)	−9.63 (0.05)	2.12 (0.04)	1.62 (0.03)
SN 2004A	183	39.11 (0.03)	37.12 (0.02)	−5.87 (0.05)	1.58 (0.04)	1.56 (0.06)
SN 2004A	282	38.87 (0.05)	36.97 (0.03)	−5.86 (0.05)	1.12 (0.01)	1.30 (0.03)
SN 2004dj	106	38.78 (0.03)	36.78 (0.03)	−15.82 (0.05)	1.64 (0.05)	2.01 (0.09)
SN 2004dj	111	38.95 (0.09)	36.75 (0.06)	−16.43 (0.05)	3.58 (0.25)	2.29 (0.23)
SN 2004dj	134	38.77 (0.04)	36.75 (0.04)	−13.95 (0.05)	1.63 (0.06)	1.85 (0.10)
SN 2004dj	140	38.89 (0.11)	36.69 (0.06)	−14.01 (0.05)	2.91 (0.28)	2.81 (0.41)
SN 2004dj	169	38.73 (0.04)	36.70 (0.04)	−11.12 (0.05)	1.63 (0.06)	1.89 (0.12)
SN 2004dj	170	38.81 (0.10)	36.68 (0.06)	−4.62 (0.05)	2.39 (0.07)	2.48 (0.12)
SN 2004dj	196	38.76 (0.06)	36.75 (0.05)	−10.21 (0.05)	1.83 (0.08)	1.46 (0.13)
SN 2004dj	223	38.71 (0.06)	36.68 (0.05)	−9.16 (0.05)	1.57 (0.04)	1.66 (0.07)
SN 2004dj	225	38.83 (0.11)	36.73 (0.06)	−4.57 (0.05)	2.27 (0.05)	2.23 (0.11)
SN 2004dj	254	38.82 (0.12)	36.75 (0.07)	−2.18 (0.05)	2.06 (0.03)	2.36 (0.09)

Table A5 – *continued*

SN name	Age since discovery[a]	$\log\left(\frac{L_{\rm tot}}{\rm ergs^{-1}}\right)$	$\log\left(\frac{L_{\rm pk}}{\rm ergs^{-1}\,\AA^{-1}}\right)$	$v_{\rm pk}$[b] (100 km s^{-1})	HWHM$_1$[c] (1000 km s^{-1})	HWHM$_2$[d] (1000 km s^{-1})
SN 2004dj	260	38.70 (0.03)	36.70 (0.03)	−1.64 (0.05)	1.66 (0.02)	1.31 (0.03)
SN 2004dj	398	38.51 (0.06)	36.67 (0.05)	1.23 (0.06)	1.07 (0.01)	1.00 (0.03)
SN 2004dj	407	38.50 (0.06)	36.66 (0.05)	0.28 (0.05)	1.07 (0.01)	0.97 (0.03)
SN 2004dj	635	37.86 (0.19)	36.14 (0.12)	−1.52 (0.05)	0.73 (0.01)	1.01 (0.02)
SN 2004dj	875	37.47 (0.03)	35.81 (0.04)	−1.14 (0.05)	0.80 (0.02)	1.03 (0.05)
SN 2004dj	905	37.42 (0.04)	35.69 (0.05)	−1.43 (0.05)	0.97 (0.04)	1.35 (0.15)
SN 2004dj	1199	37.38 (0.02)	35.53 (0.03)	−1.56 (0.05)	1.34 (0.10)	1.56 (0.25)
SN 2004et	196	38.98 (0.02)	36.98 (0.01)	−2.68 (0.05)	2.11 (0.08)	1.30 (0.05)
SN 2004et	202	38.97 (0.02)	36.97 (0.02)	−1.72 (0.05)	2.04 (0.09)	1.40 (0.06)
SN 2004et	277	38.69 (0.04)	36.76 (0.03)	−3.60 (0.05)	1.29 (0.02)	1.54 (0.06)
SN 2004et	349	38.45 (0.04)	36.54 (0.03)	−0.78 (0.05)	1.16 (0.02)	1.95 (0.14)
SN 2005ay	284	38.83 (0.04)	36.90 (0.02)	−4.49 (0.05)	1.12 (0.01)	1.75 (0.04)
SN 2005cs	303	37.74 (0.09)	35.78 (0.05)	2.75 (0.14)	1.42 (0.03)	0.97 (0.03)
SN 2006my	98	39.41 (0.01)	37.24 (0.01)	−5.36 (0.05)	3.91 (0.14)	1.81 (0.12)
SN 2006ov	82	38.33 (0.03)	36.39 (0.03)	0.88 (0.05)	1.64 (0.04)	1.27 (0.06)
SN 2007gw	186	39.16 (0.02)	37.09 (0.02)	−18.45 (0.05)	1.80 (0.27)	2.56 (0.45)
SN 2008ex	280	39.72 (0.03)	37.65 (0.04)	−0.72 (0.05)	1.51 (0.05)	2.05 (0.10)
SN 2008ij	119	39.30 (0.03)	37.33 (0.04)	1.13 (0.06)	2.33 (0.39)	2.22 (0.37)
SN 2008ij	149	38.26 (0.11)	36.32 (0.08)	−2.66 (0.05)	1.76 (0.07)	1.14 (0.08)
SN 2008ij	186	38.69 (0.04)	36.75 (0.03)	1.12 (0.06)	1.58 (0.08)	1.41 (0.09)
SN 2009ls	111	38.64 (0.02)	36.73 (0.02)	0.31 (0.05)	2.44 (0.11)	1.30 (0.05)
SN 2009ls	164	38.63 (0.02)	36.57 (0.02)	−1.78 (0.05)	2.60 (0.07)	1.90 (0.11)
SN 2011cj	227	39.32 (0.02)	37.31 (0.02)	−0.62 (0.05)	1.89 (0.08)	1.52 (0.08)
SN 2011fd	97	38.67 (0.02)	36.72 (0.02)	−11.23 (0.95)	1.25 (0.13)	1.39 (0.12)
SN 2011fd	185	39.02 (0.03)	37.03 (0.02)	−6.95 (0.05)	1.71 (0.06)	1.20 (0.04)
SN 2012A	406	38.21 (0.03)	36.44 (0.02)	−3.69 (0.05)	0.95 (0.01)	1.29 (0.04)
SN 2012A	432	38.00 (0.19)	36.05 (0.13)	−2.40 (0.05)	1.43 (0.02)	1.48 (0.05)
SN 2012aw[e]	337	38.99 (0.01)	37.08 (0.01)	−6.05 (0.05)	1.08 (0.01)	1.54 (0.03)
SN 2012aw[e]	364	38.96 (0.16)	36.97 (0.12)	−2.66 (0.05)	1.46 (0.02)	1.57 (0.04)
SN 2012ch	335	39.39 (0.02)	37.23 (0.02)	0.20 (0.05)	3.77 (0.17)	2.29 (0.22)
SN 2012ec	214	39.02 (0.06)	36.99 (0.05)	−13.64 (0.05)	2.04 (0.29)	1.97 (0.42)
SN 2012ec	393	38.46 (0.02)	36.54 (0.01)	−3.40 (0.05)	1.51 (0.03)	1.50 (0.06)
SN 2012fg[f]	171	39.36 (0.06)	37.30 (0.04)	−0.01 (0.05)	2.79 (0.58)	1.49 (0.48)
SN 2012fg[f]	211	39.23 (0.06)	37.10 (0.05)	−8.24 (0.05)	2.52 (0.19)	1.62 (0.17)
SN 2012ho	154	39.46 (0.02)	37.49 (0.01)	−7.05 (0.05)	1.98 (0.05)	1.43 (0.03)
SN 2012ho	215	39.37 (0.06)	37.29 (0.05)	−5.47 (0.05)	2.47 (0.08)	1.56 (0.08)
SN 2012ho	235	39.30 (0.06)	37.23 (0.05)	−1.87 (0.05)	2.57 (0.08)	1.40 (0.13)
SN 2012ho	237	39.21 (0.01)	37.27 (0.01)	−6.10 (0.05)	1.56 (0.02)	1.26 (0.03)
SN 2012ho	250	39.29 (0.07)	37.24 (0.06)	−3.60 (0.05)	2.07 (0.08)	1.57 (0.11)
SN 2012ho	303	39.09 (0.06)	37.21 (0.06)	−2.65 (0.05)	1.17 (0.02)	1.66 (0.07)
SN 2013ab[g]	143	39.45 (0.01)	37.45 (0.01)	0.49 (0.05)	2.60 (0.23)	1.91 (0.24)
SN 2013ab[g]	167	39.39 (0.02)	37.40 (0.02)	−0.66 (0.05)	2.16 (0.11)	1.52 (0.12)
SN 2013am[h]	256	38.09 (0.08)	36.27 (0.06)	−0.46 (0.05)	1.07 (0.05)	0.83 (0.03)
SN 2013am[h]	461	37.93 (0.14)	36.37 (0.06)	0.45 (0.05)	0.51 (0.01)	0.67 (0.03)
			K I λ7682, O I λ7774			
SN 1988A	162	39.77 (0.04)	37.74 (0.02)	11.76 (0.24)	1.59 (0.05)	1.10 (0.08)
SN 1988A	182	39.20 (0.03)	37.21 (0.01)	11.03 (0.20)	1.36 (0.03)	0.93 (0.03)
SN 1990E	195	38.72 (0.07)	36.70 (0.07)	−2.12 (1.33)	1.25 (0.10)	1.80 (0.16)
SN 1990E	304	37.98 (0.17)	36.01 (0.09)	−2.98 (1.28)	0.75 (0.02)	1.25 (0.04)
SN 1990H	193	39.39 (0.08)	37.43 (0.05)	8.11 (0.05)	1.25 (0.08)	1.57 (0.21)
SN 1992ad	225	38.51 (0.10)	36.46 (0.08)	10.28 (0.16)	2.11 (0.12)	1.29 (0.12)
SN 1992ad	286	38.11 (0.14)	36.09 (0.10)	13.36 (0.32)	1.65 (0.12)	1.03 (0.09)
SN 1992H	461	38.28 (0.20)	36.25 (0.13)	16.70 (0.48)	1.91 (0.27)	1.15 (0.29)
SN 1992H	492	38.06 (0.21)	36.08 (0.15)	8.41 (0.07)	1.69 (1.40)	1.17 (0.95)
SN 1999em	312	38.49 (0.06)	36.59 (0.02)	12.85 (0.29)	1.14 (0.03)	1.22 (0.10)
SN 1999em	418	37.97 (0.07)	36.03 (0.05)	14.30 (0.36)	1.48 (0.02)	1.17 (0.20)
SN 1999gq	83	39.19 (0.03)	37.07 (0.02)	2.63 (0.04)	2.41 (0.05)	1.39 (0.04)
SN 2001X	176	39.25 (0.02)	37.22 (0.02)	6.81 (0.04)	1.22 (0.04)	1.19 (0.04)
SN 2002hh	159	38.34 (0.01)	36.31 (0.01)	−6.49 (1.11)	1.22 (0.03)	2.21 (0.06)
SN 2002hh	394	37.29 (0.03)	35.12 (0.02)	16.33 (0.47)	2.80 (0.33)	1.35 (0.37)
SN 2003gd	138	38.43 (0.02)	36.47 (0.01)	11.09 (0.20)	1.27 (0.01)	0.89 (0.02)
SN 2003hl	149	38.59 (0.05)	36.53 (0.04)	6.24 (0.04)	1.19 (0.07)	2.18 (0.23)

Table A5 – *continued*

SN name	Age since discovery[a]	$\log\left(\frac{L_{\rm tot}}{\rm ergs^{-1}}\right)$	$\log\left(\frac{L_{\rm pk}}{\rm ergs^{-1}\,\AA^{-1}}\right)$	$v_{\rm pk}$[b] (100 km s^{-1})	HWHM$_1$[c] (1000 km s^{-1})	HWHM$_2$[d] (1000 km s^{-1})
SN 2004A	162	39.15 (0.04)	37.15 (0.02)	4.56 (0.04)	1.17 (0.03)	0.97 (0.03)
SN 2004A	183	39.07 (0.04)	37.08 (0.02)	6.86 (0.04)	1.22 (0.03)	0.94 (0.03)
SN 2004A	282	38.49 (0.03)	36.56 (0.02)	9.94 (0.15)	1.18 (0.02)	0.97 (0.04)
SN 2004dj	106	38.79 (0.04)	36.84 (0.02)	3.13 (0.04)	1.29 (0.03)	0.96 (0.04)
SN 2004dj	111	38.88 (0.08)	36.82 (0.06)	−0.53 (0.04)	1.83 (0.03)	1.96 (0.08)
SN 2004dj	134	38.78 (0.03)	36.83 (0.02)	3.10 (0.04)	1.39 (0.02)	0.89 (0.04)
SN 2004dj	140	38.82 (0.09)	36.78 (0.07)	3.18 (0.04)	1.82 (0.01)	1.57 (0.04)
SN 2004dj	169	38.66 (0.02)	36.70 (0.01)	6.20 (0.04)	1.39 (0.03)	1.19 (0.09)
SN 2004dj	170	38.70 (0.09)	36.67 (0.07)	3.17 (0.04)	1.81 (0.01)	1.39 (0.02)
SN 2004dj	196	38.62 (0.02)	36.63 (0.01)	7.01 (0.04)	1.37 (0.02)	1.32 (0.06)
SN 2004dj	223	38.45 (0.02)	36.46 (0.02)	8.56 (0.08)	1.37 (0.02)	1.17 (0.04)
SN 2004dj	225	38.55 (0.11)	36.48 (0.08)	5.20 (0.04)	1.70 (0.01)	1.70 (0.04)
SN 2004dj	254	38.47 (0.11)	36.39 (0.09)	5.20 (0.04)	1.72 (0.01)	1.63 (0.03)
SN 2004dj	260	38.31 (0.03)	36.33 (0.03)	8.56 (0.08)	1.42 (0.03)	0.89 (0.04)
SN 2004dj	398	37.88 (0.03)	35.84 (0.01)	9.36 (0.12)	1.84 (0.03)	0.95 (0.02)
SN 2004dj	407	37.86 (0.03)	35.81 (0.01)	8.61 (0.08)	1.86 (0.03)	1.02 (0.02)
SN 2004et	196	38.95 (0.02)	36.88 (0.01)	12.50 (0.27)	1.54 (0.03)	1.37 (0.05)
SN 2004et	202	38.90 (0.01)	36.89 (0.01)	11.72 (0.24)	1.48 (0.03)	1.03 (0.04)
SN 2004et	277	38.43 (0.01)	36.38 (0.01)	14.82 (0.39)	1.57 (0.03)	1.37 (0.06)
SN 2004et	349	37.99 (0.02)	35.98 (0.01)	13.26 (0.31)	1.72 (0.01)	1.06 (0.03)
SN 2005ay	284	38.37 (0.06)	36.54 (0.04)	11.89 (0.24)	1.31 (0.06)	0.70 (0.11)
SN 2005cs	157	38.23 (0.01)	36.30 (0.01)	13.42 (0.32)	1.31 (0.01)	0.93 (0.01)
SN 2005cs	303	37.64 (0.13)	35.70 (0.11)	18.44 (0.57)	1.35 (0.04)	1.10 (0.11)
SN 2006my	98	39.27 (0.02)	37.26 (0.02)	10.53 (0.18)	1.32 (0.02)	1.26 (0.04)
SN 2006ov	82	38.28 (0.02)	36.35 (0.01)	13.40 (0.32)	1.31 (0.01)	1.09 (0.03)
SN 2007gw	186	39.08 (0.04)	37.06 (0.02)	−3.18 (1.27)	1.51 (0.40)	1.62 (0.36)
SN 2008ex	280	39.43 (0.06)	37.45 (0.04)	10.09 (0.15)	1.58 (0.03)	1.06 (0.06)
SN 2008ij	119	39.38 (0.03)	37.28 (0.02)	1.59 (1.51)	1.62 (0.09)	2.04 (0.08)
SN 2008ij	149	38.13 (0.15)	36.15 (0.11)	14.55 (0.38)	1.14 (0.04)	1.04 (0.03)
SN 2008ij	186	38.64 (0.06)	36.53 (0.03)	4.45 (0.04)	1.91 (0.08)	1.35 (0.10)
SN 2009ls	164	38.53 (0.04)	36.48 (0.02)	2.50 (1.56)	1.02 (0.07)	2.07 (0.09)
SN 2011cj	227	39.15 (0.05)	37.13 (0.05)	8.68 (0.08)	1.46 (0.04)	1.28 (0.06)
SN 2011fd	97	38.87 (0.06)	36.83 (0.05)	3.00 (0.04)	1.15 (0.03)	1.46 (0.05)
SN 2011fd	185	38.91 (0.05)	36.94 (0.03)	6.81 (0.04)	1.31 (0.03)	0.92 (0.04)
SN 2012aw[e]	337	38.59 (0.01)	36.60 (0.01)	11.16 (0.21)	1.43 (0.01)	1.11 (0.03)
SN 2012aw[e]	364	38.40 (0.08)	36.38 (0.06)	11.11 (0.20)	1.58 (0.02)	1.21 (0.05)
SN 2012ch	335	39.12 (0.02)	37.03 (0.02)	14.75 (0.39)	3.73 (0.55)	0.95 (0.83)
SN 2012ec	214	38.76 (0.10)	36.81 (0.07)	11.56 (0.23)	1.02 (0.04)	1.40 (0.07)
SN 2012fg[f]	171	39.14 (0.11)	37.08 (0.09)	25.77 (0.94)	2.10 (0.48)	1.22 (0.31)
SN 2012fg[f]	211	38.80 (0.12)	36.70 (0.07)	0.59 (0.04)	1.38 (0.25)	1.40 (0.25)
SN 2012ho	154	39.41 (0.02)	37.32 (0.02)	0.57 (0.04)	1.30 (0.03)	1.88 (0.05)
SN 2012ho	215	39.10 (0.06)	36.98 (0.05)	8.00 (0.05)	1.74 (0.08)	1.97 (0.15)
SN 2012ho	235	38.99 (0.05)	36.87 (0.04)	7.99 (0.05)	1.96 (0.24)	1.53 (0.30)
SN 2012ho	237	38.92 (0.02)	36.91 (0.01)	8.29 (0.06)	1.53 (0.02)	1.16 (0.03)
SN 2012ho	250	38.85 (0.05)	36.77 (0.04)	7.98 (0.05)	1.81 (0.10)	1.50 (0.17)
SN 2012ho	303	38.44 (0.15)	36.66 (0.10)	12.83 (0.29)	0.80 (0.04)	0.74 (0.05)
SN 2013ab[g]	143	39.50 (0.01)	37.37 (0.01)	9.50 (0.12)	1.70 (0.03)	1.53 (0.04)
SN 2013ab[g]	167	39.39 (0.02)	37.27 (0.02)	10.95 (0.20)	1.74 (0.05)	1.44 (0.05)
SN 2013am[h]	256	38.13 (0.03)	36.32 (0.01)	14.00 (0.35)	0.99 (0.02)	1.11 (0.08)
SN 2013am[h]	461	37.59 (0.31)	35.74 (0.15)	18.30 (0.56)	1.32 (0.08)	0.84 (0.10)
			O I λ8446			
SN 1988A	162	38.42 (0.16)	37.05 (0.14)	−6.25 (0.04)	0.66 (0.01)	–
SN 1992ad	286	37.71 (0.11)	36.20 (0.10)	0.94 (0.05)	0.91 (0.02)	–
SN 1992H	382	38.10 (0.18)	36.62 (0.15)	2.90 (0.15)	0.62 (0.01)	–
SN 1992H	461	37.65 (0.68)	36.00 (0.61)	8.28 (0.41)	0.87 (0.17)	–
SN 2002hh	336	36.76 (0.05)	35.37 (0.05)	4.03 (0.20)	1.03 (0.06)	–
SN 2004A	282	38.31 (0.09)	36.82 (0.07)	−7.40 (0.04)	0.67 (0.01)	–
SN 2004dj	106	37.96 (0.08)	36.58 (0.06)	0.35 (0.04)	1.24 (0.02)	–
SN 2004dj	134	38.07 (0.09)	36.67 (0.06)	4.50 (0.22)	1.13 (0.03)	–
SN 2004dj	169	38.03 (0.09)	36.66 (0.06)	3.19 (0.16)	0.94 (0.01)	–
SN 2004dj	196	38.08 (0.08)	36.67 (0.06)	4.64 (0.23)	0.96 (0.01)	–
SN 2004dj	223	37.94 (0.08)	36.56 (0.06)	6.02 (0.30)	0.98 (0.01)	–

Table A5 – *continued*

SN name	Age since discovery[a]	$\log\left(\frac{L_{\rm tot}}{\rm ergs^{-1}}\right)$	$\log\left(\frac{L_{\rm pk}}{\rm ergs^{-1}\AA^{-1}}\right)$	$v_{\rm pk}$[b] (100 km s^{-1})	HWHM$_1$[c] (1000 km s^{-1})	HWHM$_2$[d] (1000 km s^{-1})
SN 2004dj	260	37.84 (0.08)	36.42 (0.07)	6.06 (0.30)	1.05 (0.02)	–
SN 2004dj	635	37.03 (0.07)	35.47 (0.07)	1.11 (0.06)	1.03 (0.02)	–
SN 2004dj	905	36.62 (0.07)	35.33 (0.07)	−0.60 (0.04)	0.97 (0.10)	–
SN 2005cs	157	36.96 (0.02)	35.77 (0.02)	5.93 (0.30)	0.58 (0.01)	–
SN 2005cs	303	37.20 (0.09)	35.68 (0.07)	−1.37 (0.04)	0.69 (0.02)	–
SN 2006ov	82	37.57 (0.03)	36.14 (0.03)	0.89 (0.04)	0.87 (0.03)	–
SN 2008ex	280	38.26 (0.09)	36.89 (0.09)	0.55 (0.04)	1.00 (0.16)	–
SN 2008ij	186	37.90 (0.19)	36.39 (0.13)	−8.12 (0.04)	0.66 (0.02)	–
SN 2011cj	227	38.29 (0.10)	36.91 (0.10)	−9.01 (0.04)	0.83 (0.02)	–
SN 2012A	406	36.98 (0.11)	35.62 (0.09)	−3.16 (0.04)	0.62 (0.02)	–
SN 2012A	432	36.76 (0.19)	35.18 (0.16)	−7.16 (0.04)	0.88 (0.20)	–
SN 2013am[h]	256	37.70 (0.15)	36.50 (0.11)	−0.09 (0.04)	0.28 (0.01)	–
SN 2013am[h]	461	37.10 (0.26)	35.85 (0.18)	−0.11 (0.04)	0.43 (0.02)	–

Notes. Uncertainties are in parentheses.
[a]Phases of spectra are in rest-frame days since discovery using the redshift and discovery date presented in Table A1.
[b]For doublets and blends, $v_{\rm pk}$ is calculated with respect to the bluer component.
[c]HWHM$_1$ is measured for the blue component of a doublet/blend or the only component of a singlet.
[d]HWHM$_2$ is measured for the red component of a doublet/blend and is left blank for a singlet.
[e]SN 2012aw is also known as PTF12bvh.
[f]SN 2012fg is also known as PTF12jxe.
[g]SN 2013ab is also known as iPTF13ut.
[h]SN 2013am is also known as iPTF13aaz.

Table A6. Spectral-feature measurements of magnesium.

SN name	Age since discovery[a]	$\log\left(\frac{L_{\rm tot}}{\rm ergs^{-1}}\right)$	$\log\left(\frac{L_{\rm pk}}{\rm ergs^{-1}\AA^{-1}}\right)$	$v_{\rm pk}$ (100 km s^{-1})	HWHM (1000 km s^{-1})
		Mg I] λ4571			
SN 1992ad	225	38.36 (0.04)	36.78 (0.04)	9.35 (0.47)	3.88 (0.15)
SN 1992ad	286	38.15 (0.05)	36.47 (0.05)	−5.13 (0.07)	3.78 (0.11)
SN 1992H	203	39.11 (0.08)	37.37 (0.07)	−1.05 (0.07)	2.76 (0.07)
SN 1992H	221	39.01 (0.03)	37.33 (0.03)	4.05 (0.20)	3.06 (0.05)
SN 1992H	382	38.60 (0.06)	36.93 (0.05)	−3.50 (0.07)	2.07 (0.04)
SN 1992H	425	38.66 (0.06)	36.66 (0.05)	−0.48 (0.07)	4.77 (0.08)
SN 1992H	461	38.33 (0.11)	36.50 (0.11)	3.19 (0.16)	4.64 (0.18)
SN 1992H	492	38.30 (0.08)	36.35 (0.07)	0.32 (0.07)	5.38 (0.21)
SN 1999em	312	38.35 (0.09)	36.57 (0.05)	7.17 (0.36)	2.36 (0.06)
SN 1999em	332	38.35 (0.04)	36.54 (0.03)	9.64 (0.48)	2.83 (0.02)
SN 1999em	418	38.22 (0.05)	36.45 (0.04)	0.74 (0.07)	2.42 (0.05)
SN 1999em	516	37.35 (0.07)	35.68 (0.05)	0.66 (0.07)	2.14 (0.05)
SN 2001X	176	38.71 (0.08)	37.07 (0.08)	9.86 (0.49)	1.91 (0.04)
SN 2002hh	394	35.58 (0.21)	34.10 (0.15)	15.25 (0.76)	1.28 (0.07)
SN 2003gd	138	38.16 (0.05)	36.35 (0.04)	12.85 (0.64)	2.64 (0.02)
SN 2004A	162	38.63 (0.07)	36.95 (0.06)	8.48 (0.42)	2.47 (0.06)
SN 2004A	183	38.54 (0.08)	36.85 (0.07)	8.23 (0.41)	2.14 (0.02)
SN 2004A	282	38.30 (0.05)	36.59 (0.03)	−0.77 (0.07)	2.21 (0.04)
SN 2004dj	106	38.45 (0.06)	36.80 (0.05)	1.28 (0.07)	2.01 (0.04)
SN 2004dj	134	38.35 (0.06)	36.67 (0.06)	1.12 (0.07)	2.21 (0.06)
SN 2004dj	169	38.19 (0.06)	36.55 (0.06)	2.54 (0.13)	2.11 (0.05)
SN 2004dj	196	38.22 (0.05)	36.55 (0.06)	2.46 (0.12)	2.25 (0.05)
SN 2004dj	223	38.12 (0.05)	36.46 (0.04)	2.57 (0.13)	2.28 (0.04)
SN 2004dj	260	38.05 (0.04)	36.39 (0.04)	5.16 (0.26)	2.40 (0.05)
SN 2004dj	398	37.96 (0.02)	36.24 (0.02)	0.03 (0.07)	2.54 (0.03)
SN 2004dj	407	37.97 (0.02)	36.22 (0.01)	1.27 (0.07)	2.60 (0.03)
SN 2004dj	635	37.47 (0.03)	35.82 (0.03)	−2.58 (0.07)	2.60 (0.05)
SN 2004et	196	38.41 (0.02)	36.61 (0.02)	13.61 (0.68)	3.33 (0.02)
SN 2004et	202	38.25 (0.05)	36.55 (0.06)	13.65 (0.68)	2.91 (0.05)
SN 2004et	277	38.11 (0.02)	36.32 (0.02)	8.52 (0.43)	3.00 (0.02)

Table A6 – *continued*

SN name	Age since discovery[a]	$\log\left(\frac{L_{\rm tot}}{\rm ergs^{-1}}\right)$	$\log\left(\frac{L_{\rm pk}}{\rm ergs^{-1}\AA^{-1}}\right)$	$v_{\rm pk}$ (100 km s^{-1})	HWHM (1000 km s^{-1})
SN 2004et	349	37.87 (0.02)	36.09 (0.02)	4.65 (0.23)	2.87 (0.03)
SN 2005ay	284	37.99 (0.07)	36.70 (0.07)	−2.54 (0.07)	1.92 (0.23)
SN 2005cs	303	37.22 (0.06)	35.66 (0.06)	−0.61 (0.07)	2.19 (0.12)
SN 2006ov	82	37.75 (0.03)	36.32 (0.03)	−0.35 (0.07)	1.62 (0.03)
SN 2007gw	186	38.68 (0.05)	36.94 (0.05)	−12.17 (0.07)	2.76 (0.09)
SN 2008ex	280	38.71 (0.12)	37.05 (0.11)	1.17 (0.07)	2.05 (0.07)
SN 2008ij	186	38.04 (0.09)	36.48 (0.09)	0.66 (0.07)	1.79 (0.04)
SN 2011cj	227	38.85 (0.03)	37.27 (0.02)	−0.04 (0.07)	2.88 (0.07)
SN 2011fd	97	38.17 (0.07)	36.64 (0.06)	6.54 (0.33)	1.83 (0.05)
SN 2011fd	185	38.49 (0.04)	36.86 (0.04)	−1.33 (0.07)	2.78 (0.06)
SN 2012A	406	37.34 (0.16)	35.85 (0.11)	−7.20 (0.07)	1.26 (0.03)
SN 2012A	432	37.82 (0.05)	35.91 (0.04)	−0.26 (0.07)	3.90 (0.07)
SN 2012aw[b]	337	38.10 (0.02)	36.33 (0.01)	5.80 (0.29)	2.88 (0.04)
SN 2012aw[b]	364	38.45 (0.07)	36.54 (0.06)	7.06 (0.35)	3.32 (0.07)
SN 2012ec	214	38.44 (0.04)	37.08 (0.04)	−3.85 (0.07)	1.49 (0.05)
SN 2012ec	393	37.95 (0.05)	36.57 (0.06)	−7.25 (0.07)	1.54 (0.05)
SN 2012fg[c]	171	39.09 (0.22)	37.30 (0.18)	−7.31 (0.07)	2.41 (0.03)
SN 2012ho	215	39.06 (0.02)	37.14 (0.02)	15.77 (0.79)	5.21 (0.12)
SN 2012ho	235	39.10 (0.02)	37.14 (0.02)	8.69 (0.43)	5.40 (0.13)
SN 2012ho	237	38.80 (0.03)	37.00 (0.02)	3.11 (0.16)	3.32 (0.03)
SN 2012ho	250	39.09 (0.05)	37.10 (0.05)	18.51 (0.93)	6.75 (0.34)
SN 2012ho	303	38.44 (0.18)	36.96 (0.11)	−6.51 (0.07)	1.47 (0.07)
SN 2013ab[d]	143	38.90 (0.02)	37.28 (0.02)	14.87 (0.74)	2.02 (0.02)
SN 2013ab[d]	167	38.88 (0.04)	37.20 (0.04)	9.74 (0.49)	2.26 (0.04)
SN 2013am[e]	256	36.88 (0.07)	35.46 (0.06)	−1.33 (0.07)	1.09 (0.03)

Notes. Uncertainties are in parentheses.
[a]Phases of spectra are in rest-frame days since discovery using the redshift and discovery date presented in Table A1.
[b]SN 2012aw is also known as PTF12bvh.
[c]SN 2012fg is also known as PTF12jxe.
[d]SN 2013ab is also known as iPTF13ut.
[e]SN 2013am is also known as iPTF13aaz.

Table A7. Spectral-feature measurements of calcium.

SN name	Age since discovery[a]	$\log\left(\frac{L_{\rm tot}}{\rm ergs^{-1}}\right)$	$\log\left(\frac{L_{\rm pk}}{\rm ergs^{-1}\AA^{-1}}\right)$	$v_{\rm pk}$[b] (100 km s^{-1})	HWHM$_1$[c] (1000 km s^{-1})	HWHM$_2$[d] (1000 km s^{-1})
			[Ca II] λλ7291,7324			
SN 1988A	162	39.67 (0.05)	37.90 (0.04)	−2.67 (0.54)	0.66 (0.02)	1.12 (0.03)
SN 1988A	182	39.20 (0.05)	37.45 (0.05)	−2.68 (0.54)	0.72 (0.02)	0.94 (0.02)
SN 1988H	119	39.34 (0.03)	37.60 (0.04)	−0.82 (0.04)	0.86 (0.05)	1.06 (0.08)
SN 1989L	182	39.01 (0.04)	37.27 (0.04)	0.95 (0.72)	0.73 (0.03)	0.97 (0.05)
SN 1990E	195	38.77 (0.05)	37.01 (0.05)	1.74 (0.09)	1.65 (0.40)	1.01 (0.47)
SN 1990E	304	38.57 (0.04)	36.83 (0.03)	3.47 (0.17)	1.20 (0.42)	1.14 (0.59)
SN 1990H	193	39.17 (0.08)	37.40 (0.09)	−7.42 (0.04)	1.48 (0.25)	0.79 (0.22)
SN 1990K	147	39.25 (0.04)	37.33 (0.04)	4.09 (0.88)	1.13 (0.11)	1.82 (0.20)
SN 1990K	205	39.17 (0.02)	37.27 (0.01)	8.97 (0.45)	1.16 (0.09)	1.33 (0.08)
SN 1992ad	225	39.21 (0.02)	37.40 (0.02)	2.11 (0.11)	1.45 (0.69)	1.34 (1.79)
SN 1992ad	286	38.93 (0.01)	37.13 (0.01)	1.27 (0.06)	1.46 (1.04)	1.12 (1.45)
SN 1992bt	235	39.06 (0.16)	37.42 (0.11)	−4.05 (0.04)	0.97 (0.03)	0.31 (0.03)
SN 1992H	382	39.11 (0.05)	37.29 (0.06)	−6.20 (0.37)	0.81 (0.03)	1.05 (0.06)
SN 1992H	425	38.80 (0.05)	36.81 (0.04)	5.31 (0.27)	1.73 (0.54)	2.01 (2.23)
SN 1992H	461	38.82 (0.12)	36.84 (0.09)	4.47 (0.22)	1.66 (0.89)	1.80 (3.08)
SN 1992H	492	38.59 (0.09)	36.58 (0.07)	5.37 (0.27)	1.78 (2.65)	2.40 (1.19)
SN 1993G	114	39.01 (0.10)	37.20 (0.06)	3.54 (0.18)	1.22 (0.03)	0.55 (0.01)
SN 1993K	282	39.13 (0.07)	37.32 (0.07)	3.31 (0.17)	0.77 (0.08)	1.25 (0.13)
SN 1999em	312	39.13 (0.06)	37.42 (0.04)	−4.58 (0.45)	0.74 (0.02)	0.76 (0.05)
SN 1999em	332	39.09 (0.06)	37.37 (0.04)	−4.56 (0.45)	0.70 (0.02)	0.84 (0.05)
SN 1999em	418	38.77 (0.06)	37.11 (0.03)	−5.43 (0.41)	0.70 (0.03)	0.69 (0.08)

Table A7 – *continued*

SN name	Age since discovery[a]	$\log\left(\frac{L_{\rm tot}}{\rm ergs^{-1}}\right)$	$\log\left(\frac{L_{\rm pk}}{\rm ergs^{-1}\,\AA^{-1}}\right)$	$v_{\rm pk}$[b] (100 km s^{-1})	HWHM$_1$[c] (1000 km s^{-1})	HWHM$_2$[d] (1000 km s^{-1})
SN 1999gq	83	39.14 (0.02)	37.34 (0.02)	2.39 (0.12)	1.82 (0.05)	0.67 (0.11)
SN 2001X	176	39.09 (0.03)	37.28 (0.03)	−7.16 (0.32)	1.03 (0.12)	1.41 (0.11)
SN 2002hh	159	38.27 (0.01)	36.33 (0.01)	3.01 (0.15)	1.90 (0.70)	3.02 (1.81)
SN 2002hh	336	37.41 (0.04)	35.64 (0.05)	2.18 (0.11)	1.25 (0.20)	0.93 (0.23)
SN 2002hh	394	37.56 (0.01)	35.63 (0.01)	0.48 (0.04)	1.73 (0.02)	1.11 (0.05)
SN 2003gd	138	38.84 (0.05)	37.01 (0.04)	3.37 (0.17)	0.80 (0.02)	0.90 (0.03)
SN 2003hl	149	38.56 (0.04)	36.76 (0.03)	−7.27 (0.31)	0.83 (0.04)	1.21 (0.06)
SN 2004A	162	39.12 (0.05)	37.28 (0.05)	−6.62 (0.35)	0.79 (0.06)	1.27 (0.08)
SN 2004A	183	39.07 (0.08)	37.26 (0.07)	−6.60 (0.35)	0.71 (0.03)	0.94 (0.03)
SN 2004A	282	38.86 (0.09)	37.07 (0.07)	−4.98 (0.43)	0.65 (0.01)	0.82 (0.01)
SN 2004dj	106	38.70 (0.05)	36.87 (0.06)	0.50 (0.04)	1.35 (0.07)	0.82 (0.08)
SN 2004dj	111	38.86 (0.04)	36.83 (0.04)	−2.44 (0.04)	2.27 (0.96)	2.29 (3.01)
SN 2004dj	134	38.71 (0.07)	36.89 (0.08)	0.51 (0.04)	1.23 (0.11)	0.96 (0.22)
SN 2004dj	140	38.82 (0.05)	36.85 (0.05)	−2.24 (0.04)	1.50 (0.48)	1.99 (1.19)
SN 2004dj	169	38.66 (0.06)	36.89 (0.06)	2.12 (0.11)	1.23 (0.05)	0.66 (0.07)
SN 2004dj	170	38.84 (0.06)	36.87 (0.05)	1.64 (0.08)	1.90 (8.92)	2.56 (3.95)
SN 2004dj	196	38.75 (0.06)	36.97 (0.06)	2.96 (0.15)	0.95 (0.07)	1.25 (0.23)
SN 2004dj	223	38.68 (0.06)	36.91 (0.06)	2.94 (0.15)	1.05 (0.07)	0.91 (0.10)
SN 2004dj	225	38.81 (0.07)	36.94 (0.06)	5.51 (0.28)	1.65 (0.88)	1.36 (1.43)
SN 2004dj	254	38.86 (0.08)	36.95 (0.06)	1.54 (0.08)	1.60 (1.27)	1.69 (4.26)
SN 2004dj	260	38.69 (0.04)	36.91 (0.04)	2.13 (0.11)	1.17 (0.06)	0.91 (0.10)
SN 2004dj	398	38.50 (0.09)	36.75 (0.07)	0.48 (0.04)	0.79 (0.01)	0.66 (0.02)
SN 2004dj	407	38.48 (0.09)	36.73 (0.07)	0.48 (0.04)	0.77 (0.02)	0.69 (0.02)
SN 2004dj	635	37.81 (0.19)	36.08 (0.15)	−0.35 (0.04)	0.61 (0.01)	0.64 (0.01)
SN 2004dj	905	37.24 (0.03)	35.59 (0.03)	−1.05 (0.04)	0.64 (0.02)	0.52 (0.02)
SN 2004et	196	39.16 (0.03)	37.45 (0.03)	8.72 (0.44)	1.42 (0.04)	0.67 (0.08)
SN 2004et	202	39.17 (0.03)	37.47 (0.03)	8.72 (0.44)	1.28 (0.04)	0.70 (0.06)
SN 2004et	349	38.81 (0.04)	37.10 (0.04)	9.48 (0.47)	1.08 (1.09)	1.16 (2.55)
SN 2005ay	284	38.78 (0.06)	36.99 (0.05)	−6.15 (0.37)	0.65 (0.02)	1.00 (0.02)
SN 2005cs	157	37.77 (0.02)	36.23 (0.02)	−1.71 (0.04)	0.52 (0.01)	0.44 (0.01)
SN 2005cs	303	37.91 (0.08)	36.25 (0.06)	2.06 (0.10)	0.60 (0.24)	1.01 (0.63)
SN 2006my	98	39.29 (0.01)	37.54 (0.01)	−3.00 (0.53)	0.68 (0.02)	1.06 (0.03)
SN 2006ov	82	38.37 (0.02)	36.65 (0.02)	1.48 (0.07)	0.67 (0.02)	0.72 (0.04)
SN 2007gw	186	38.82 (0.02)	37.16 (0.02)	2.89 (0.14)	1.15 (3.86)	1.07 (2.77)
SN 2008ex	280	39.59 (0.01)	37.78 (0.01)	5.78 (0.29)	1.59 (0.46)	1.37 (1.13)
SN 2008ij	119	39.34 (0.02)	37.50 (0.02)	10.75 (0.54)	1.86 (1.65)	1.95 (3.16)
SN 2008ij	149	38.33 (0.05)	36.50 (0.05)	4.14 (0.21)	1.08 (0.49)	1.31 (0.85)
SN 2008ij	186	38.84 (0.02)	36.96 (0.02)	−1.50 (0.60)	1.50 (0.16)	1.11 (0.14)
SN 2009ls	111	38.50 (0.03)	36.80 (0.03)	3.28 (0.16)	1.49 (1.70)	1.75 (4.47)
SN 2009ls	164	38.51 (0.01)	36.68 (0.01)	−3.11 (0.52)	2.43 (1.59)	1.91 (8.18)
SN 2011cj	227	39.20 (0.04)	37.45 (0.04)	−4.02 (0.48)	0.90 (0.04)	0.77 (0.04)
SN 2011fd	97	38.69 (0.04)	37.04 (0.04)	4.58 (0.23)	1.29 (0.77)	1.04 (2.50)
SN 2011fd	185	39.04 (0.04)	37.49 (0.04)	3.80 (0.19)	1.13 (1.58)	1.38 (2.46)
SN 2012A	406	38.36 (0.03)	36.65 (0.03)	−5.46 (0.40)	0.50 (0.02)	0.76 (0.02)
SN 2012A	432	38.07 (0.08)	36.23 (0.06)	5.48 (0.27)	1.16 (0.49)	1.48 (1.35)
SN 2012aw[e]	337	38.93 (0.01)	37.26 (0.01)	6.90 (0.34)	0.97 (0.03)	0.70 (0.03)
SN 2012aw[e]	364	38.97 (0.05)	37.14 (0.04)	6.72 (0.34)	1.36 (0.16)	1.45 (1.05)
SN 2012ch	335	39.42 (0.02)	37.50 (0.01)	10.02 (0.50)	1.84 (3.93)	2.24 (1.32)
SN 2012ec	214	38.63 (0.08)	36.92 (0.08)	−6.08 (0.37)	0.68 (0.12)	1.13 (0.19)
SN 2012ec	393	38.03 (0.02)	36.38 (0.02)	−1.07 (0.04)	0.79 (0.20)	0.58 (0.13)
SN 2012fg[f]	171	39.53 (0.04)	37.54 (0.02)	−3.01 (0.04)	2.37 (9.81)	2.75 (5.18)
SN 2012fg[f]	211	39.23 (0.02)	37.40 (0.02)	1.29 (0.06)	1.39 (0.12)	0.75 (0.12)
SN 2012ho	154	39.52 (0.01)	37.77 (0.01)	3.74 (0.19)	1.22 (0.06)	1.30 (0.18)
SN 2012ho	215	39.52 (0.04)	37.63 (0.03)	4.64 (0.23)	1.33 (0.66)	1.94 (2.40)
SN 2012ho	235	39.37 (0.04)	37.57 (0.03)	3.07 (0.15)	1.31 (2.85)	1.75 (9.05)
SN 2012ho	237	39.26 (0.01)	37.63 (0.01)	7.75 (0.39)	1.01 (0.66)	1.04 (1.14)
SN 2012ho	250	39.38 (0.05)	37.55 (0.04)	4.52 (0.23)	1.43 (1.32)	1.68 (7.67)
SN 2012ho	303	39.14 (0.03)	37.53 (0.02)	7.59 (0.38)	1.13 (2.28)	1.05 (2.23)
SN 2013ab[g]	143	39.21 (0.01)	37.50 (0.01)	11.65 (0.58)	1.45 (3.67)	1.26 (2.03)
SN 2013ab[g]	167	39.25 (0.01)	37.48 (0.01)	13.38 (0.67)	1.15 (0.61)	1.29 (1.06)
SN 2013am[h]	256	38.53 (0.04)	36.89 (0.04)	1.36 (0.07)	0.38 (0.01)	0.53 (0.01)
SN 2013am[h]	461	38.40 (0.03)	36.82 (0.02)	1.56 (0.08)	0.40 (0.01)	0.46 (0.01)

Table A7 – *continued*

SN name	Age since discovery[a]	$\log\left(\frac{L_{\rm tot}}{\rm ergs^{-1}}\right)$	$\log\left(\frac{L_{\rm pk}}{\rm ergs^{-1}\AA^{-1}}\right)$	$v_{\rm pk}$[b] (100 km s^{-1})	HWHM$_1$[c] (1000 km s^{-1})	HWHM$_2$[d] (1000 km s^{-1})
			Ca II λλ8498,8542			
SN 1988A	162	39.75 (0.03)	37.95 (0.02)	−3.70 (0.04)	0.55 (0.05)	1.04 (0.01)
SN 1988A	182	39.31 (0.03)	37.53 (0.02)	−3.00 (0.03)	0.63 (0.07)	0.96 (0.01)
SN 1988H	119	39.55 (0.02)	37.67 (0.02)	−6.24 (0.04)	0.63 (0.11)	1.40 (0.03)
SN 1989L	182	39.40 (0.04)	37.58 (0.02)	3.29 (0.16)	0.53 (0.06)	1.07 (0.01)
SN 1990E	195	38.98 (0.04)	37.07 (0.03)	−10.09 (0.04)	0.63 (0.03)	1.66 (0.07)
SN 1990E	304	38.43 (0.06)	36.65 (0.04)	−4.46 (0.03)	0.77 (0.13)	1.04 (0.09)
SN 1990K	147	39.05 (0.10)	37.24 (0.06)	−3.72 (0.04)	0.51 (0.04)	1.26 (0.06)
SN 1990K	205	38.92 (0.05)	37.04 (0.04)	2.67 (0.13)	0.63 (0.05)	1.57 (0.06)
SN 1992ad	225	38.84 (0.03)	37.06 (0.01)	−4.21 (0.04)	0.65 (0.02)	1.18 (0.01)
SN 1992ad	286	38.16 (0.11)	36.42 (0.07)	−2.09 (0.04)	0.54 (0.05)	1.00 (0.08)
SN 1992H	382	38.78 (0.09)	37.01 (0.08)	0.51 (0.04)	0.49 (0.05)	0.97 (0.04)
SN 1992H	425	38.44 (0.09)	36.53 (0.08)	3.06 (0.15)	0.82 (0.67)	1.52 (0.74)
SN 1992H	461	38.26 (0.25)	36.40 (0.18)	7.90 (0.40)	0.72 (0.35)	1.43 (0.16)
SN 1993G	114	39.24 (0.18)	37.59 (0.09)	−5.00 (0.04)	0.57 (0.04)	0.51 (0.01)
SN 1993K	282	38.55 (0.17)	36.94 (0.13)	−5.29 (0.04)	0.21 (0.06)	0.77 (0.07)
SN 1999em	312	39.01 (0.03)	37.37 (0.02)	−0.63 (0.04)	0.39 (0.02)	0.79 (0.01)
SN 1999em	418	38.24 (0.05)	36.50 (0.02)	0.13 (0.04)	0.34 (0.04)	0.87 (0.01)
SN 1999gq	83	39.20 (0.03)	37.51 (0.03)	−12.31 (0.04)	0.37 (0.05)	1.22 (0.02)
SN 2001X	176	39.32 (0.03)	37.59 (0.02)	−6.85 (0.04)	0.97 (0.08)	0.80 (0.01)
SN 2002hh	159	38.58 (0.01)	36.73 (0.01)	−10.85 (0.04)	1.08 (0.25)	1.65 (0.15)
SN 2002hh	394	37.33 (0.01)	35.42 (0.01)	−4.47 (0.04)	1.50 (3.09)	1.76 (2.37)
SN 2003gd	138	38.95 (0.04)	37.21 (0.02)	−0.02 (0.03)	0.88 (0.06)	0.81 (0.01)
SN 2003hl	149	38.64 (0.04)	36.82 (0.02)	−7.59 (0.04)	0.51 (0.05)	1.13 (0.03)
SN 2004A	162	39.35 (0.04)	37.62 (0.03)	−6.86 (0.04)	0.72 (0.03)	0.76 (0.01)
SN 2004A	183	39.36 (0.04)	37.64 (0.03)	−4.06 (0.03)	0.59 (0.04)	0.79 (0.01)
SN 2004A	282	39.08 (0.03)	37.33 (0.02)	−2.60 (0.04)	0.37 (0.08)	0.95 (0.01)
SN 2004dj	106	38.98 (0.02)	37.25 (0.01)	−8.80 (0.04)	0.57 (0.06)	1.62 (0.13)
SN 2004dj	111	39.08 (0.12)	37.26 (0.10)	−6.71 (0.04)	0.86 (0.02)	1.30 (0.01)
SN 2004dj	140	39.14 (0.13)	37.29 (0.10)	−6.59 (0.04)	0.79 (0.04)	1.29 (0.01)
SN 2004dj	169	39.14 (0.02)	37.29 (0.01)	−4.44 (0.03)	0.64 (0.02)	1.15 (0.01)
SN 2004dj	170	39.18 (0.14)	37.31 (0.10)	−2.98 (0.04)	0.54 (0.30)	1.38 (0.02)
SN 2004dj	196	39.18 (0.01)	37.30 (0.01)	−3.05 (0.03)	0.74 (0.07)	1.18 (0.04)
SN 2004dj	223	39.06 (0.01)	37.22 (0.01)	−0.96 (0.04)	0.77 (0.01)	1.07 (0.01)
SN 2004dj	225	39.14 (0.14)	37.27 (0.10)	−2.94 (0.04)	0.68 (0.19)	1.32 (0.01)
SN 2004dj	254	39.06 (0.14)	37.20 (0.10)	−2.98 (0.04)	1.12 (0.34)	1.26 (0.02)
SN 2004dj	260	38.93 (0.02)	37.10 (0.02)	−0.30 (0.03)	0.80 (0.08)	1.07 (0.02)
SN 2004dj	398	38.22 (0.08)	36.49 (0.06)	1.04 (0.05)	0.61 (0.17)	0.89 (0.03)
SN 2004dj	407	38.16 (0.09)	36.42 (0.06)	−0.33 (0.04)	0.50 (0.14)	0.91 (0.03)
SN 2004dj	635	37.37 (0.05)	35.49 (0.03)	0.25 (0.03)	0.86 (0.05)	1.19 (0.05)
SN 2004et	196	39.20 (0.02)	37.40 (0.01)	−4.44 (0.04)	0.72 (0.37)	1.25 (0.03)
SN 2004et	202	39.15 (0.02)	37.38 (0.02)	−5.16 (0.04)	0.72 (0.26)	1.19 (0.03)
SN 2004et	277	38.77 (0.04)	37.06 (0.03)	−3.83 (0.03)	0.68 (0.06)	0.96 (0.02)
SN 2004et	349	38.25 (0.02)	36.54 (0.02)	−1.03 (0.03)	0.92 (0.38)	0.99 (0.04)
SN 2005ay	284	38.82 (0.06)	37.11 (0.04)	−3.66 (0.04)	0.53 (0.04)	0.81 (0.01)
SN 2005cs	157	38.23 (0.01)	36.51 (0.01)	7.19 (0.36)	0.73 (0.40)	1.02 (0.63)
SN 2005cs	303	38.09 (0.04)	36.27 (0.01)	6.14 (0.31)	0.47 (0.03)	1.00 (0.01)
SN 2006my	98	39.42 (0.01)	37.72 (0.01)	−0.93 (0.04)	1.63 (0.62)	0.95 (0.09)
SN 2006ov	82	38.65 (0.01)	36.89 (0.01)	2.73 (0.14)	0.68 (0.07)	0.92 (0.01)
SN 2008ex	280	39.43 (0.06)	37.70 (0.04)	−8.93 (0.04)	0.55 (0.17)	0.98 (0.03)
SN 2008ij	119	39.48 (0.02)	37.57 (0.02)	3.18 (0.04)	1.50 (0.01)	0.71 (0.03)
SN 2008ij	149	38.27 (0.06)	36.56 (0.03)	−11.06 (0.04)	0.99 (1.22)	1.11 (2.81)
SN 2008ij	186	38.84 (0.02)	37.00 (0.01)	−6.81 (0.04)	1.21 (2.46)	1.34 (1.71)
SN 2009ls	111	38.84 (0.02)	37.03 (0.02)	−13.93 (0.04)	1.28 (0.03)	0.79 (0.29)
SN 2009ls	164	38.72 (0.02)	36.76 (0.01)	−5.71 (0.04)	0.73 (0.02)	1.87 (0.05)
SN 2011cj	227	39.38 (0.04)	37.58 (0.03)	−3.71 (0.04)	0.78 (0.09)	0.91 (0.02)
SN 2011fd	97	38.85 (0.05)	37.09 (0.02)	−8.86 (0.04)	0.61 (0.05)	1.08 (0.02)
SN 2011fd	185	39.34 (0.04)	37.54 (0.03)	−3.91 (0.03)	0.40 (0.03)	1.10 (0.01)
SN 2012A	406	37.73 (0.05)	36.09 (0.02)	−3.02 (0.04)	0.46 (0.04)	0.81 (0.01)
SN 2012A	432	37.24 (0.13)	35.38 (0.12)	10.93 (0.04)	0.69 (0.42)	0.84 (0.37)
SN 2012aw[e]	337	38.97 (0.01)	37.25 (0.01)	−2.60 (0.03)	0.50 (0.02)	0.86 (0.01)
SN 2012aw[e]	364	38.70 (0.11)	36.88 (0.08)	−1.01 (0.03)	1.23 (1.20)	1.15 (0.17)

Table A7 – *continued*

SN name	Age since discovery[a]	$\log\left(\frac{L_{\rm tot}}{\rm ergs^{-1}}\right)$	$\log\left(\frac{L_{\rm pk}}{\rm ergs^{-1}\AA^{-1}}\right)$	$v_{\rm pk}$[b] (100 km s^{-1})	HWHM$_1$[c] (1000 km s^{-1})	HWHM$_2$[d] (1000 km s^{-1})
SN 2012ch	335	38.91 (0.05)	37.11 (0.04)	−2.42 (0.03)	1.52 (1.82)	1.08 (0.57)
SN 2012ec	214	38.66 (0.13)	36.97 (0.07)	−4.13 (0.04)	0.89 (0.12)	0.66 (0.03)
SN 2012ec	393	37.91 (0.03)	36.14 (0.03)	−3.24 (0.03)	0.85 (0.24)	0.72 (0.12)
SN 2012fg[f]	171	39.28 (0.05)	37.39 (0.03)	−13.89 (0.04)	1.01 (0.67)	1.17 (0.97)
SN 2012fg[f]	211	38.99 (0.05)	37.17 (0.05)	−12.96 (0.04)	0.83 (0.10)	0.67 (0.07)
SN 2012ho	154	39.53 (0.01)	37.70 (0.01)	−8.85 (0.04)	0.67 (0.06)	1.56 (0.02)
SN 2012ho	215	39.33 (0.06)	37.45 (0.05)	−6.02 (0.04)	1.63 (1.40)	1.28 (5.37)
SN 2012ho	235	39.17 (0.07)	37.33 (0.06)	−4.57 (0.04)	1.48 (1.60)	1.25 (3.42)
SN 2012ho	237	39.28 (0.01)	37.53 (0.01)	−5.76 (0.04)	0.58 (0.02)	1.00 (0.01)
SN 2012ho	250	39.06 (0.07)	37.20 (0.05)	−5.90 (0.04)	1.52 (3.24)	1.34 (8.76)
SN 2012ho	303	38.92 (0.05)	37.22 (0.03)	−4.82 (0.04)	0.77 (0.08)	0.75 (0.02)
SN 2013ab[g]	143	39.27 (0.01)	37.55 (0.01)	−6.38 (0.04)	0.90 (0.06)	0.93 (0.02)
SN 2013ab[g]	167	39.36 (0.03)	37.60 (0.02)	−6.46 (0.04)	0.77 (0.25)	1.03 (0.06)
SN 2013am[h]	256	38.77 (0.04)	37.14 (0.03)	2.12 (0.11)	0.70 (0.09)	0.62 (0.01)
SN 2013am[h]	461	37.87 (0.07)	36.25 (0.04)	2.74 (0.14)	0.50 (0.02)	0.57 (0.01)
			Ca II λ8662			
SN 1988A	162	39.77 (0.02)	37.96 (0.02)	5.75 (0.29)	2.07 (0.02)	–
SN 1988A	182	39.30 (0.01)	37.46 (0.01)	5.72 (0.29)	1.95 (0.02)	–
SN 1988H	119	39.51 (0.02)	37.71 (0.01)	−4.39 (0.03)	1.73 (0.01)	–
SN 1989L	182	39.04 (0.03)	37.34 (0.03)	3.11 (0.16)	1.41 (0.02)	–
SN 1990E	195	38.90 (0.03)	37.27 (0.03)	−9.42 (0.03)	1.75 (0.03)	–
SN 1990E	304	38.66 (0.03)	36.88 (0.03)	0.42 (0.03)	1.40 (0.02)	–
SN 1990K	147	38.99 (0.08)	37.29 (0.09)	5.78 (0.29)	1.58 (0.03)	–
SN 1990K	205	38.69 (0.07)	37.12 (0.06)	17.57 (0.88)	0.97 (0.03)	–
SN 1992ad	225	38.74 (0.04)	37.13 (0.03)	−9.04 (0.03)	1.12 (0.02)	–
SN 1992ad	286	38.10 (0.05)	36.49 (0.04)	−9.57 (0.03)	1.18 (0.04)	–
SN 1992H	382	38.54 (0.11)	36.98 (0.10)	4.51 (0.23)	0.91 (0.02)	–
SN 1992H	425	38.24 (0.18)	36.53 (0.16)	−0.45 (0.03)	1.57 (0.18)	–
SN 1992H	461	38.06 (0.42)	36.34 (0.27)	14.14 (0.71)	1.19 (0.05)	–
SN 1993G	114	38.98 (0.14)	37.47 (0.12)	−3.79 (0.03)	0.71 (0.02)	–
SN 1993K	282	38.36 (0.27)	36.94 (0.22)	−1.25 (0.03)	0.55 (0.03)	–
SN 1999em	312	38.77 (0.04)	37.16 (0.04)	−1.33 (0.03)	0.93 (0.02)	–
SN 1999em	418	37.93 (0.04)	36.34 (0.03)	0.02 (0.03)	0.92 (0.02)	–
SN 1999gq	83	39.03 (0.01)	37.40 (0.01)	−12.87 (0.03)	1.88 (0.04)	–
SN 2001X	176	39.18 (0.01)	37.49 (0.01)	−4.76 (0.03)	1.35 (0.03)	–
SN 2002hh	159	38.64 (0.01)	36.91 (0.01)	−6.63 (0.03)	2.67 (0.03)	–
SN 2002hh	336	37.21 (0.01)	35.65 (0.01)	−3.84 (0.03)	1.95 (0.07)	–
SN 2002hh	394	37.37 (0.02)	35.58 (0.02)	2.67 (0.13)	2.11 (0.04)	–
SN 2003gd	138	38.67 (0.02)	37.01 (0.03)	3.36 (0.17)	1.08 (0.01)	–
SN 2003hl	149	38.25 (0.02)	36.77 (0.02)	−6.49 (0.03)	1.48 (0.23)	–
SN 2004A	162	39.10 (0.03)	37.47 (0.02)	−6.07 (0.03)	1.18 (0.03)	–
SN 2004A	183	39.07 (0.03)	37.47 (0.03)	−4.70 (0.03)	0.96 (0.02)	–
SN 2004A	282	38.71 (0.04)	37.11 (0.04)	−3.99 (0.03)	0.90 (0.02)	–
SN 2004dj	106	38.67 (0.02)	37.10 (0.02)	−8.16 (0.03)	1.19 (0.02)	–
SN 2004dj	111	38.99 (0.09)	37.15 (0.07)	−1.50 (0.03)	1.95 (0.03)	–
SN 2004dj	134	38.76 (0.03)	37.07 (0.02)	−4.02 (0.03)	1.27 (0.04)	–
SN 2004dj	140	38.88 (0.11)	37.10 (0.10)	−4.48 (0.03)	1.94 (0.06)	–
SN 2004dj	169	38.66 (0.02)	37.04 (0.02)	−0.21 (0.03)	1.92 (0.03)	–
SN 2004dj	170	38.73 (0.13)	37.05 (0.12)	−1.22 (0.03)	1.79 (0.06)	–
SN 2004dj	196	38.67 (0.02)	37.01 (0.02)	1.20 (0.06)	1.77 (0.02)	–
SN 2004dj	223	38.55 (0.02)	36.92 (0.02)	2.49 (0.12)	1.47 (0.02)	–
SN 2004dj	225	38.67 (0.16)	36.96 (0.15)	−1.15 (0.03)	1.76 (0.07)	–
SN 2004dj	254	38.60 (0.18)	36.89 (0.16)	−1.15 (0.03)	1.67 (0.07)	–
SN 2004dj	260	38.47 (0.03)	36.79 (0.03)	0.46 (0.03)	1.29 (0.02)	–
SN 2004dj	398	37.74 (0.06)	36.24 (0.05)	1.12 (0.06)	0.82 (0.01)	–
SN 2004dj	407	37.79 (0.06)	36.19 (0.05)	0.42 (0.03)	0.91 (0.01)	–
SN 2004dj	635	37.10 (0.04)	35.46 (0.02)	−0.97 (0.03)	1.59 (0.03)	–
SN 2004et	196	39.08 (0.02)	37.45 (0.02)	0.98 (0.05)	1.68 (0.05)	–
SN 2004et	202	39.07 (0.02)	37.42 (0.01)	3.06 (0.15)	1.54 (0.02)	–
SN 2004et	277	38.66 (0.02)	37.01 (0.01)	1.70 (0.08)	1.32 (0.02)	–
SN 2004et	349	38.12 (0.02)	36.48 (0.01)	0.39 (0.03)	1.23 (0.02)	–
SN 2005ay	284	38.51 (0.03)	36.90 (0.03)	−2.82 (0.03)	1.21 (0.02)	–

Table A7 – *continued*

SN name	Age since discovery[a]	$\log\left(\frac{L_{\rm tot}}{\rm ergs^{-1}}\right)$	$\log\left(\frac{L_{\rm pk}}{\rm ergs^{-1}\,\AA^{-1}}\right)$	$v_{\rm pk}$[b] (100 km s^{-1})	HWHM$_1$[c] (1000 km s^{-1})	HWHM$_2$[d] (1000 km s^{-1})
SN 2005cs	157	37.84 (0.01)	36.29 (0.01)	9.15 (0.46)	1.00 (0.01)	–
SN 2005cs	303	37.22 (0.11)	35.78 (0.10)	1.91 (0.10)	0.87 (0.05)	–
SN 2006my	98	39.16 (0.01)	37.52 (0.01)	0.05 (0.03)	1.34 (0.02)	–
SN 2006ov	82	38.17 (0.01)	36.60 (0.01)	7.24 (0.36)	1.26 (0.04)	–
SN 2008ex	280	39.37 (0.03)	37.79 (0.04)	−3.95 (0.03)	1.80 (0.03)	–
SN 2008ij	119	39.57 (0.01)	37.74 (0.01)	7.52 (0.38)	2.34 (0.03)	–
SN 2008ij	149	38.09 (0.06)	36.62 (0.05)	−4.32 (0.03)	1.78 (0.16)	–
SN 2008ij	186	38.51 (0.04)	37.04 (0.04)	−2.94 (0.03)	1.27 (0.03)	–
SN 2009ls	111	38.83 (0.01)	37.18 (0.01)	−3.60 (0.03)	2.45 (0.03)	–
SN 2009ls	164	38.58 (0.01)	37.02 (0.01)	−2.90 (0.03)	1.60 (0.01)	–
SN 2011cj	227	39.14 (0.05)	37.49 (0.04)	−3.23 (0.03)	1.17 (0.02)	–
SN 2011fd	97	38.59 (0.03)	37.01 (0.03)	−6.98 (0.03)	1.20 (0.03)	–
SN 2011fd	185	38.93 (0.04)	37.35 (0.03)	−6.25 (0.03)	0.99 (0.02)	–
SN 2012A	406	37.34 (0.05)	35.91 (0.04)	−2.34 (0.03)	0.80 (0.02)	–
SN 2012A	432	36.76 (0.13)	35.26 (0.14)	1.93 (0.10)	1.37 (0.37)	–
SN 2012aw[e]	337	38.60 (0.01)	37.08 (0.01)	−2.68 (0.03)	1.03 (0.01)	–
SN 2012aw[e]	364	38.53 (0.04)	36.77 (0.03)	4.19 (0.21)	1.79 (0.02)	–
SN 2012ch	335	38.44 (0.02)	37.07 (0.02)	1.87 (0.09)	1.98 (0.70)	–
SN 2012ec	214	38.46 (0.10)	36.87 (0.11)	1.62 (0.08)	1.07 (0.04)	–
SN 2012ec	393	37.49 (0.03)	36.12 (0.02)	1.52 (0.08)	0.78 (0.06)	–
SN 2012fg[f]	171	39.13 (0.04)	37.45 (0.04)	−18.36 (0.03)	2.35 (0.21)	–
SN 2012fg[f]	211	39.03 (0.03)	37.27 (0.04)	−5.83 (0.03)	1.91 (0.09)	–
SN 2012ho	154	39.53 (0.01)	37.90 (0.01)	−6.02 (0.03)	1.65 (0.02)	–
SN 2012ho	215	39.27 (0.03)	37.55 (0.03)	−1.86 (0.03)	1.81 (0.04)	–
SN 2012ho	235	39.11 (0.04)	37.39 (0.04)	−1.86 (0.03)	1.69 (0.02)	–
SN 2012ho	237	39.17 (0.01)	37.60 (0.01)	−2.73 (0.03)	1.24 (0.02)	–
SN 2012ho	250	38.97 (0.04)	37.25 (0.04)	−3.24 (0.03)	1.66 (0.03)	–
SN 2012ho	303	38.80 (0.05)	37.20 (0.03)	−4.54 (0.03)	1.02 (0.02)	–
SN 2013ab[g]	143	39.04 (0.01)	37.60 (0.01)	−4.94 (0.03)	1.43 (0.02)	–
SN 2013ab[g]	167	39.19 (0.02)	37.62 (0.01)	−1.84 (0.03)	1.57 (0.03)	–
SN 2013am[h]	256	38.02 (0.07)	36.75 (0.05)	0.46 (0.03)	0.36 (0.01)	–
SN 2013am[h]	461	37.35 (0.09)	36.14 (0.08)	−0.69 (0.03)	0.36 (0.01)	–

Notes. Uncertainties are in parentheses.
[a]Phases of spectra are in rest-frame days since discovery using the redshift and discovery date presented in Table A1.
[b]For doublets, $v_{\rm pk}$ is calculated with respect to the stronger component.
[c]HWHM$_1$ is measured for the blue component of a doublet or the only component of a singlet.
[d]HWHM$_2$ is measured for the red component of a doublet and is left blank for a singlet.
[e]SN 2012aw is also known as PTF12bvh.
[f]SN 2012fg is also known as PTF12jxe.
[g]SN 2013ab is also known as iPTF13ut.
[h]SN 2013am is also known as iPTF13aaz.

Table A8. Spectral-feature measurements of iron.

SN name	Age since discovery[a]	$\log\left(\frac{L_{\rm tot}}{\rm ergs^{-1}}\right)$	$\log\left(\frac{L_{\rm pk}}{\rm ergs^{-1}\,\AA^{-1}}\right)$	$v_{\rm pk}$ (100 km s^{-1})	HWHM (1000 km s^{-1})
			Fe II λ5018		
SN 1988A	162	39.30 (0.04)	37.50 (0.03)	9.13 (0.46)	2.28 (0.03)
SN 1992ad	225	38.51 (0.04)	36.83 (0.03)	−5.04 (0.06)	2.18 (0.04)
SN 1992ad	286	38.17 (0.08)	36.53 (0.06)	−3.92 (0.06)	1.91 (0.04)
SN 1992H	203	39.24 (0.07)	37.56 (0.05)	−3.12 (0.06)	2.50 (0.04)
SN 1992H	221	39.38 (0.03)	37.50 (0.02)	0.52 (0.06)	2.95 (0.03)
SN 1992H	382	38.51 (0.07)	36.81 (0.06)	3.82 (0.19)	2.49 (0.09)
SN 1992H	425	38.41 (0.09)	36.54 (0.09)	2.58 (0.13)	3.33 (0.28)
SN 1999em	312	38.44 (0.06)	36.62 (0.04)	8.96 (0.45)	2.20 (0.02)
SN 1999em	332	38.39 (0.05)	36.55 (0.04)	10.08 (0.50)	2.45 (0.03)
SN 1999em	418	38.13 (0.05)	36.31 (0.05)	6.54 (0.33)	2.39 (0.02)
SN 1999em	516	37.35 (0.10)	35.56 (0.07)	5.36 (0.27)	2.18 (0.04)

Table A8 – *continued*

SN name	Age since discovery[a]	$\log\left(\frac{L_{\rm tot}}{\rm ergs^{-1}}\right)$	$\log\left(\frac{L_{\rm pk}}{\rm ergs^{-1}\,\AA^{-1}}\right)$	$v_{\rm pk}$ (100 km s^{-1})	HWHM (1000 km s^{-1})
SN 1999gq	83	38.97 (0.03)	37.19 (0.02)	−3.34 (0.06)	2.74 (0.05)
SN 2001X	176	39.01 (0.04)	37.21 (0.03)	3.68 (0.18)	2.10 (0.02)
SN 2002hh	336	36.75 (0.12)	35.17 (0.11)	−3.65 (0.06)	1.71 (0.03)
SN 2002hh	394	36.07 (0.19)	34.51 (0.14)	−4.64 (0.06)	1.15 (0.03)
SN 2003gd	138	38.20 (0.05)	36.41 (0.03)	10.70 (0.54)	2.20 (0.03)
SN 2004A	162	38.64 (0.09)	37.12 (0.08)	−3.35 (0.06)	1.57 (0.04)
SN 2004A	183	38.78 (0.09)	36.98 (0.08)	−1.80 (0.06)	2.25 (0.06)
SN 2004A	282	38.44 (0.06)	36.69 (0.05)	−4.25 (0.06)	1.91 (0.06)
SN 2004dj	106	38.69 (0.04)	36.87 (0.05)	−5.37 (0.06)	2.70 (0.08)
SN 2004dj	111	38.61 (0.16)	36.81 (0.14)	7.03 (0.35)	3.65 (0.08)
SN 2004dj	134	38.55 (0.05)	36.71 (0.05)	1.56 (0.08)	2.62 (0.07)
SN 2004dj	140	38.52 (0.17)	36.67 (0.13)	9.70 (0.48)	3.63 (0.11)
SN 2004dj	169	38.44 (0.05)	36.58 (0.05)	4.00 (0.20)	2.77 (0.06)
SN 2004dj	170	38.42 (0.16)	36.57 (0.11)	9.70 (0.48)	3.61 (0.09)
SN 2004dj	196	38.44 (0.05)	36.59 (0.05)	1.61 (0.08)	2.68 (0.06)
SN 2004dj	223	38.33 (0.06)	36.47 (0.05)	7.51 (0.38)	2.56 (0.05)
SN 2004dj	225	38.46 (0.14)	36.49 (0.14)	1.69 (0.08)	4.08 (0.13)
SN 2004dj	254	38.41 (0.15)	36.45 (0.14)	1.69 (0.08)	3.96 (0.12)
SN 2004dj	260	38.23 (0.04)	36.40 (0.04)	1.68 (0.08)	2.45 (0.04)
SN 2004dj	398	37.94 (0.02)	36.14 (0.02)	−0.66 (0.06)	2.48 (0.04)
SN 2004dj	407	37.97 (0.02)	36.10 (0.02)	−0.66 (0.06)	2.83 (0.04)
SN 2004dj	635	37.49 (0.02)	35.70 (0.02)	−4.32 (0.06)	3.34 (0.09)
SN 2004et	196	38.64 (0.02)	36.77 (0.02)	11.95 (0.60)	2.85 (0.02)
SN 2004et	202	38.61 (0.02)	36.69 (0.01)	10.85 (0.54)	3.04 (0.04)
SN 2004et	277	38.30 (0.02)	36.42 (0.02)	8.49 (0.42)	2.74 (0.04)
SN 2004et	349	37.91 (0.03)	36.12 (0.02)	7.23 (0.36)	2.30 (0.03)
SN 2005ay	284	38.33 (0.17)	36.78 (0.13)	−5.07 (0.06)	1.24 (0.02)
SN 2005cs	157	37.30 (0.07)	35.74 (0.04)	5.25 (0.26)	2.03 (0.09)
SN 2005cs	303	37.10 (0.08)	35.59 (0.07)	3.14 (0.16)	1.91 (0.11)
SN 2006my	98	39.09 (0.02)	37.30 (0.01)	11.25 (0.56)	2.30 (0.02)
SN 2006ov	82	37.93 (0.05)	36.28 (0.03)	5.51 (0.28)	1.81 (0.03)
SN 2008ex	280	38.87 (0.06)	37.19 (0.05)	6.25 (0.31)	1.86 (0.03)
SN 2008ij	119	39.24 (0.05)	37.26 (0.06)	9.63 (0.48)	3.46 (0.04)
SN 2008ij	149	37.62 (0.17)	36.16 (0.14)	−4.82 (0.06)	1.20 (0.05)
SN 2008ij	186	38.30 (0.05)	36.60 (0.04)	2.29 (0.11)	2.13 (0.05)
SN 2009ls	111	38.81 (0.03)	36.77 (0.02)	2.30 (0.12)	3.88 (0.05)
SN 2009ls	164	38.30 (0.03)	36.37 (0.02)	5.87 (0.29)	3.59 (0.10)
SN 2011cj	227	39.08 (0.25)	37.53 (0.15)	−7.22 (0.06)	1.12 (0.02)
SN 2011fd	97	38.59 (0.43)	37.12 (0.22)	−6.00 (0.06)	0.81 (0.02)
SN 2011fd	185	38.76 (0.42)	37.30 (0.21)	−6.02 (0.06)	0.81 (0.02)
SN 2012A	406	37.14 (0.34)	36.18 (0.19)	−7.11 (0.06)	0.24 (0.01)
SN 2012A	432	38.18 (0.51)	36.42 (0.30)	−5.18 (0.06)	1.58 (0.05)
SN 2012aw[b]	337	38.32 (0.01)	36.52 (0.01)	4.68 (0.23)	2.26 (0.02)
SN 2012aw[b]	364	38.41 (0.10)	36.52 (0.08)	6.57 (0.33)	2.97 (0.09)
SN 2012ch	335	39.14 (0.08)	37.27 (0.08)	2.58 (0.13)	4.27 (0.15)
SN 2012ec	214	38.64 (0.14)	37.09 (0.11)	−5.89 (0.06)	1.98 (0.14)
SN 2012ec	393	37.90 (0.10)	36.66 (0.08)	−7.36 (0.06)	0.84 (0.05)
SN 2012fg[c]	171	39.09 (0.12)	37.24 (0.11)	−13.01 (0.06)	2.97 (0.17)
SN 2012fg[c]	211	38.72 (0.10)	37.12 (0.10)	−8.27 (0.06)	1.46 (0.08)
SN 2012ho	154	39.26 (0.05)	37.49 (0.07)	−6.65 (0.06)	2.99 (0.07)
SN 2012ho	215	39.08 (0.08)	37.23 (0.06)	1.24 (0.06)	2.95 (0.04)
SN 2012ho	235	39.02 (0.10)	37.19 (0.09)	3.54 (0.18)	2.93 (0.04)
SN 2012ho	237	38.84 (0.08)	37.20 (0.09)	−6.55 (0.06)	2.42 (0.11)
SN 2012ho	250	39.01 (0.11)	37.14 (0.09)	1.29 (0.06)	3.16 (0.06)
SN 2012ho	303	38.70 (0.14)	37.05 (0.15)	−6.40 (0.06)	2.54 (0.10)
SN 2013ab[d]	143	39.25 (0.02)	37.37 (0.01)	11.85 (0.59)	3.01 (0.03)
SN 2013ab[d]	167	39.11 (0.03)	37.30 (0.03)	9.53 (0.48)	2.58 (0.04)
SN 2013am[e]	256	37.10 (0.06)	35.45 (0.08)	7.35 (0.37)	2.60 (0.15)
			Fe II λ5527		
SN 1988A	162	39.44 (0.04)	37.73 (0.04)	4.34 (0.22)	2.24 (0.06)
SN 1989L	182	38.66 (0.04)	37.01 (0.04)	4.23 (0.21)	2.82 (0.10)
SN 1990E	151	38.46 (0.07)	36.67 (0.07)	1.86 (0.09)	3.42 (0.12)

Table A8 – *continued*

SN name	Age since discovery[a]	$\log\left(\frac{L_{\rm tot}}{\rm ergs^{-1}}\right)$	$\log\left(\frac{L_{\rm pk}}{\rm ergs^{-1}\,\AA^{-1}}\right)$	$v_{\rm pk}$ (100 km s^{-1})	HWHM (1000 km s^{-1})
SN 1992ad	225	38.51 (0.02)	36.72 (0.02)	−0.79 (0.05)	2.87 (0.03)
SN 1992ad	286	38.12 (0.04)	36.30 (0.04)	−7.44 (0.05)	3.52 (0.11)
SN 1992H	203	39.32 (0.06)	37.54 (0.06)	−1.75 (0.05)	2.94 (0.05)
SN 1992H	221	39.23 (0.02)	37.43 (0.01)	0.40 (0.05)	3.72 (0.05)
SN 1992H	382	38.57 (0.06)	36.70 (0.05)	−1.71 (0.05)	3.41 (0.05)
SN 1992H	492	38.08 (0.11)	36.23 (0.10)	8.66 (0.43)	2.96 (0.28)
SN 1999em	312	38.32 (0.04)	36.55 (0.03)	5.85 (0.29)	2.20 (0.05)
SN 1999em	332	38.29 (0.05)	36.52 (0.05)	0.50 (0.05)	2.51 (0.05)
SN 1999em	418	37.87 (0.04)	36.17 (0.04)	2.50 (0.13)	2.08 (0.04)
SN 1999em	516	37.13 (0.06)	35.42 (0.04)	0.48 (0.05)	1.38 (0.09)
SN 1999gq	83	38.80 (0.03)	37.14 (0.03)	2.83 (0.14)	2.67 (0.05)
SN 2001X	176	38.86 (0.04)	37.22 (0.03)	3.53 (0.18)	1.90 (0.03)
SN 2002hh	159	36.87 (0.11)	35.36 (0.08)	−3.84 (0.05)	1.25 (0.02)
SN 2002hh	394	36.35 (0.10)	34.68 (0.08)	−3.82 (0.05)	2.29 (0.14)
SN 2003gd	138	38.10 (0.04)	36.41 (0.03)	1.12 (0.06)	2.11 (0.05)
SN 2003hl	149	37.96 (0.14)	36.38 (0.12)	1.27 (0.06)	1.20 (0.09)
SN 2004A	162	38.72 (0.05)	37.12 (0.05)	0.14 (0.05)	1.91 (0.05)
SN 2004A	183	38.60 (0.07)	37.03 (0.07)	2.28 (0.11)	1.80 (0.06)
SN 2004A	282	38.24 (0.07)	36.61 (0.07)	0.08 (0.05)	1.71 (0.04)
SN 2004dj	106	38.45 (0.04)	36.84 (0.04)	−5.68 (0.05)	2.34 (0.06)
SN 2004dj	134	38.25 (0.05)	36.69 (0.05)	−3.60 (0.05)	2.17 (0.06)
SN 2004dj	140	38.64 (0.04)	36.66 (0.04)	7.32 (0.37)	5.13 (0.08)
SN 2004dj	169	38.13 (0.03)	36.56 (0.03)	−0.47 (0.05)	2.69 (0.07)
SN 2004dj	170	38.62 (0.03)	36.58 (0.03)	12.58 (0.63)	4.79 (0.08)
SN 2004dj	196	38.05 (0.04)	36.54 (0.04)	−2.58 (0.05)	2.23 (0.05)
SN 2004dj	223	38.06 (0.03)	36.41 (0.03)	−1.43 (0.05)	2.79 (0.07)
SN 2004dj	225	38.53 (0.03)	36.48 (0.02)	9.93 (0.50)	4.44 (0.07)
SN 2004dj	254	38.46 (0.03)	36.41 (0.02)	9.93 (0.50)	4.46 (0.06)
SN 2004dj	260	38.06 (0.01)	36.30 (0.01)	0.78 (0.05)	3.36 (0.06)
SN 2004dj	398	37.82 (0.02)	36.04 (0.02)	−0.32 (0.05)	2.46 (0.05)
SN 2004dj	407	37.81 (0.02)	36.03 (0.02)	0.85 (0.05)	2.59 (0.06)
SN 2004dj	635	37.26 (0.04)	35.64 (0.04)	−1.32 (0.05)	2.18 (0.04)
SN 2004dj	875	36.80 (0.01)	35.49 (0.03)	−1.09 (0.05)	1.15 (0.08)
SN 2004dj	905	36.66 (0.02)	35.42 (0.02)	−0.74 (0.05)	1.07 (0.03)
SN 2004dj	1199	36.72 (0.01)	35.50 (0.01)	−2.94 (0.05)	1.48 (0.06)
SN 2004et	196	38.68 (0.01)	36.82 (0.01)	7.12 (0.36)	3.18 (0.05)
SN 2004et	202	38.60 (0.02)	36.76 (0.01)	8.24 (0.41)	3.09 (0.04)
SN 2004et	277	38.17 (0.01)	36.37 (0.01)	4.95 (0.25)	2.90 (0.05)
SN 2004et	349	37.69 (0.04)	36.03 (0.03)	4.86 (0.24)	2.25 (0.04)
SN 2005ay	284	38.25 (0.11)	36.64 (0.11)	3.74 (0.19)	1.69 (0.06)
SN 2005cs	157	37.59 (0.03)	36.00 (0.02)	1.15 (0.06)	1.82 (0.03)
SN 2005cs	303	37.51 (0.07)	35.67 (0.06)	7.28 (0.36)	2.64 (0.07)
SN 2006my	98	38.97 (0.02)	37.24 (0.02)	10.06 (0.50)	2.50 (0.03)
SN 2006ov	82	37.94 (0.04)	36.29 (0.04)	5.80 (0.29)	1.85 (0.04)
SN 2007gw	186	38.78 (0.06)	37.04 (0.05)	−13.09 (0.05)	2.56 (0.16)
SN 2008ij	119	39.15 (0.03)	37.27 (0.03)	6.66 (0.33)	4.11 (0.06)
SN 2008ij	149	38.06 (0.12)	36.26 (0.08)	0.36 (0.05)	2.11 (0.06)
SN 2008ij	186	38.34 (0.06)	36.59 (0.04)	0.33 (0.05)	2.06 (0.04)
SN 2009ls	111	38.49 (0.02)	36.76 (0.01)	5.17 (0.26)	2.97 (0.05)
SN 2009ls	164	38.23 (0.03)	36.44 (0.03)	5.17 (0.26)	2.85 (0.04)
SN 2011cj	227	38.91 (0.05)	37.25 (0.05)	1.50 (0.08)	2.57 (0.06)
SN 2011fd	97	38.37 (0.06)	36.76 (0.06)	5.12 (0.26)	1.78 (0.05)
SN 2011fd	185	38.60 (0.09)	36.92 (0.08)	1.73 (0.09)	2.14 (0.08)
SN 2012A	406	37.04 (0.26)	35.49 (0.15)	−3.21 (0.05)	1.05 (0.03)
SN 2012A	432	37.56 (0.04)	35.60 (0.04)	3.11 (0.16)	4.78 (0.14)
SN 2012aw[b]	337	38.22 (0.01)	36.57 (0.01)	4.04 (0.20)	1.81 (0.02)
SN 2012aw[b]	364	38.47 (0.06)	36.46 (0.04)	4.94 (0.25)	3.81 (0.05)
SN 2012ec	214	38.62 (0.11)	37.02 (0.09)	13.15 (0.66)	1.77 (0.06)
SN 2012ec	393	38.25 (0.03)	36.42 (0.04)	10.45 (0.52)	4.61 (0.18)
SN 2012fg[c]	171	39.10 (0.09)	37.17 (0.08)	−8.06 (0.05)	3.47 (0.38)
SN 2012fg[c]	211	38.78 (0.13)	36.93 (0.10)	−0.34 (0.05)	2.89 (0.08)
SN 2012ho	154	39.14 (0.04)	37.40 (0.04)	1.25 (0.06)	3.32 (0.08)

Table A8 – *continued*

SN name	Age since discovery[a]	$\log\left(\frac{L_{\rm tot}}{\rm ergs^{-1}}\right)$	$\log\left(\frac{L_{\rm pk}}{\rm ergs^{-1}\AA^{-1}}\right)$	$v_{\rm pk}$ (100 km s^{-1})	HWHM (1000 km s^{-1})
SN 2012ho	215	38.99 (0.03)	37.11 (0.03)	−6.18 (0.05)	3.95 (0.10)
SN 2012ho	235	39.00 (0.05)	37.07 (0.04)	−6.06 (0.05)	3.95 (0.07)
SN 2012ho	237	38.62 (0.02)	36.97 (0.02)	0.22 (0.05)	2.02 (0.05)
SN 2012ho	250	38.98 (0.05)	37.04 (0.04)	−1.94 (0.05)	3.88 (0.05)
SN 2012ho	303	38.21 (0.26)	36.94 (0.14)	−2.06 (0.05)	0.80 (0.05)
SN 2013ab[d]	143	39.45 (0.01)	37.41 (0.02)	17.69 (0.88)	4.93 (0.05)
SN 2013ab[d]	167	39.11 (0.01)	37.31 (0.01)	13.15 (0.66)	3.56 (0.08)
SN 2013am[e]	256	37.26 (0.06)	35.86 (0.04)	3.60 (0.18)	0.89 (0.02)
			[Fe II] λ7155		
SN 1988A	162	39.27 (0.04)	37.62 (0.04)	0.75 (0.04)	1.55 (0.03)
SN 1988A	182	38.76 (0.03)	37.19 (0.03)	0.68 (0.04)	1.30 (0.02)
SN 1988H	119	38.78 (0.02)	37.20 (0.02)	−0.69 (0.04)	1.87 (0.05)
SN 1989L	182	38.61 (0.04)	37.08 (0.03)	3.50 (0.04)	1.49 (0.02)
SN 1990E	304	37.60 (0.13)	36.20 (0.13)	2.74 (0.04)	0.78 (0.04)
SN 1992ad	225	38.26 (0.03)	36.74 (0.02)	−2.98 (0.04)	1.58 (0.04)
SN 1992H	382	38.27 (0.04)	36.77 (0.03)	−5.21 (0.04)	1.48 (0.16)
SN 1992H	425	38.06 (0.04)	36.52 (0.04)	−6.11 (0.04)	1.68 (0.39)
SN 1992H	461	37.92 (0.13)	36.37 (0.11)	−8.49 (0.04)	1.66 (0.38)
SN 1992H	492	37.69 (0.12)	36.23 (0.12)	−2.83 (0.04)	1.57 (0.38)
SN 1993G	114	37.78 (0.35)	36.48 (0.26)	7.49 (0.20)	0.43 (0.07)
SN 1993K	282	38.08 (0.39)	36.67 (0.27)	5.45 (0.09)	0.44 (0.02)
SN 1999em	312	38.24 (0.04)	36.76 (0.03)	0.35 (0.04)	1.22 (0.02)
SN 1999em	332	38.29 (0.03)	36.70 (0.02)	2.01 (0.04)	1.43 (0.02)
SN 1999em	418	37.96 (0.03)	36.40 (0.02)	1.99 (0.04)	1.31 (0.01)
SN 2001X	176	38.71 (0.03)	37.21 (0.03)	−3.06 (0.04)	1.37 (0.01)
SN 2002hh	159	37.62 (0.02)	36.09 (0.02)	−6.35 (0.04)	2.68 (0.09)
SN 2002hh	336	36.90 (0.04)	35.35 (0.04)	−4.78 (0.04)	2.05 (0.09)
SN 2002hh	394	36.85 (0.01)	35.25 (0.02)	−3.99 (0.04)	1.65 (0.12)
SN 2003gd	138	38.02 (0.04)	36.49 (0.04)	1.02 (0.04)	1.11 (0.01)
SN 2003hl	149	37.76 (0.05)	36.34 (0.05)	−5.50 (0.04)	0.96 (0.17)
SN 2004A	162	38.66 (0.03)	37.08 (0.02)	−4.26 (0.04)	1.74 (0.04)
SN 2004A	183	38.63 (0.04)	37.05 (0.04)	−3.50 (0.04)	1.29 (0.02)
SN 2004A	282	38.42 (0.06)	36.82 (0.05)	−4.27 (0.04)	0.94 (0.01)
SN 2004dj	106	38.16 (0.02)	36.65 (0.02)	−10.55 (0.04)	1.92 (0.04)
SN 2004dj	134	38.18 (0.03)	36.63 (0.03)	−11.35 (0.04)	1.64 (0.03)
SN 2004dj	140	38.13 (0.06)	36.59 (0.06)	−12.60 (0.04)	1.92 (0.16)
SN 2004dj	169	38.19 (0.02)	36.58 (0.02)	−10.46 (0.04)	1.63 (0.03)
SN 2004dj	170	38.19 (0.06)	36.55 (0.06)	−12.44 (0.04)	1.52 (0.05)
SN 2004dj	196	38.22 (0.03)	36.60 (0.03)	−8.87 (0.04)	1.49 (0.03)
SN 2004dj	223	38.08 (0.03)	36.50 (0.03)	−8.07 (0.04)	1.40 (0.03)
SN 2004dj	225	38.24 (0.05)	36.52 (0.05)	−4.46 (0.04)	1.25 (0.03)
SN 2004dj	254	38.09 (0.05)	36.49 (0.05)	−2.72 (0.04)	1.09 (0.01)
SN 2004dj	260	38.05 (0.03)	36.45 (0.03)	−8.05 (0.04)	1.39 (0.03)
SN 2004dj	398	37.89 (0.02)	36.26 (0.02)	−2.96 (0.04)	1.28 (0.01)
SN 2004dj	407	37.86 (0.03)	36.24 (0.02)	−2.98 (0.04)	1.25 (0.01)
SN 2004dj	635	37.30 (0.08)	35.74 (0.06)	−2.07 (0.04)	1.00 (0.01)
SN 2004dj	875	36.99 (0.01)	35.50 (0.03)	−1.32 (0.04)	0.90 (0.04)
SN 2004dj	905	36.98 (0.03)	35.42 (0.03)	−1.28 (0.04)	1.44 (0.06)
SN 2004et	196	38.38 (0.02)	36.84 (0.02)	4.43 (0.04)	2.07 (0.01)
SN 2004et	202	38.36 (0.02)	36.85 (0.02)	3.71 (0.04)	1.57 (0.03)
SN 2004et	277	38.12 (0.02)	36.53 (0.02)	5.34 (0.09)	1.54 (0.01)
SN 2004et	349	37.89 (0.02)	36.27 (0.02)	6.11 (0.13)	1.46 (0.02)
SN 2005ay	284	38.35 (0.03)	36.69 (0.02)	−0.58 (0.04)	1.27 (0.02)
SN 2005cs	157	37.29 (0.02)	35.91 (0.02)	−0.29 (0.04)	1.12 (0.04)
SN 2005cs	303	37.19 (0.07)	35.70 (0.06)	3.78 (0.04)	0.96 (0.01)
SN 2006my	98	38.65 (0.01)	37.21 (0.01)	−0.32 (0.04)	1.43 (0.02)
SN 2006ov	82	37.69 (0.03)	36.16 (0.02)	2.58 (0.04)	1.11 (0.02)
SN 2008ex	280	39.04 (0.03)	37.47 (0.03)	3.06 (0.04)	1.84 (0.04)
SN 2008ij	186	38.16 (0.02)	36.54 (0.02)	−1.44 (0.04)	2.06 (0.06)
SN 2011cj	227	38.80 (0.03)	37.21 (0.03)	−2.99 (0.04)	1.77 (0.04)
SN 2011fd	185	38.35 (0.04)	36.88 (0.04)	−3.42 (0.04)	1.16 (0.04)
SN 2012A	406	37.37 (0.04)	35.88 (0.05)	2.42 (0.04)	1.14 (0.02)

Table A8 – *continued*

SN name	Age since discovery[a]	$\log\left(\frac{L_{\rm tot}}{\rm ergs^{-1}}\right)$	$\log\left(\frac{L_{\rm pk}}{\rm ergs^{-1}\,\AA^{-1}}\right)$	$v_{\rm pk}$ (100 km s^{-1})	HWHM (1000 km s^{-1})
SN 2012A	432	37.47 (0.11)	35.69 (0.10)	−2.87 (0.04)	1.59 (0.02)
SN 2012aw[b]	337	38.22 (0.01)	36.81 (0.01)	2.71 (0.04)	1.24 (0.01)
SN 2012aw[b]	364	38.30 (0.08)	36.70 (0.08)	0.17 (0.04)	1.50 (0.01)
SN 2012ec	214	38.34 (0.07)	36.84 (0.07)	−0.82 (0.04)	1.05 (0.02)
SN 2012ec	393	37.88 (0.02)	36.34 (0.01)	−0.63 (0.04)	1.34 (0.03)
SN 2012ho	154	38.67 (0.02)	37.28 (0.02)	−3.95 (0.04)	1.62 (0.06)
SN 2012ho	215	38.48 (0.05)	37.04 (0.05)	−6.40 (0.04)	1.97 (0.20)
SN 2012ho	235	38.55 (0.06)	36.97 (0.06)	−3.36 (0.04)	2.03 (0.10)
SN 2012ho	237	38.54 (0.02)	37.00 (0.02)	−6.31 (0.04)	1.36 (0.04)
SN 2012ho	250	38.45 (0.06)	36.95 (0.07)	−1.90 (0.04)	1.47 (0.22)
SN 2012ho	303	38.30 (0.09)	36.84 (0.08)	−0.99 (0.04)	1.27 (0.06)
SN 2013ab[d]	143	38.72 (0.01)	37.29 (0.01)	2.60 (0.04)	2.57 (0.08)
SN 2013ab[d]	167	38.76 (0.01)	37.21 (0.01)	2.23 (0.04)	2.44 (0.04)
SN 2013am[e]	256	37.80 (0.05)	36.38 (0.04)	1.61 (0.04)	0.61 (0.01)
SN 2013am[e]	461	37.61 (0.07)	36.22 (0.05)	2.13 (0.04)	0.59 (0.02)

Notes. Uncertainties are in parentheses.
[a]Phases of spectra are in rest-frame days since discovery using the redshift and discovery date presented in Table A1.
[b]SN 2012aw is also known as PTF12bvh.
[c]SN 2012fg is also known as PTF12jxe.
[d]SN 2013ab is also known as iPTF13ut.
[e]SN 2013am is also known as iPTF13aaz.

Table A9. Late-time light curves.

SN name	Filter	No. of points	MJD range	Slope[a]	Photometry reference
SN 1988A	*B*	3	47531–47623	0.985 (0.124)	Benetti, Cappellaro & Turatto (1991)
SN 1988A	*V*	4	47339–47623	1.075 (0.023)	Benetti et al. (1991)
SN 1988A	*R*	5	47362–47689	0.855 (0.036)	Ruiz-Lapuente et al. (1990)
SN 1990E	*B*	3	48076–48188	0.619 (0.326)	Schmidt et al. (1993)
SN 1990E	*V*	10	48084–48244	0.912 (0.094)	Schmidt et al. (1993)
SN 1990E	*R*	13	48084–48272	0.889 (0.059)	Schmidt et al. (1993)
SN 1990E	*I*	13	48084–48272	0.959 (0.054)	Schmidt et al. (1993)
SN 1992H	*B*	11	48808–49105	0.757 (0.011)	Clocchiatti et al. (1996)
SN 1992H	*V*	10	48833–49105	0.997 (0.010)	Clocchiatti et al. (1996)
SN 1992H	*R*	6	49009–49101	1.443 (0.029)	Clocchiatti et al. (1996)
SN 1999em	*B*	7	51614–51812	0.585 (0.059)	Faran et al. (2014a)
SN 1999em	*V*	10	51614–51819	0.929 (0.017)	Faran et al. (2014a)
SN 1999em	*R*	10	51614–51819	0.965 (0.010)	Faran et al. (2014a)
SN 1999em	*I*	10	51614–51819	0.950 (0.018)	Faran et al. (2014a)
SN 1999gq	Unf[b]	10	51615–51698	0.685 (0.166)	Ganeshalingam et al. (2010)[c]
SN 2001X	*B*	3	52088–52109	1.413 (0.963)	Faran et al. (2014a)
SN 2001X	*V*	4	52088–52109	1.348 (0.060)	Faran et al. (2014a)
SN 2001X	*R*	4	52088–52109	0.995 (0.241)	Faran et al. (2014a)
SN 2001X	*I*	4	52088–52109	1.330 (0.233)	Faran et al. (2014a)
SN 2002hh	*V*	10	52744–52846	0.938 (0.176)	Pozzo et al. (2006)
SN 2002hh	*R*	12	52744–52855	1.011 (0.048)	Pozzo et al. (2006)
SN 2002hh	*I*	12	52744–52855	1.005 (0.047)	Pozzo et al. (2006)
SN 2003gd	*B*	6	52849–52882	0.460 (0.230)	Faran et al. (2014a)
SN 2003gd	*V*	7	52849–52888	0.830 (0.092)	Faran et al. (2014a)
SN 2003gd	*R*	7	52849–52888	0.845 (0.052)	Faran et al. (2014a)
SN 2003gd	*I*	7	52849–52888	0.986 (0.053)	Faran et al. (2014a)
SN 2003hl[d]	*V*	–	–	0.800 (0.000)	Olivares E. et al. (2010)
SN 2004A	*B*	13	53157–53246	0.716 (0.014)	Gurugubelli et al. (2008)
SN 2004A	*V*	17	53139–53255	1.102 (0.008)	Gurugubelli et al. (2008)
SN 2004A	*R*	21	53137–53255	0.841 (0.007)	Gurugubelli et al. (2008)
SN 2004A	*I*	17	53146–53255	0.955 (0.009)	Gurugubelli et al. (2008)
SN 2004dj	*B*	8	53339–53374	0.618 (0.051)	Ganeshalingam et al. (2010)[c]
SN 2004dj	*V*	9	53335–53374	1.116 (0.032)	Ganeshalingam et al. (2010)[c]
SN 2004dj	*R*	11	53327–53374	0.454 (0.015)	Ganeshalingam et al. (2010)[c]

Table A9 – *continued*

SN name	Filter	No. of points	MJD range	Slope[a]	Photometry reference
SN 2004dj	*I*	11	53327–53374	0.357 (0.015)	Ganeshalingam et al. (2010)[c]
SN 2004et	*B*	25	53436–53698	0.758 (0.006)	Sahu et al. (2006)
SN 2004et	*V*	28	53454–53811	1.139 (0.004)	Sahu et al. (2006)
SN 2004et	*R*	30	53454–53811	1.251 (0.003)	Sahu et al. (2006)
SN 2004et	*I*	27	53454–53731	1.285 (0.004)	Sahu et al. (2006)
SN 2005ay	*V*	4	53680–53688	1.169 (0.072)	Tsvetkov et al. (2006)
SN 2005ay	*R*	6	53680–53852	0.923 (0.122)	Tsvetkov et al. (2006)
SN 2005cs	*B*	9	53699–53859	0.301 (0.189)	Pastorello et al. (2009)
SN 2005cs	*V*	23	53699–53926	0.402 (0.032)	Pastorello et al. (2009)
SN 2005cs	*R*	19	53699–53926	0.630 (0.021)	Pastorello et al. (2009)
SN 2005cs	*I*	21	53699–53926	0.714 (0.021)	Pastorello et al. (2009)
SN 2006my	Unf[b]	12	54099–54148	0.889 (0.063)	Ganeshalingam et al. (2010)[c]
SN 2006ov	*V*	18	54120–54206	0.243 (0.088)	Spiro et al. (2014)
SN 2006ov	*R*	16	54126–54206	1.166 (0.105)	Spiro et al. (2014)
SN 2006ov	*I*	8	54121–54206	1.135 (0.085)	Spiro et al. (2014)
SN 2007gw	Unf[b]	6	54503–54626	0.420 (0.410)	Ganeshalingam et al. (2010)[c]
SN 2008ex	*V*	8	54975–55042	0.962 (0.088)	Ganeshalingam et al. (2010)[c]
SN 2008ex	*R*	10	54971–55042	1.072 (0.060)	Ganeshalingam et al. (2010)[c]
SN 2008ex	*I*	11	54971–55042	1.047 (0.057)	Ganeshalingam et al. (2010)[c]
SN 2012A	*B*	7	56077–56326	0.604 (0.060)	Tomasella et al. (2013)
SN 2012A	*V*	10	56077–56344	0.807 (0.040)	Tomasella et al. (2013)
SN 2012A	*R*	10	56077–56344	0.886 (0.040)	Tomasella et al. (2013)
SN 2012A	*I*	5	56221–56326	1.164 (0.098)	Tomasella et al. (2013)
SN 2012aw[e]	*B*	14	56219–56332	0.603 (0.015)	Ganeshalingam et al. (2010)[c]
SN 2012aw[e]	*V*	27	56219–56421	0.893 (0.004)	Ganeshalingam et al. (2010)[c]
SN 2012aw[e]	*R*	27	56219–56421	1.005 (0.003)	Ganeshalingam et al. (2010)[c]
SN 2012aw[e]	*I*	26	56219–56421	1.096 (0.003)	Ganeshalingam et al. (2010)[c]
SN 2012ec	*B*	3	56283–56303	1.794 (1.808)	Barbarino et al. (2015)
SN 2012ec	*V*	4	56283–56306	1.306 (0.389)	Barbarino et al. (2015)
SN 2012ec	*R*	5	56278–56306	0.942 (0.538)	Barbarino et al. (2015)
SN 2012ec	*I*	3	56290–56306	0.683 (1.051)	Barbarino et al. (2015)
SN 2012fg[f]	*B*	33	56337–56445	1.064 (0.313)	Rubin, private communication
SN 2012fg[f]	*V*	24	56337–56445	1.234 (0.105)	Rubin, private communication
SN 2012fg[f]	*R*	24	56337–56445	1.583 (0.022)	Rubin, private communication
SN 2012fg[f]	*I*	24	56337–56445	1.590 (0.131)	Rubin, private communication
SN 2012ho	Unf[b]	32	56473–56541	0.892 (0.144)	Ganeshalingam et al. (2010)[c]
SN 2013ab[g]	*B*	23	56459–56524	0.342 (0.069)	Bose et al. (2015)
SN 2013ab[g]	*V*	29	56455–56528	0.992 (0.028)	Bose et al. (2015)
SN 2013ab[g]	*R*	22	56459–56529	0.804 (0.023)	Bose et al. (2015)
SN 2013ab[g]	*I*	16	56475–56529	1.364 (0.046)	Bose et al. (2015)
SN 2013am[h]	*V*	4	56603–56688	0.409 (0.100)	Zhang et al. (2014)
SN 2013am[h]	*R*	5	56603–56716	0.380 (0.171)	Zhang et al. (2014)
SN 2013am[h]	*I*	5	56603–56716	0.523 (0.108)	Zhang et al. (2014)

[a]Slopes and uncertainties are in units of mag per 100 d; uncertainties are in parentheses.
[b]'Unf' is unfiltered KAIT data (Ganeshalingam et al. 2010).
[c]These data are previously unpublished but the observations and data reduction pipeline are described in Ganeshalingam et al. (2010).
[d] Olivares E. et al. (2010) provide only a linear fit for the late-time *V*-band magnitude versus time with the slope listed here.
[e]SN 2012aw is also known as PTF12bvh.
[f]SN 2012fg is also known as PTF12jxe.
[g]SN 2013ab is also known as iPTF13ut.
[h]SN 2013am is also known as iPTF13aaz.

Table A10. Interpolated/extrapolated photometry at spectral epochs.

SN name	MJD[a]	Age since discovery[b]	*B* (mag)[c]	*V* (mag)[c]	*R* (mag)[c]	*I* (mag)[c]	Unf.[d] (mag)[c]
SN 1988A	47339.262	162	18.17 (0.09)	17.24 (0.05)	16.10 (0.09)	–	–
SN 1988A	47359.195	182	18.37 (0.09)	17.45 (0.05)	16.27 (0.09)	–	–
SN 1988H	47343.245	119	18.69 (0.09)	17.48 (0.04)	–	–	–
SN 1990E	48089.000	151	20.48 (0.02)	18.92 (0.09)	17.55 (0.12)	16.70 (0.06)	–
SN 1990E	48103.479	165	20.57 (0.02)	19.05 (0.09)	17.67 (0.12)	16.84 (0.06)	–
SN 1990E	48133.000	195	20.75 (0.02)	19.32 (0.09)	17.94 (0.12)	17.12 (0.06)	–
SN 1990E	48242.214	303	21.43 (0.02)	20.32 (0.09)	18.91 (0.12)	18.17 (0.06)	–
SN 1990K	48184.356	147	20.14 (0.10)	19.06 (0.08)	17.93 (0.11)	–	–
SN 1990K	48242.163	205	20.62 (0.10)	19.54 (0.08)	18.72 (0.11)	–	–
SN 1992H	48867.208	202	18.99 (0.05)	17.80 (0.06)	16.30 (0.06)	–	–
SN 1992H	48886.144	221	19.13 (0.05)	17.99 (0.06)	16.57 (0.06)	–	–
SN 1992H	49047.470	382	20.35 (0.05)	19.59 (0.06)	18.90 (0.06)	–	–
SN 1992H	49091.435	425	20.69 (0.05)	20.03 (0.06)	19.53 (0.06)	–	–
SN 1992H	49127.000	461	20.96 (0.05)	20.39 (0.06)	20.04 (0.06)	–	–
SN 1992H	49158.000	492	21.19 (0.05)	20.70 (0.06)	20.49 (0.06)	–	–
SN 1999em	51793.515	312	19.12 (0.07)	18.17 (0.03)	17.23 (0.03)	16.75 (0.02)	–
SN 1999em	51813.494	332	19.24 (0.07)	18.36 (0.03)	17.42 (0.03)	16.94 (0.02)	–
SN 1999em	51899.000	418	19.74 (0.07)	19.15 (0.03)	18.25 (0.03)	17.75 (0.02)	–
SN 1999em	51997.244	516	20.32 (0.07)	20.06 (0.03)	19.19 (0.03)	18.68 (0.02)	–
SN 1999gq	51618.399	83	–	–	–	–	17.17 (0.27)
SN 2001X	52144.206	176	19.67 (0.20)	18.28 (0.02)	17.23 (0.03)	16.97 (0.02)	–
SN 2002hh	52737.499	159	–	19.39 (0.21)	17.23 (0.14)	15.80 (0.12)	–
SN 2002hh	52914.170	336	–	21.05 (0.21)	19.02 (0.14)	17.57 (0.12)	–
SN 2002hh	52972.211	394	–	21.60 (0.21)	19.60 (0.14)	18.16 (0.12)	–
SN 2003gd	52940.372	138	19.37 (0.06)	18.14 (0.04)	17.10 (0.05)	16.61 (0.04)	–
SN 2003hl	53021.178	148	–	21.11 (0.04)	–	–	–
SN 2004A	53176.403	162	19.45 (0.07)	17.90 (0.02)	17.11 (0.01)	16.68 (0.02)	–
SN 2004A	53197.367	183	19.60 (0.07)	18.13 (0.02)	17.29 (0.01)	16.88 (0.02)	–
SN 2004A	53296.230	282	20.31 (0.07)	19.22 (0.02)	18.12 (0.01)	17.82 (0.02)	–
SN 2004dj	53323.000	105	16.18 (0.02)	14.85 (0.03)	14.28 (0.02)	13.79 (0.02)	–
SN 2004dj	53328.529	111	16.21 (0.02)	14.92 (0.03)	14.30 (0.02)	13.81 (0.02)	–
SN 2004dj	53351.525	134	16.35 (0.02)	15.17 (0.03)	14.40 (0.02)	13.89 (0.02)	–
SN 2004dj	53357.267	140	16.39 (0.02)	15.24 (0.03)	14.43 (0.02)	13.91 (0.02)	–
SN 2004dj	53386.432	169	16.57 (0.02)	15.56 (0.03)	14.56 (0.02)	14.01 (0.02)	–
SN 2004dj	53387.235	170	16.58 (0.02)	15.57 (0.03)	14.57 (0.02)	14.02 (0.02)	–
SN 2004dj	53413.426	196	16.74 (0.02)	15.86 (0.03)	14.69 (0.02)	14.11 (0.02)	–
SN 2004dj	53440.272	223	16.90 (0.02)	16.16 (0.03)	14.81 (0.02)	14.21 (0.02)	–
SN 2004dj	53442.332	225	16.92 (0.02)	16.19 (0.03)	14.82 (0.02)	14.21 (0.02)	–
SN 2004dj	53471.233	254	17.09 (0.02)	16.51 (0.03)	14.95 (0.02)	14.32 (0.02)	–
SN 2004dj	53477.182	260	17.13 (0.02)	16.58 (0.03)	14.97 (0.02)	14.34 (0.02)	–
SN 2004dj	53615.494	398	17.99 (0.02)	18.12 (0.03)	15.60 (0.02)	14.83 (0.02)	–
SN 2004dj	53624.499	407	18.04 (0.02)	18.22 (0.03)	15.64 (0.02)	14.86 (0.02)	–
SN 2004dj	53852.292	635	19.45 (0.02)	20.76 (0.03)	16.68 (0.02)	15.68 (0.02)	–
SN 2004dj	54092.484	875	20.93 (0.02)	23.44 (0.03)	17.77 (0.02)	16.53 (0.02)	–
SN 2004dj	54122.398	905	21.12 (0.02)	23.77 (0.03)	17.90 (0.02)	16.64 (0.02)	–
SN 2004dj	54416.603	1199	22.94 (0.02)	27.06 (0.03)	19.24 (0.02)	17.69 (0.02)	–
SN 2004et	53471.494	196	17.89 (0.05)	16.13 (0.08)	14.95 (0.13)	14.43 (0.06)	–
SN 2004et	53477.421	202	17.93 (0.05)	16.20 (0.08)	15.02 (0.13)	14.51 (0.06)	–
SN 2004et	53552.428	277	18.50 (0.05)	17.05 (0.08)	15.96 (0.13)	15.47 (0.06)	–
SN 2004et	53624.354	349	19.05 (0.05)	17.87 (0.08)	16.86 (0.13)	16.40 (0.06)	–
SN 2005ay	53741.579	284	–	19.39 (0.06)	18.32 (0.06)	–	–
SN 2005cs	53706.659	157	21.54 (0.06)	19.36 (0.13)	17.96 (0.10)	17.09 (0.09)	–
SN 2005cs	53852.529	303	21.98 (0.06)	19.95 (0.13)	18.88 (0.10)	18.13 (0.09)	–
SN 2006my	54145.661	98	–	–	–	–	17.73 (0.03)
SN 2006ov	54145.654	82	–	20.09 (0.08)	19.09 (0.09)	18.57 (0.12)	–
SN 2007gw	54525.500	186	–	–	–	–	19.42 (0.19)
SN 2008ex	54979.455	280	–	19.92 (0.09)	18.71 (0.08)	18.07 (0.09)	–
SN 2012A	56340.305	406	20.97 (0.11)	20.08 (0.09)	19.15 (0.14)	19.21 (0.09)	–
SN 2012A	56366.145	432	21.12 (0.11)	20.29 (0.09)	19.38 (0.14)	19.51 (0.09)	–
SN 2012aw[e]	56340.323	337	18.95 (0.04)	17.83 (0.04)	17.00 (0.04)	16.48 (0.06)	–
SN 2012aw[e]	56367.343	364	19.12 (0.04)	18.08 (0.04)	17.27 (0.04)	16.78 (0.06)	–
SN 2012ec	56365.000	213	20.30 (0.06)	18.82 (0.06)	17.65 (0.04)	17.23 (0.08)	–
SN 2012ec	56545.543	393	23.54 (0.06)	21.18 (0.06)	19.36 (0.04)	18.47 (0.08)	–

Table A10 – *continued*

SN name	MJD[a]	Age since discovery[b]	*B* (mag)[c]	*V* (mag)[c]	*R* (mag)[c]	*I* (mag)[c]	Unf.[d] (mag)[c]
SN 2012fg[f]	56381.301	171	21.40 (0.75)	20.24 (0.16)	19.72 (0.08)	19.70 (0.17)	–
SN 2012fg[f]	56422.301	211	21.84 (0.75)	20.74 (0.16)	20.37 (0.08)	20.35 (0.17)	–
SN 2012ho	56422.611	154	–	–	–	–	18.13 (0.16)
SN 2012ho	56484.387	215	–	–	–	–	18.68 (0.16)
SN 2012ho	56504.339	235	–	–	–	–	18.86 (0.16)
SN 2012ho	56506.551	237	–	–	–	–	18.88 (0.16)
SN 2012ho	56520.295	250	–	–	–	–	19.00 (0.16)
SN 2012ho	56573.439	303	–	–	–	–	19.47 (0.16)
SN 2013ab[g]	56484.348	143	18.96 (0.06)	17.64 (0.07)	16.85 (0.03)	16.65 (0.05)	–
SN 2013ab[g]	56508.212	167	19.04 (0.06)	17.88 (0.07)	17.05 (0.03)	16.97 (0.05)	–
SN 2013am[h]	56629.632	256	–	20.75 (0.01)	19.26 (0.03)	17.95 (0.04)	–
SN 2013am[h]	56834.287	461	–	21.59 (0.01)	20.03 (0.03)	19.02 (0.04)	–

[a]Modified JD (if not rounded to the whole day, modified JD at the mid-point of the observation).
[b]Phases of spectra are in rest-frame days since discovery using the redshift and discovery date presented in Table A1.
[c]Uncertainties on the photometry are in parentheses.
[d]'Unf' is unfiltered KAIT magnitudes (Ganeshalingam et al. 2010).
[e]SN 2012aw is also known as PTF12bvh.
[f]SN 2012fg is also known as PTF12jxe.
[g]SN 2013ab is also known as iPTF13ut.
[h]SN 2013am is also known as iPTF13aaz.

This paper has been typeset from a TEX/LATEX file prepared by the author.